COMPARATIVE ANALYSIS OF ELECTRICAL AND MECHANICAL FAULT SIGNATURES IN INDUCTION MOTORS

A Thesis

by

ARVIND M. VENUGOPAL

Submitted to the Office of Graduate Studies of
Texas A&M University
in partial fulfillment of the requirements for the degree of

MASTER OF SCIENCE

December 2003

Major Subject: Mechanical Engineering

COMPARATIVE ANALYSIS OF ELECTRICAL AND MECHANICAL FAULT SIGNATURES IN INDUCTION MOTORS

A Thesis

by

ARVIND M. VENUGOPAL

Submitted to Texas A&M University
in partial fulfillment of the requirements
for the degree of

MASTER OF SCIENCE

Approved as to style and content by:

Alexander G. Parlos (Chair of Committee)	John M. Vance (Member)
Edgar Sanchez-Sinencio (Member)	Dennis L. O'Neal (Interim Head of Department)

December 2003

Major Subject: Mechanical Engineering

ABSTRACT

Comparative Analysis of Electrical and Mechanical
Fault Signatures in Induction Motors. (December 2003)
Arvind M. Venugopal, B.E., University of Madras, Chennai, India
Chair of Advisory Committee: Dr.Alexander G. Parlos

This research deals with the comparison of fault signatures in induction motors. The primary objective is to study and analyze the similarities in the electrical and mechanical fault signatures, and to determine the suitability of the former for effective motor fault detection. Currently, vibration analysis is the dominant means for mechanical fault detection for use in condition-based maintenance. The use of electrical signatures for mechanical fault detection in electric motors is becoming of interest. Due to its cost-effective nature and ease of use, electrical sensors are pre-installed at the motor switchgear by manufacturers. However in order to achieve this for mechanical faults, a systematic comparison between the vibration signatures and electric current signatures must be performed to study the effectiveness of such an approach. The behavior of vibration signatures as measured through tri-ax accelerometers installed at both in-board and out-board sides, and the three phase motor current signatures as compared to their corresponding healthy baselines is analyzed through a sequence of signal processing algorithms. The procedure is carried out for different types of mechanical faults including broken rotor bars, air-gap eccentricity, mechanical imbalance and deteriorating bearings staged on motors of different make and power rating. A comparison is then made between the two fault indicators derived from mechanical and electrical measurements, respectively.

To My Parents

ACKNOWLEDGMENTS

I would like to convey my sincere thanks and gratitude to my committee chair and advisor, Dr. Alexander G. Parlos, for his patience, continuous guidance, technical support and advice through the course of my research work. I also thank Dr. Vance and Dr. Sanchez for their time, interest and support in my research. Last but not least, I would like to acknowledge and thank the other students in the NIML Lab for offering me help whenever I needed it.

TABLE OF CONTENTS

CHAPTER Page

LIST OF TABLES

LIST OF FIGURES

FIGURE Page

FIGURE Page

FIGURE Page

FIGURE Page

FIGURE Page

FIGURE Page

FIGURE Page

CHAPTER I

AN INTRODUCTION TO INDUCTION MOTOR FAULT DIAGNOSIS

A. Problem Definition

Induction motors play a key role in the successful operation of a variety of industrial processes and real-world applications. In order to prevent productivity losses and achieve minimum machinery downtime, it is extremely important that such motors are constantly monitored and diagnosed for potential faults. Sources of these failures may range from mechanical faults such as broken rotor bars, damaged motor bearings and air-gap eccentricities to electrical faults such as stator winding shorts and supply voltage imbalance. A majority of these faults is often based on the physical degradation of parts, and hence require much attention. While preventive and periodic maintenance are techniques often employed in industry, unnecessary replacement of healthy motor parts is a major problem associated with it. It is in this context that the usefulness of a system with capabilities to detect and diagnose mechanical faults can be realized. Early detection of faults also allows for reduction in downtime due to unexpected failures [1].

B. Types of Induction Motor Faults

Faults in induction motors can be broadly classified into faults based on the electrical condition (electrical faults) and faults based on the mechanical condition (mechanical faults) of the motor. Electrical faults include faults like excessive power supply imbalance and stator winding shorts, and mechanical faults include faults like bearing

---

The journal model is *IEEE Transactions on Automatic Control*.

defects and rotor faults. The fact that the vibration signature analysis of a machine will primarily be helpful when applied to analyzing the mechanical condition of a machine drives the focus of the intended work on the different types of mechanical faults. According to the results of a recent motor reliability survey [2], the majority (about 80 %) of the electric machine component failures are caused due to problems with the three main components of the machine namely the stator, the rotor and the bearings. A brief overview of the different forms of mechanical faults follows.

Despite the rugged architecture of the squirrel-cage construction, rotor faults occur in induction motors, especially in larger machines. Startup transients and high centrifugal forces created by load fluctuations propagate the defect once it is initiated. While mechanical signature monitoring promises to be an easy detection method for such faults, methods have also been developed using frequency component monitoring of the current spectrum associated with broken rotor bars. Rolling element bearings, which are the most common type of bearings used to provide rotor supports in induction motors, generally consist of an outer ring, an inner ring and a set of roller balls for rotating in the raceways. Localized fatigue caused due to continual stresses, improper lubrication, corrosion and improper installation are a few modes through which bearing faults may occur. Air-gap eccentricity is another mechanical fault type, and can be classified into static and dynamic air-gap eccentricities. When the positioning of the stator or the rotor (during the commissioning stage) is incorrect or when there is an ovality of the core, static air-gap eccentricity is caused. Dynamic air-gap eccentricity can be caused by bearing wear, bearing misalignment, bent rotor shaft and so on. Both types of eccentricities can cause a lot of damage to the bearings, core, windings and the rotor cage. Additional mechanical faults appear in induction motors, but are not further explained here.

C. Literature Review

Several methods have been proposed to detect and diagnose incipient motor faults. These include both electrical faults and mechanical faults. An enormous amount of research has been done and a variety of literature has been published toward detecting mechanical faults. An important area of research is in the detection of broken rotor bars. Elkasabgy and Eastham [3] demonstrated that the detection of the presence of a broken bar could actually be carried out in three distinct ways: a) Motor Current Signature Analysis (MCSA), which involves frequency analysis of the motor's stator current for monitoring frequency components associated with faults; b) Use of internal or external search coils to measure variations in the magnetic flux density as a function of time; c) Monitoring the twice-slip frequency components induced in the motor torque. Payne et al. [4],[5] performed an investigation into detection and diagnosis of broken rotor bars by the use of vibration and phase current analysis. Emphasis was made on demonstrating higher potential with the use of current spectra while experimental results proved encouraging for both current spectra based and vibration spectra based fault diagnosis.

Another area of concentration for motor fault detection and diagnosis has been damaged bearings and air-gap rotor eccentricities. Schoen et al. [6] addressed the application of motor current spectral analysis for the detection of rolling element bearing damage in induction motors. They correlated the relationship between vibration and current frequencies caused by incipient bearing failure, and showed experimentally that this relationship is verified by the vibration and current spectra of an induction machine with bearing faults in them. Yazici and Kliman [7] developed a statistical time-frequency based method for detecting bearing damage and broken rotor bars. They used an algorithm that is trained to recognize healthy operating condition, and

flag new operating modes, thus indicating the presence of faults. Trzynadlowski and Ritchie [8] performed a comparative analysis of line current, input power and estimated torque. These were used as signals from which broken bar fault information could be extracted. They concluded that the input power is the best signal to use due to its high magnitude of fault indicating peaks.

Cameron et al. [9] developed a unified monitoring strategy, and selected line current and frame vibration as the monitored parameters to produce signature patterns uniquely identifiable as characteristic of eccentricity. Thomson et al. [10] were able to successfully demonstrate the identification of faults in the motor spectral components. An industrial case study was presented to show that the spectral components of the stator current associated with eccentricity were identifiable in the FFT. These were notably absent after the correction of the defect. Kim [11],[12] presents an alternative approach to MCSA by using the overall distortion of the stator current as an indicator for the presence of a fault. This approach has the advantage of being insensitive to uncertainty in the frequencies at which faults appear in the current. M. Benbouzid et al. [13] demonstrated the use of stator current processing for the detection and localization of faults in an induction motor. P. D. McFadden and J. D. Smith [14] used the signal average of vibration to show valuable results in detecting local defects in a gear. While the paper in the IEEE Transactions on Industrial Electronics by M. Benbouzid [15] provides a tutorial overview of induction motor fault diagnosis by the use of motor signature analysis, the paper in the IEEE Transactions on Energy Conversions [16] focuses on providing a detailed bibliography of all relevant previous work toward induction motor fault detection and diagnosis.

D. Research Objectives and Proposed Approach

1. Objectives

The significance of the causes and effects of mechanical faults drives the necessity for an integrated system that would allow for detection capabilities. The primary objective of the present research is to compare electrical and mechanical fault signatures in induction motors, and to arrive at the selection of a suitable fault detection scheme for mechanical faults. Mechanical faults such as air-gap eccentricity, broken rotor bars, mechanical imbalance and damaged bearings are considered for the same. The ultimate goal of this research is to be able to detect mechanical faults based on the electrical signatures. With its low cost (eliminate expensive vibration sensors for the purpose) and their ease of installation/use makes the use of electrical sensors the preferred method for induction motor fault detection. However for mechanical faults, in order to achieve this, a systematic comparison of the vibration signatures and current signatures is to be performed to study the effectiveness of the approach. Scalability of the scheme across motors of different motor ratings along with adaptability of the scheme with different types of mechanical fault types is also to be studied.

2. Proposed Approach

The difference in machine condition between a healthy motor and a faulty one forms the basis for fault detection. In the case of motor mechanical faults, this difference is often visualized through the line current spectra and vibration spectra. A baseline healthy set of data for constant levels of loading will be obtained by recording all phases of line currents and all axes of vibration (axial, radial and tangential). A similar procedure will be followed to obtain data sets for different fault cases. Each faulty case will then be considered individually with respect to the baseline healthy

data. This is planned to be carried out through the observation of the pattern and magnitude of the vibration data.

During the analysis of vibration information, each channel of information will be processed separately and passed through a series of stages before fault detection can be made. Data sets obtained through the data acquisition medium, will then be joined together into arrays of data ready to be processed and the data sets will be appropriately either downsampled or upsampled according to the processing requirements. These data sets will then be passed through a moving window root mean square algorithm to compute the vibration-based mechanical fault indicator.

After the computation of these indicators, the difference between the fault indicators for the faulty and healthy motors will provide information for the detection of faults. Statistical consistency will be verified by repeating the processing for multiple sets of data. While analyzing the electrical signatures, the fundamental component of the signal will be removed from the original signal before carrying out the moving window root mean square of the signal data. This will be done through multi-resolution signal processing using the wavelet packet decomposition technique.

The above procedure to analyze the vibration and current spectra will be repeated for motors of different ratings, to demonstrate the scalability of the comparison and the fault detection scheme. After the results obtained from the electrical and vibration signatures are observed, a comparative analysis will be performed to validate the effectiveness of the approach.

E. Contributions of the Research

The following are some of the key contributions of this research toward induction motor condition assessment and fault diagnosis:

- Analysis and systematic comparison of electrical and mechanical fault signatures in induction motors, to provide the means for selecting a cost-effective approach in the detection of mechanical faults.
- Demonstration of the scalability of the developed approach for machines of different ratings and manufacturers.
- Demonstration of the adaptability of the approach to mechanical faults of different nature.

F. Organization of the Thesis

The rest of the thesis report is organized as follows. In Chapter II the experimental set-ups are described for both large and small machines. While providing an overview of the different fault detection methods, this chapter also explains the various steps involved in the signal processing performed. This is done through descriptions of the algorithms based on the electrical and mechanical signatures. Chapter III presents the results and the systematic comparison of the electrical and mechanical fault signatures for the various fault cases. Each fault case is individually considered, and the corresponding results are also graphically presented. Discussions based on motor ratings and loading conditions are also presented. Finally, in Chapter IV a summary of this work is presented along with the conclusions drawn from the results.

CHAPTER II

EXPERIMENTAL WORK AND SIGNAL PROCESSING FOR FAULT INDICATOR GENERATION

A. Description of Experimental Setups and Data Acquisition

1. Small Machine Set-up

The small machine experiments were conducted on a 3 - ϕ, 4 pole, 3 hp motor manufactured by Marathon Incorporate and located at Networked Intelligent Machines Lab, 167 Wisenbaker Engineering Research Center, Texas A&M University. The motor was powered by auto-transformers and loaded from the supply mains. Experiments were conducted at a steady state of operation with constant loading. A dual module 16-channel National Instruments data acquisition system was used to collect data. The six vibration signals were sampled at 40000 samples per second (and downsampled to 4000 samples per second at a later stage), while the three phases of currents and three phases of voltages were sampled at 4000 samples per second. Figure [1] shows a picture of the Small Machine Set-up.

2. Large Machine Set-up

The large machine experiments were performed on two motors: a)3 - ϕ, 8 pole, 800 hp motor manufactured by Allis Chambers and b) 3 - ϕ, 6 pole, 500 hp motor manufactured by General Electric. They were conducted at the Public Service Electric and Gas Motor Repair Facility, Sewaran, New Jersey. The motors were loaded using a dynamometer. Experiments were performed both at constant levels of loading and varying load levels. Only steady state data were considered for processing in this research. A 13- channel IOTech Data Acquisition System was used to record three

Fig. 1. Small Machine Set-up

phase voltages, three line currents, the speed and six vibration signals. The signals were sampled at 40000 samples per second and were eventually downsampled to 4000 samples per second while processing. Figure [2] shows a picture of the Large Machine Set-up.

B. Description of the Experiments Conducted

1. Small Machines

This section describes the experiments that were done for different cases of bearing faults. Four different deteriorating bearings were chosen and used for the same, but the nature of the deterioration in the various bearings was not known. For the single fault cases, bearings were replaced at one end of the rotor (fan end) while maintaining the bearing at the other end (shaft end) healthy. For the double fault cases, the bearings were replaced at both ends. While a single faulty bearing was maintained at one end, the other end was introduced with a different faulty bearing for each experiment. As the experiments performed for the single and double faults

Fig. 2. Large Machine Set-up

were done using different rotors, baseline healthy data was also obtained separately for each of the corresponding rotors. Also, for one of the cases, the motor was loaded to 25% of its rated capacity and experiments performed for a healthy baseline and with both bearings defective.

2. Large Machines

Experiments were conducted for different types of faults. For this research, data corresponding to faults namely broken rotor bars, air-gap eccentricity, and mechanical imbalance, were used. Steady state data corresponding to 100 percent and 50 percent loading conditions were used for the different cases. The experiments for 1/2 broken bar, 1 broken bar, 2 broken bars, 4 broken bars, and two different cases of air-gap eccentricities were all done on the Allis Chamber motor. The experiments for the imbalance case was done on the G.E. motor. As data for these faults are from different motors, separate healthy baselines for the corresponding cases were considered for analysis.

C. Fault Detection Methods and the Signal Processing Approach

A system fault may be detected when there is a deviation in its operating characteristics away from its normal operation. In order to identify such a fault, it is required to observe the system parameters in cases of healthy as well as faulty operations of the system. A fault detection scheme adopted for this purpose can be data-driven, knowledge-based or model-based. In data-driven methods, the data collected during the normal operating condition are compared with data collected in the presence of specific faults in the machine. This allows for the development of fault indicators to detect and diagnose machine faults. While knowledge-based methods involve developing relationships between observed symptoms (effects) and unknown faults (causes) and thereby arriving at a logical conclusion to help diagnose faults, model-based methods use the system input and output data to estimate information about the system. For large scale systems containing a number of inputs, outputs and/or states, data-driven methods have proved to be successful when applied to statistically significant lengths of data sets.

A majority of the motor fault detection systems developed so far have been based on data-driven methods (also known as signal-based methods). With this in mind, this research focuses on the application of advanced signal processing algorithms and development of vibration-based mechanical fault indicators and current-based mechanical fault indicators for the detection of mechanical faults. Figure [3] shows the Signal Processing Approach to Fault Diagnosis.

Looking into fault specific individual frequencies produced in the signals requires some knowledge about the design of the machine (or of its components) which some users may not possess. Hence they are not considered while developing the fault indicators. The moving average root mean square is used as the main technique for

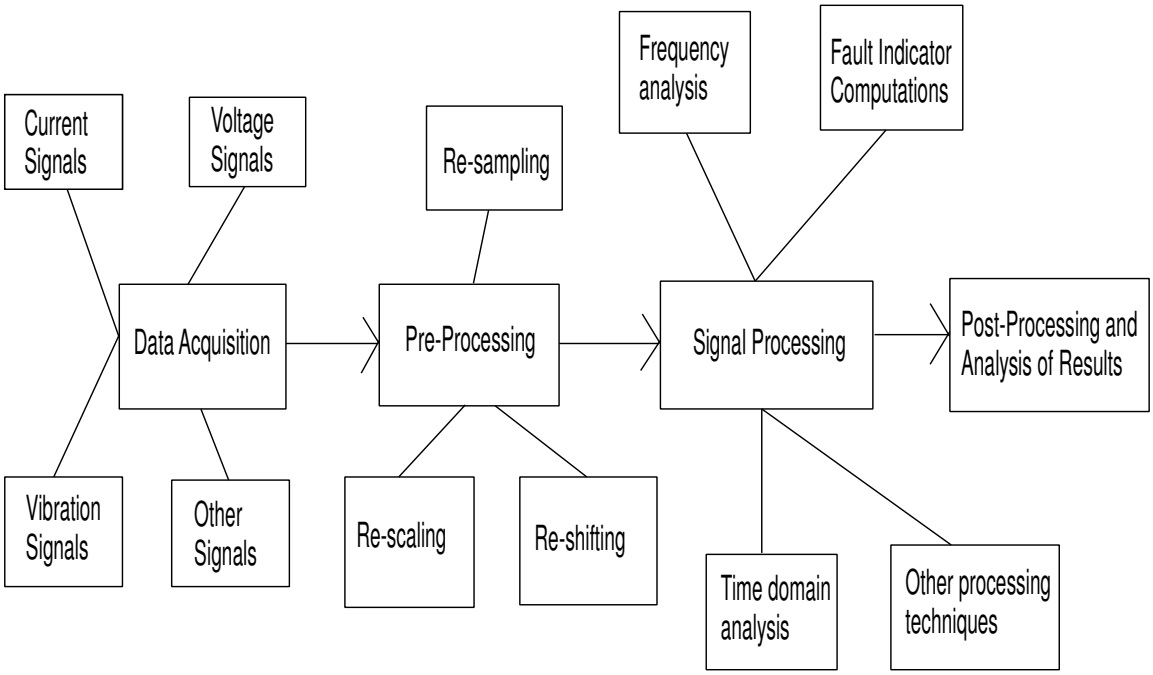

Fig. 3. Signal Processing Approach to Fault Diagnosis

computing indicators, and the wavelet packet decomposition is used for the harmonic separation of the current signals.

Wavelet Packet Decomposition: Although Fourier methods (transforms) have been often employed to decompose signals into sinusoids of different frequencies, its limitation with respect to not being able to retain temporal localization of the signal suggest the employment of an alternative means [17]. Stationarity is desired at steady state operating conditions. But in order to obtain stationarity, not only should the loading conditions and supply conditions remain constant, but the entire spectrum of harmonics has to remain invariant. This means that even though individual frequencies might not be changing location, their magnitude might be changing over time. This is the reason Wavelet packets are used instead of the Fourier based methods (Fast Fourier Transform and Short Time Fourier Transform). In addition to achieving time-localization in such non-stationary signals, the use of wavelet packets also allows for a flexible time-frequency resolution by including a scale parameter. The discrete wavelet transform (DWT) of a signal y(n) uses dyadic scales and is defined by the following expression:

$$C(a,b) = C(j,k) = \sum_{n \in Z} y(n) h_{j,k}(n), \tag{2.1}$$
$$a = 2^j, \quad b = k2^j = ka, \quad j \in N, \quad k \in Z,$$

where a is the scaling parameter, b is the position parameter,and $h_{j,k}(n)$ is the wavelet filter. The DWT of a signal produces a) approximation coefficients and b) detail coefficients. The approximation coefficients contain the low-frequency information of the signal and the detail coefficients contain the high-frequency information of the signal. The signal is then reconstructed into the desired composition (de-noising,

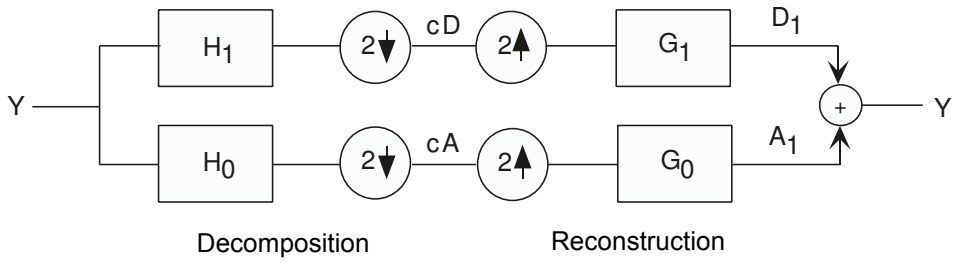

Fig. 4. Two-Channel Filter Bank

frequency isolations are a couple of options) by the use of an Inverse discrete wavelet transform (IDWT). The IDWT of the wavelet coefficient C(j,k) is defined as :

$$y(n) = \sum_{j \in Z} \sum_{k \in Z} C(j,k) g_{j,k}(n), \tag{2.2}$$

where $g_{j,k}(n)$ is the scaling filter. Successive decomposition of the wavelet coefficients allows for a multi-level analysis to be carried out.

A two-channel filter bank (shown in Figure [4]) will give a perfect loss-less reconstruction of an original signal. In the wavelet analysis, only the approximations are decomposed at each level (shown in Figure [5]). But in the wavelet packet analysis tree both the approximation and the detail coefficients are decomposed at every level (shown in Figure [6]). Wavelet analysis has been used for machinery diagnostics [18] and feature extraction for vibration monitoring [19]. In this research, the wavelet packet decomposition and reconstruction are used to separate the fundamental component and the harmonics of the current signals.

The following sections explain the steps involved in the computation of the fault indicators.

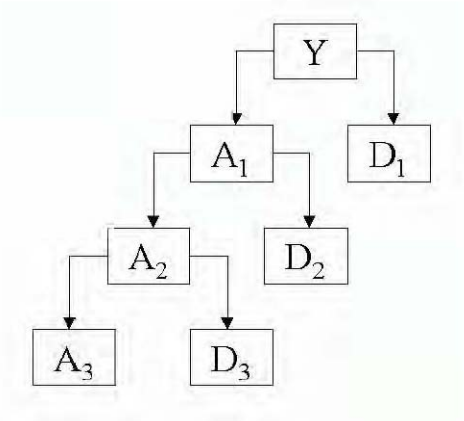

Fig.5.WaveletAnalysisTree

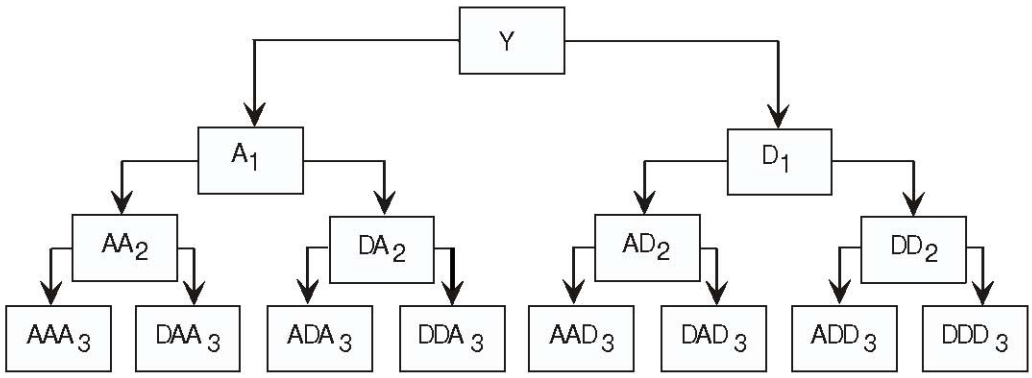

Fig.6.WaveletPacketAnalysisTree

D. Processing of Electrical Signals

The electrical signatures refer to the measurements corresponding to the induction motor's three phases of currents. Line currents and voltages are acquired through a V/I sensor system connected between the motor and the acquisition hardware.

Signals representing each of the three phases of currents, is initially passed through a downsampling stage, where the data is set to a sampling frequency of 4000 Hertz. In the case of the small motor, the data itself is acquired at a sampling rate of 4000 Hertz and hence does not need any downsampling.

It has been observed that usually the fundamental component of the current signal hides certain fault characteristics associated with mechanical faults. To solve this problem, a wavelet packet decomposition based algorithm is developed, by which the fundamental component of the signal is removed, and the harmonics are obtained as output. This is then passed through a moving average rms algorithm and the output obtained from the algorithm gives information about the actual condition of the machine. These are hence termed indicators of the machine condition. As current signatures are being analyzed, these are called current-based mechanical fault indicators.

1. Downsampling and Scaling

All signals are downsampled to a sampling rate of 4000 samples per second before any further data processing. This includes all three phases of currents and six channels of vibrations (three inboard and three outboard) for the healthy and faulty cases.

Before processing the downsampled data, scaling compensations for any scale changes made during the experiments were taken care of. Any biases that might have occurred during one or more of the experiments were also taken care of by forcing a

zero-mean to the signals.

2. Harmonic Separation using Wavelet Packet Decomposition

While analyzing the current signals, it has been observed in the past that the fundamental frequency component often causes difficulty in identifying certain characteristics associated with mechanical faults. To overcome this issue, the fundamental component of the signal was removed from the signal by the use of a wavelet packet decomposition algorithm. The output obtained thus took out the fundamental frequency component (60 Hz) providing information about the harmonics.

3. Moving Average Root Mean Square Algorithm

A root mean square computation is performed over a moving window, continuing through the length of the signal. The window size is usually set to an optimum number of points, obtained through the product of the number of points per cycle and the number of cycles per window. For the computation of indicators in this research, the number of points per cycle was fixed at 268, and the number of cycles per window was set to 12. The moving of the windows was done at a rate of one window at a time. In other words, the window's moving distance was maintained as one second. This algorithm was applied to directly to the vibration signals, and applied to the current signals after they were passed through the harmonic separation stage using wavelet packet decomposition.

The moving window root mean square value of a signal 'x(t)' is defined as follows

$$x_{RMS}(l) = \sqrt{\int_{t_1+lp}^{t_2+lp} x(t)^2 dt}, \quad l = 0, 1, \ldots, m, \tag{2.3}$$

where $t_2 - t_1$ is the size of the moving window, with a moving window distance of p and $m = (t_N - t_2)/p$. In the above expression, the units of t_1, t_2, t_N and p are

seconds, while l does not have units.

4. Current-Based Mechanical Fault Indicator

After passing the scaled and downsampled current signals through the wavelet packet algorithm, the harmonics are passed through a moving average root mean square algorithm. The output obtained indicates the machine health, and hence are indicators of the condition of the machine. As they are calculated using current signals as the source, they are termed current-based mechanical fault indicators. Healthy baselines are obtained when processing current signals from the healthy motor data, and fault indicators are obtained from the analysis of faulty motor data.

This procedure (shown in Figure [7]) is carried out for the healthy motor as well as for cases with specific pre-determined mechanical faults in the motor. The value obtained from the healthy conditions is defined as the baseline value, and an increase with respect to this baseline value of the mechanical indicator will indicate a mechanical fault in the motor.

E. Processing of Mechanical Signals

The mechanical signatures refer to the measurements corresponding to the vibration in the inboard and outboard sides of the motor. All the three axes of vibration (along the axis of the motor, perpendicular to the axis of the motor parallel the plane of the test-bed, and perpendicular to the axis of the motor in a plane normal to the test-bed) are measured using tri-axial accelerometers are installed on the surface of the motor casing.

Each of the six vibration signals is individually passed through a downsampling stage, where the data is set to a sampling frequency of 4000 Hertz. It is then passed

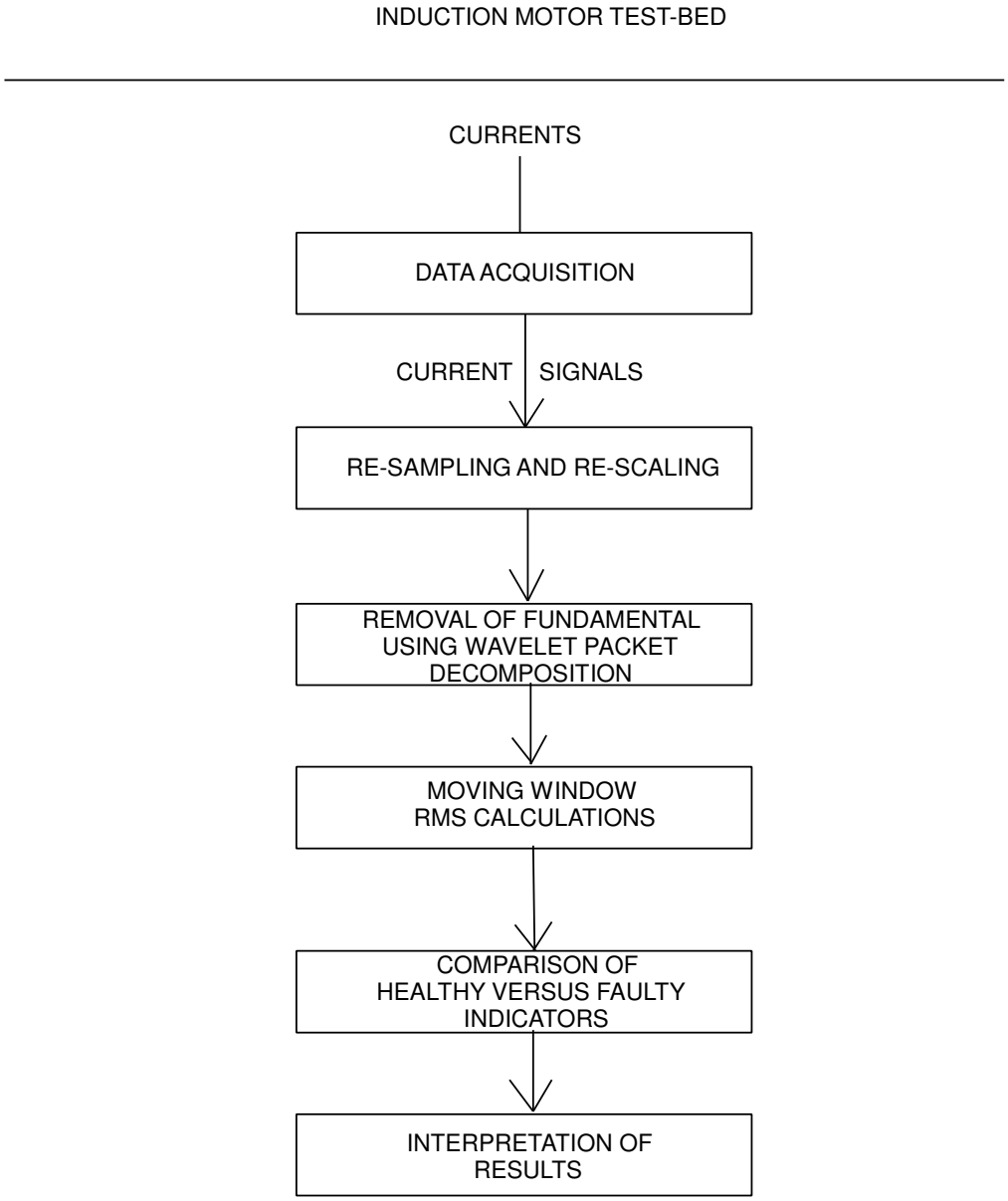

Fig. 7. Process-Flow Diagram for the Analysis of Electrical Signatures

through a moving average root mean square algorithm and the output obtained from the algorithm gives information about the actual condition of the machine. They are hence termed indicators of the machine condition. As vibration signatures are being analyzed, these are called vibration-based mechanical indicators. The use of information like ball-pass frequencies requires additional knowledge one might not have in the field, and hence is not considered during the computation of the fault indicators in the Bearing Fault cases. Unlike the current signals, harmonic separation using wavelet packet decomposition is not performed but the signal is directly passed through the moving rms algorithm.

1. Downsampling and Scaling

All signals are downsampled to a sampling rate of 4000 samples per second before any further data processing. This includes all three phases of currents and six channels of vibrations (three inboard and three outboard) for the healthy and faulty cases.

Before processing the downsampled data, scaling compensations for any scale changes made during the experiments were taken care of. Any biases that might have occurred during one or more of the experiments were also taken care of by forcing a zero-mean to the signals.

2. Moving Average Root Mean Square Algorithm

A root mean square computation is performed over a moving window, continuing through the length of the signal. The window size is usually set to an optimum number of points, obtained through the product of the number of points per cycle and the number of cycles per window. For the computation of indicators in this research, the number of points per cycle was fixed at 268, and the number of cycles per window was set to 12. The moving of the windows was done at a rate of one

window at one time. In other words, the window's moving distance was maintained as one second. This algorithm was applied to directly to the vibration signals, and applied to the current signals after they were passed through the harmonic separation stage using wavelet packet decomposition.

The moving window root mean square value of a signal 'x(t)' is defined as follows

$$x_{RMS}(l) = \sqrt{\int_{t_1+lp}^{t_2+lp} x(t)^2 dt}, \quad l = 0, 1, \ldots, m, \tag{2.4}$$

where $t_2 - t_1$ is the size of the moving window, with a moving window distance of p and $m = (t_N - t_2)/p$. In the above expression, the units of t_1, t_2, t_N and p are seconds, while l does not have units.

3. Vibration-Based Mechanical Fault Indicator

The vibration signals are scaled, downsampled and then passed through the moving average root mean square algorithm. The output obtained gives the machine health, and hence are indicators of the condition of the machine. As they are calculated using the vibration signals, they are termed vibration-based mechanical fault indicators. Healthy baselines are obtained when processing vibration signals from the healthy motor data, and fault indicators are obtained from the analysis of faulty motor data.

The above-mentioned steps (shown in Figure [8]) are carried out for the healthy motor as well as for cases with specific pre-determined mechanical faults in the motor. The value obtained from the healthy conditions is defined as the baseline value, and an increase with respect to this baseline value of the mechanical indicator will indicate a mechanical fault in the motor.

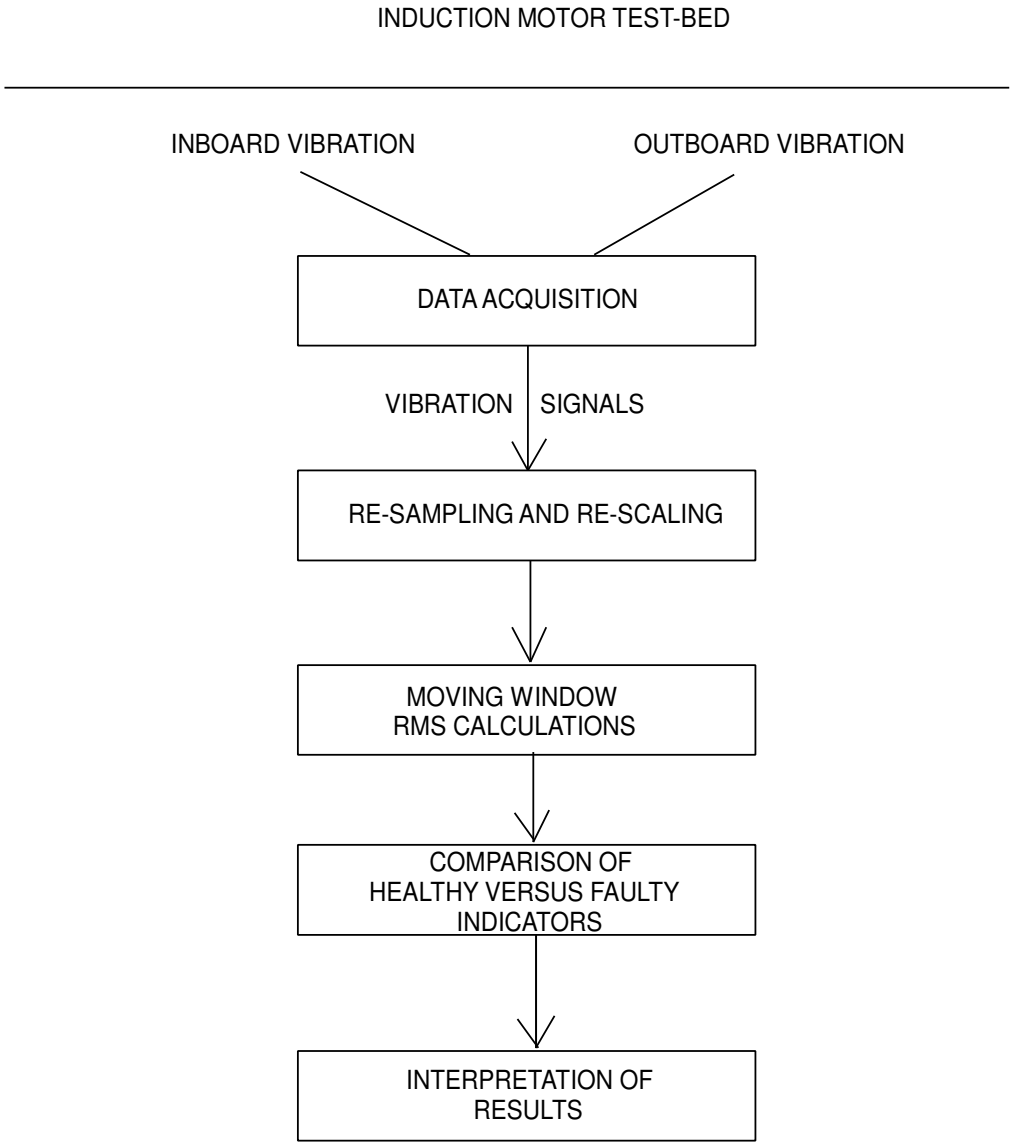

Fig. 8. Process-Flow Diagram for the Analysis of Mechanical Signatures

F. Chapter Summary

In this chapter, the experimental setups for the large machine and the small machine were described. The specifications for the corresponding data acquisition systems were also mentioned. The procedure of the experiments conducted for the large and the small machines was explained in detail. Finally the various steps in the actual data processing were given, and the two types of mechanical fault indicators being developed were discussed.

CHAPTER III

COMPARISON OF ELECTRICAL AND MECHANICAL FAULT SIGNATURES

In order to compare the mechanical and electrical fault signatures, healthy and faulty mechanical conditions were created. For doing this, depending on the type of fault, either a certain part of the motor was replaced with a faulty one or certain settings were altered to create a faulty motor condition. To determine the effects of loading and the motor ratings, different sized motors were used and studied when operating under certain loading conditions. Experiments for Fault I (Bad Bearings) were conducted on a 3 hp Motor located at Texas A&M University. Experiments for Fault II (Broken Rotor Bars) and Fault III (Air-Gap Eccentricity) were conducted on a 800 hp Motor. Experiments for Fault IV (Mechanical Imbalance) were conducted on a 500 hp Motor. The experiments on the large motors (800 hp and 500 hp motors) located at the Public Service Electric and Gas Motor Repair Facility, Sewaran, New Jersey were conducted in 1997, and their data has been used for this research. The experiments on the small motor (3 hp motor) located at the Networked Intelligent Machines Laboratory located in 167 Wisenbaker Engineering research Center, Texas A&M University were conducted during the course of this research. Table 1 shows the list of staged fault experiments.

Table I. List of Staged Fault Experiments

Fault	Rating	Manufacturer	Fault-Case	Description
Fault I	3 hp	Marathon	Single Bearing Fault Four Cases	Faulty bearing at the fan end
	3 hp	Marathon	Double Bearing Fault Five Cases	Faulty bearing at both ends
Fault II	800 hp	Allis Chambers	Broken Rotor Bars	Half broken bar
	800 hp	Allis Chambers	Broken Rotor Bars	One broken bar
	800 hp	Allis Chambers	Broken Rotor Bars	Two broken bars
	800 hp	Allis Chambers	Broken Rotor Bars	Four broken bars
Fault III	800 hp	Allis Chambers	Air-gap Eccentricity Case 1	Offset 25%Up-Inboard
	800 hp	Allis Chambers	Air-gap Eccentricity Case 2	Offset 20%Down, 10%Right-Outboard and 25%Up-Inboard
Fault IV	500 hp	G.E.	Mechanical Imbalance	Rotor Imbalance

A. Fault I: Bad Bearings

The healthy baseline data was obtained using a motor with healthy bearings at both ends. In order to demonstrate the independence of the desired overall objectives of the research from the specifics of the type of fault in the bearing, the defective bearings were randomly chosen. However, the severity of the fault itself does affect the magnitude of the results obtained. To account for this, the experiments were split into two parts. In the first part, one of the bearings in the motor was left healthy, while the other bearing was replaced with a faulty one. Four such cases

were considered and termed as Single Deteriorating Bearing Cases. In the second part, both the bearings in the motor were replaced with faulty ones. Four such cases were considered and termed as Double Faulty Bearing Cases. To study the effects of loading, an additional case of double bearing fault experiments were performed where the motor was loaded to as much as 25% of its rated capacity.

1. Single Deteriorating Bearing

While the raw vibration signals are indicative of the mechanical condition of the motor (although it does not indicate the type of fault in the motor), we realize that it is difficult to draw any conclusions by merely looking at the raw current signals. The vibration-based mechanical fault indicators calculated through the moving window averaging algorithm shows a significant increase from the healthy operating conditions. We can see a similar pattern with the current-based mechanical fault indicators as well, although the magnitudes of the mean percentage increase are a lot lesser in comparison to the vibration-based mechanical indicators. This is observed to be consistent for the various single bearing fault cases. The pattern obtained through the fault indicators allow for the detection of faults, but the identification of the type of fault through the developed fault indicators is not considered for this research.

For Single Bearing Fault Case 1, Figures [9]-[13] show the raw vibration signal, vibration-based indicator, raw current signal, current-based indicator and the comparison chart between the two indicators, respectively. We can see that the mean percentage increase of the current-based indicators is about 37.3% as compared to 51.3% of the vibration-based indicator.

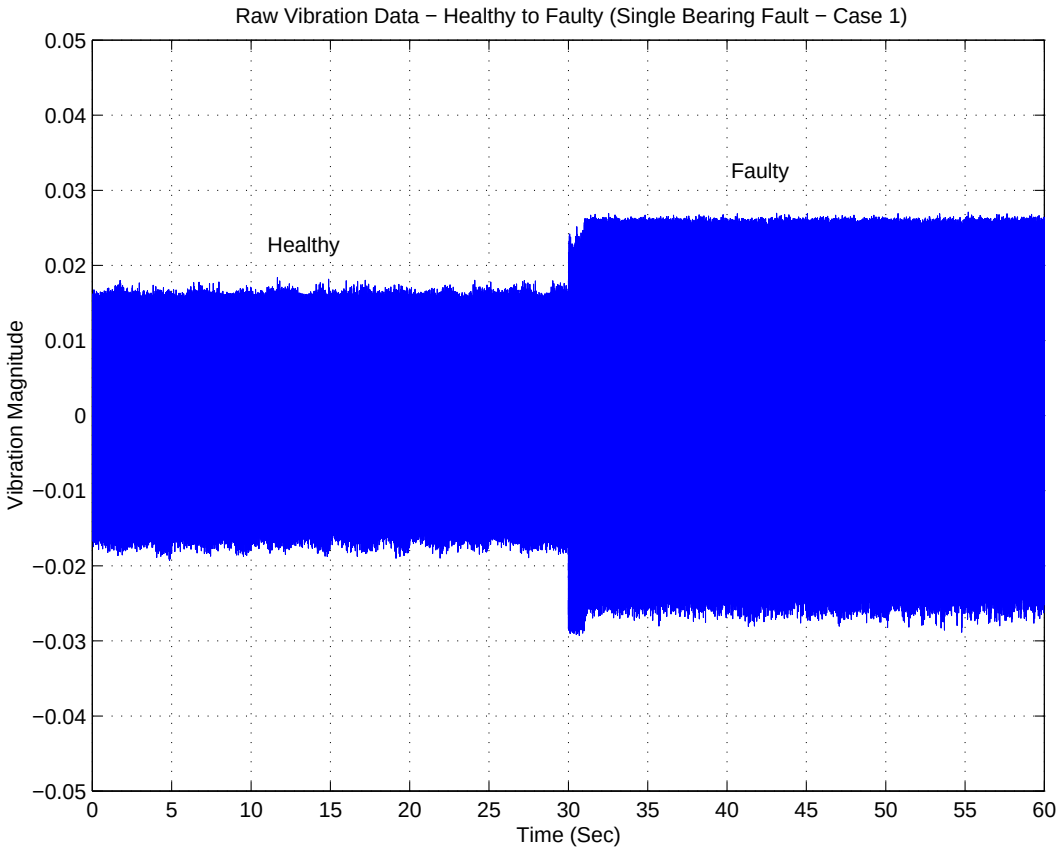

Fig. 9. Raw Vibration Signal - Single Bearing Fault - Case 1

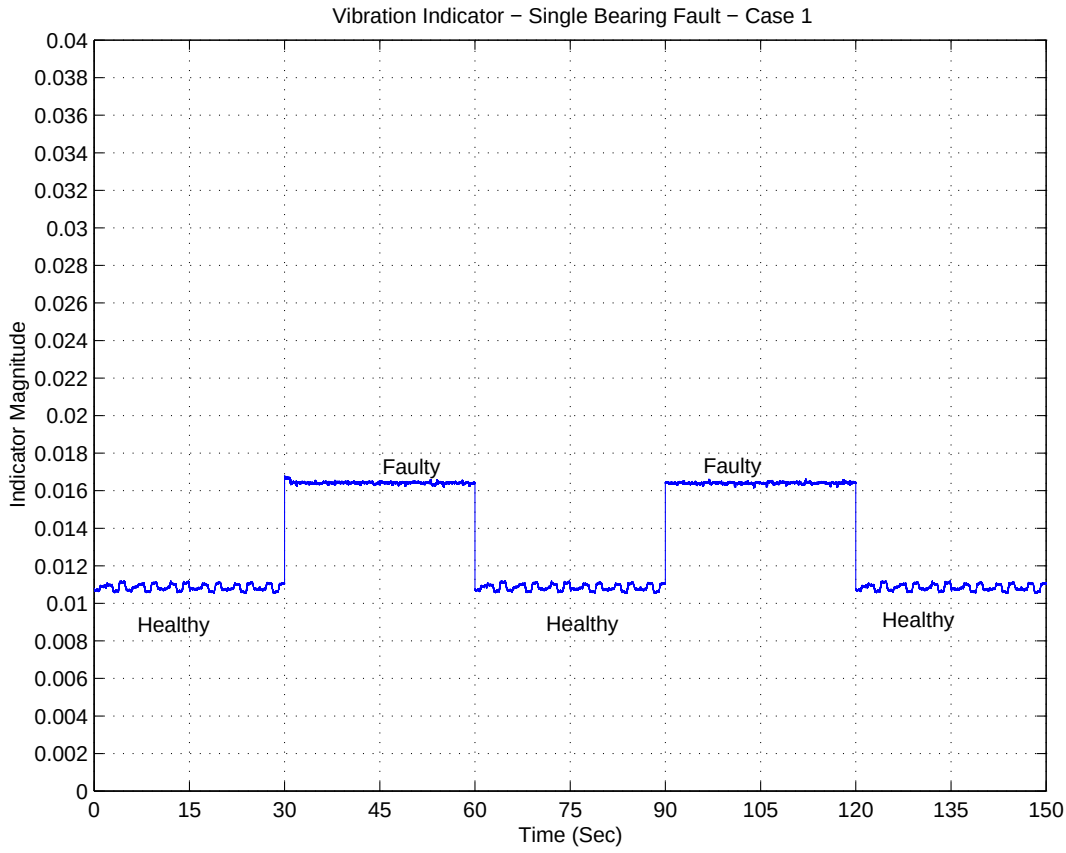

Fig. 10. Vibration-based Mechanical Indicator - Single Bearing Fault - Case 1

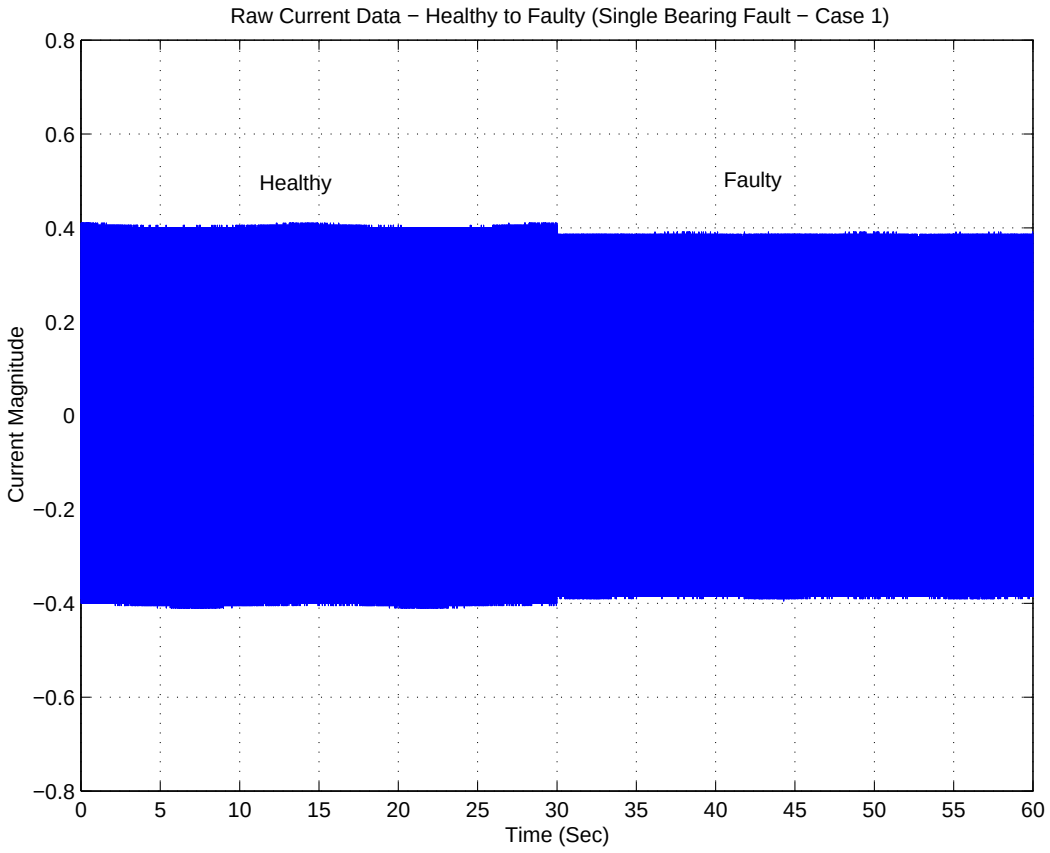

Fig. 11. Raw Current Signal - Single Bearing Fault - Case 1

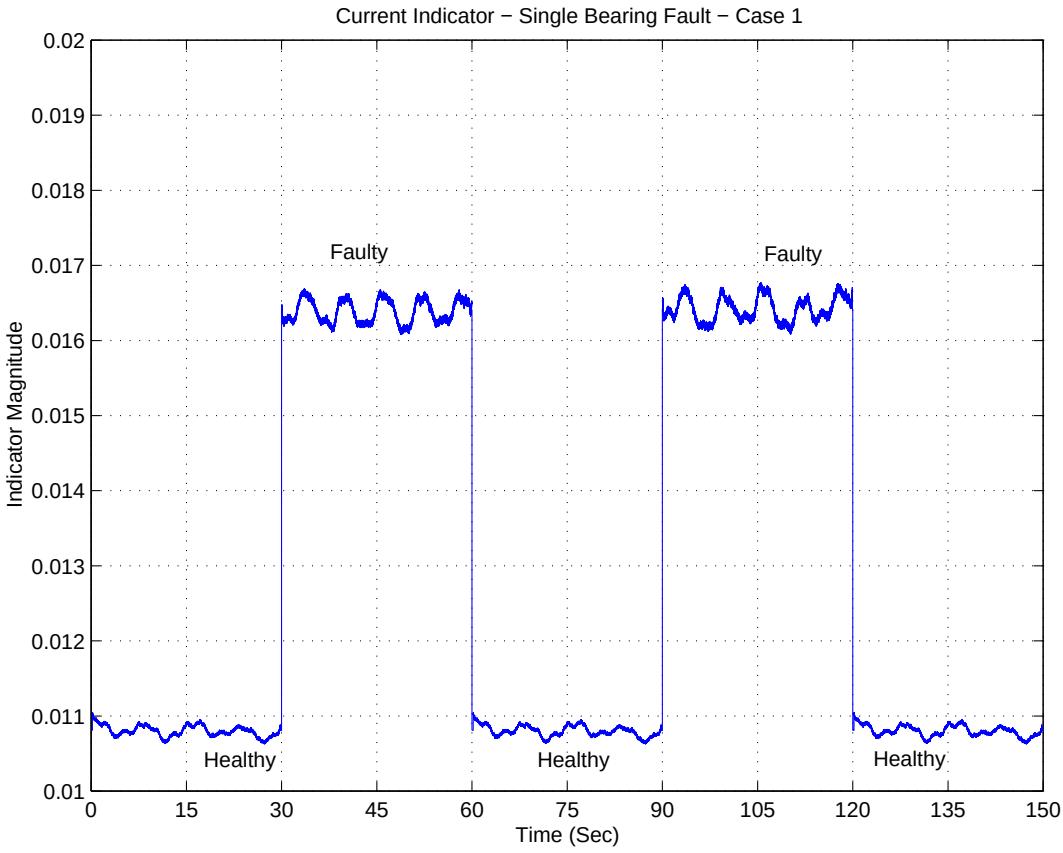

Fig. 12. Current-based Mechanical Indicator - Single Bearing Fault - Case 1

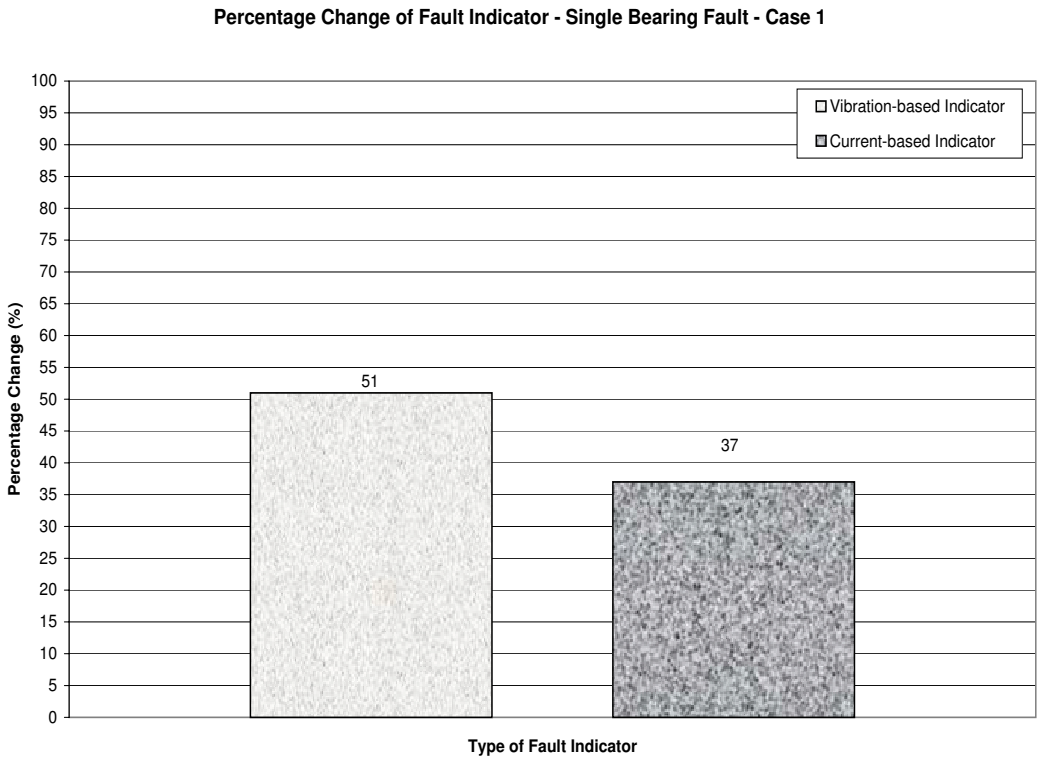

Fig. 13. Comparison of Current-based and Vibration-based Mechanical Fault Indicators - Single Bearing Fault - Case 1

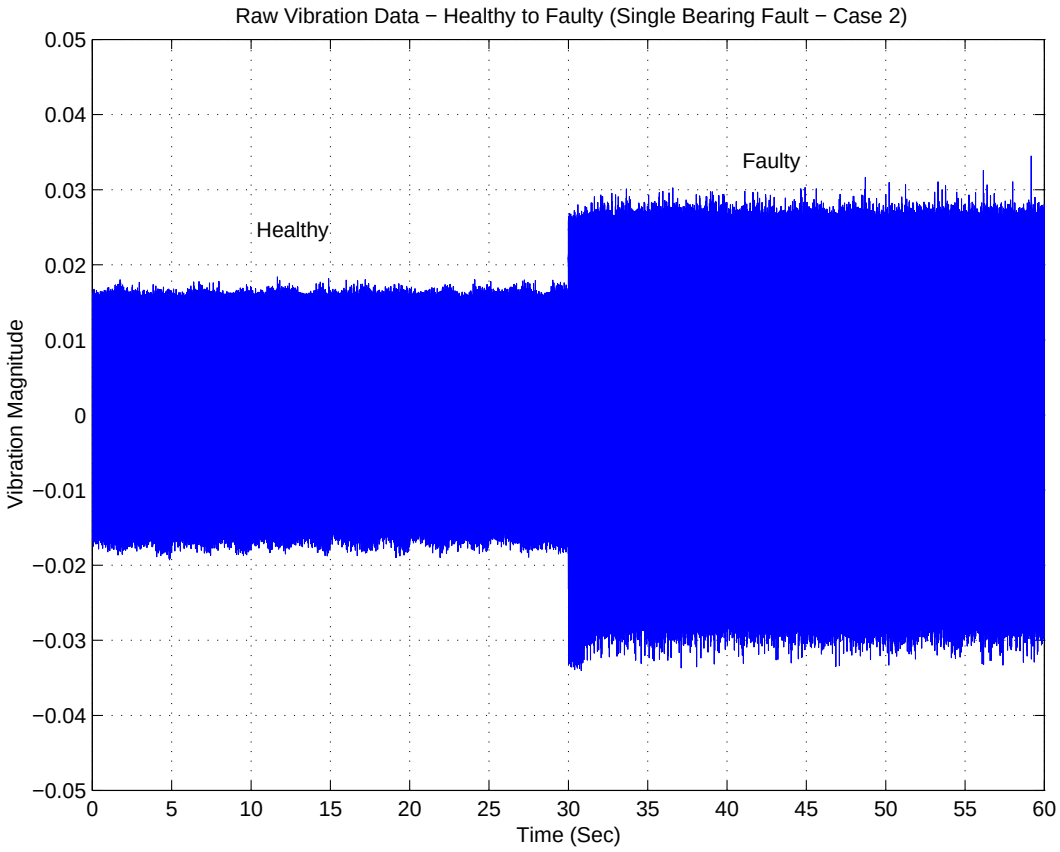

Fig. 14. Raw Vibration Signal - Single Bearing Fault - Case 2

For Single Bearing Fault Case 2, Figures [14]-[18] show the raw vibration signal, vibration-based indicator, raw current signal, current-based indicator and the comparison chart between the two indicators, respectively. We can observe that the mean percentage increase of the electrical indicators is about 4.3% as compared to 72.4% of the mechanical indicator.

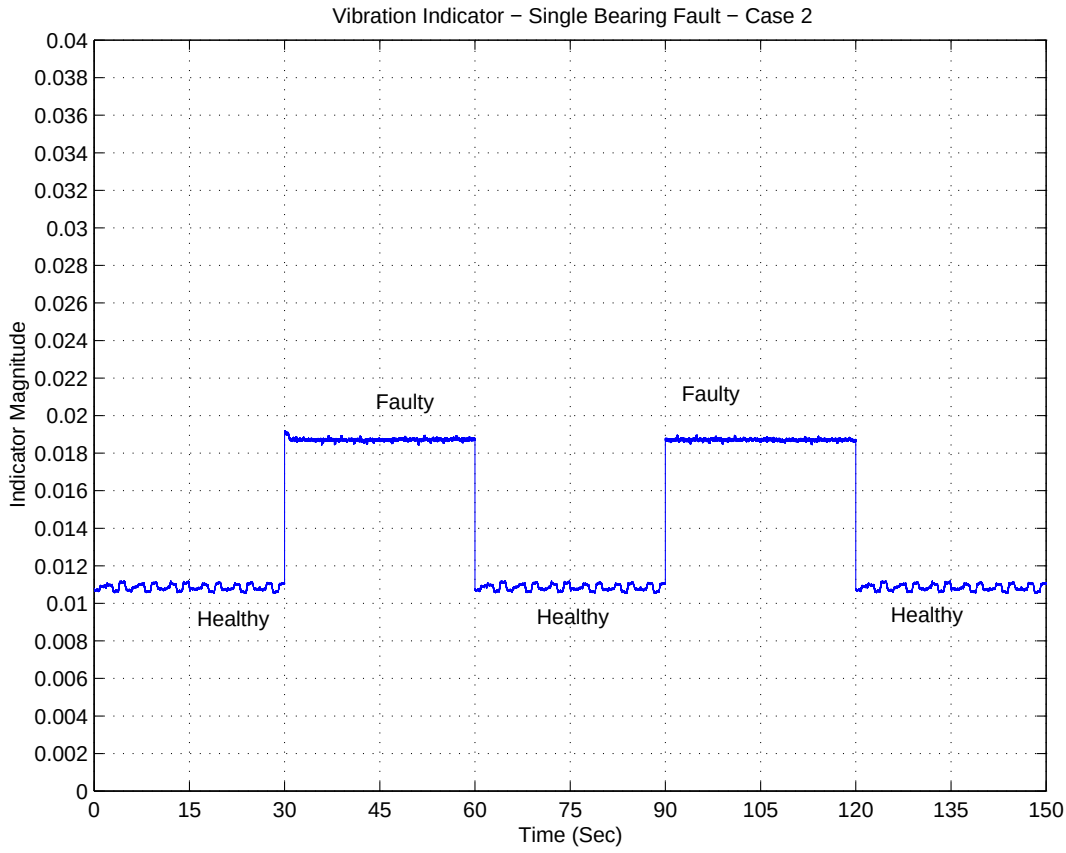

Fig. 15. Vibration-based Mechanical Indicator - Single Bearing Fault - Case 2

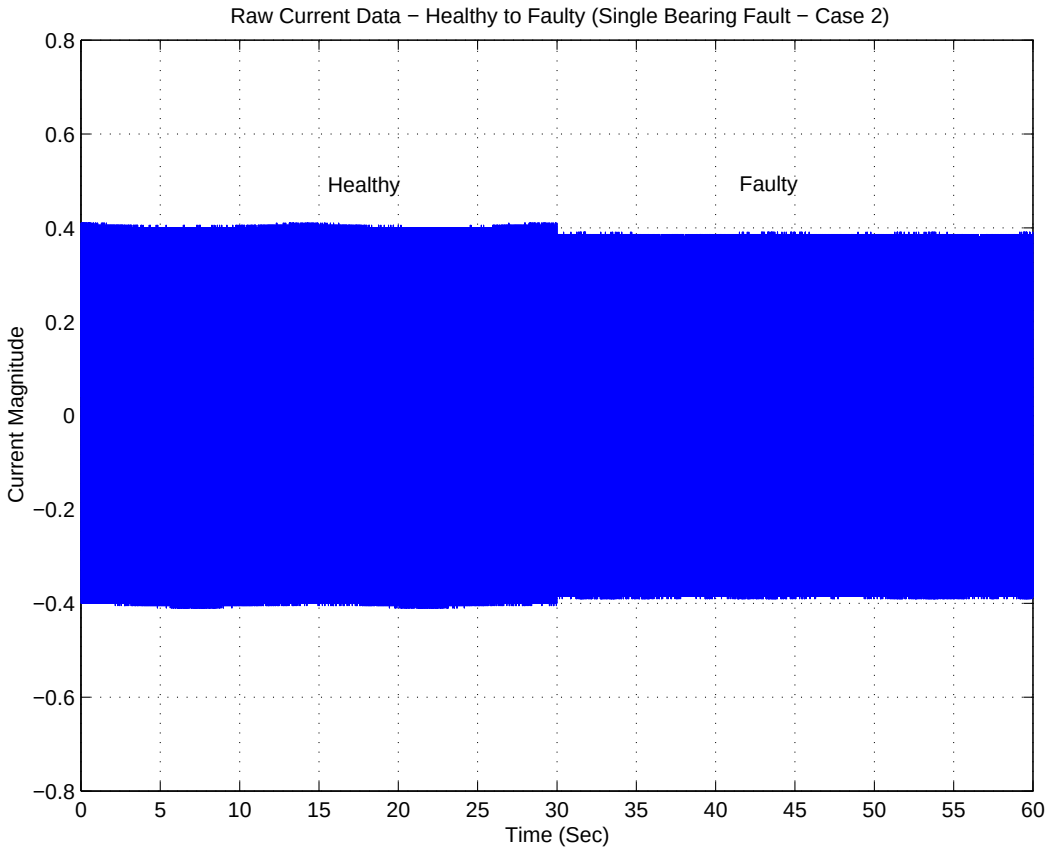

Fig. 16. Raw Current Signal - Single Bearing Fault - Case 2

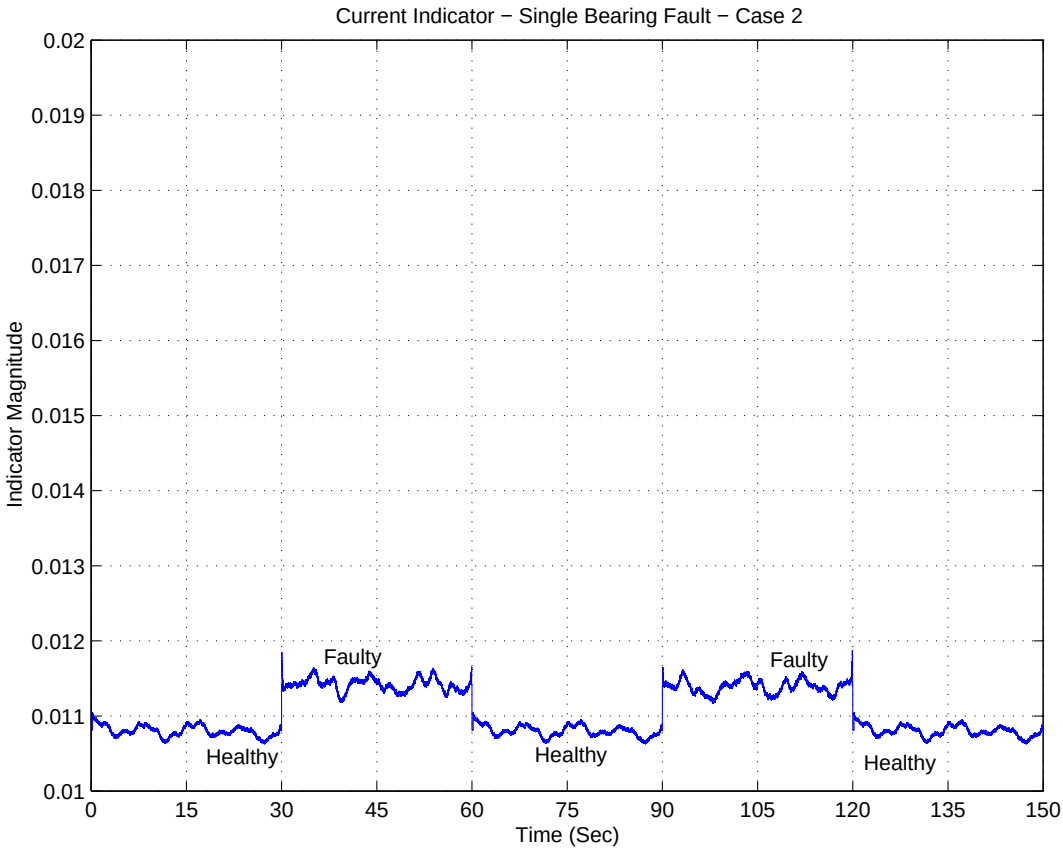

Fig. 17. Current-based Mechanical Indicator - Single Bearing Fault - Case 2

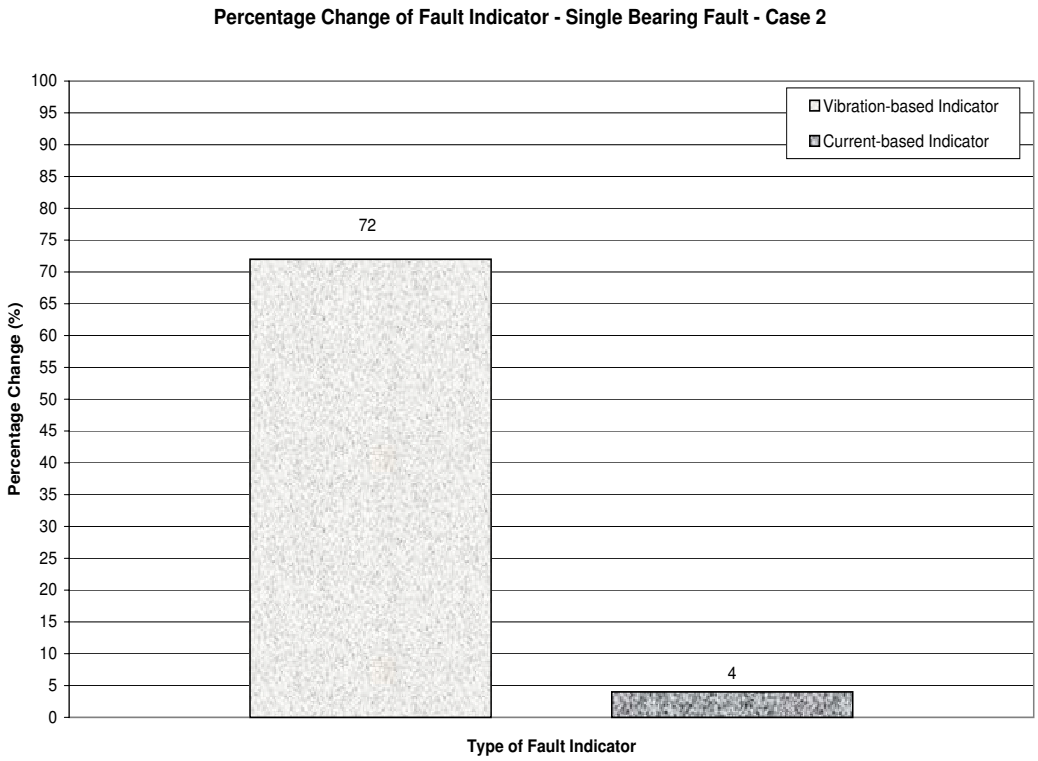

Fig. 18. Comparison of Current-based and Vibration-based Mechanical Fault Indicators - Single Bearing Fault - Case 2

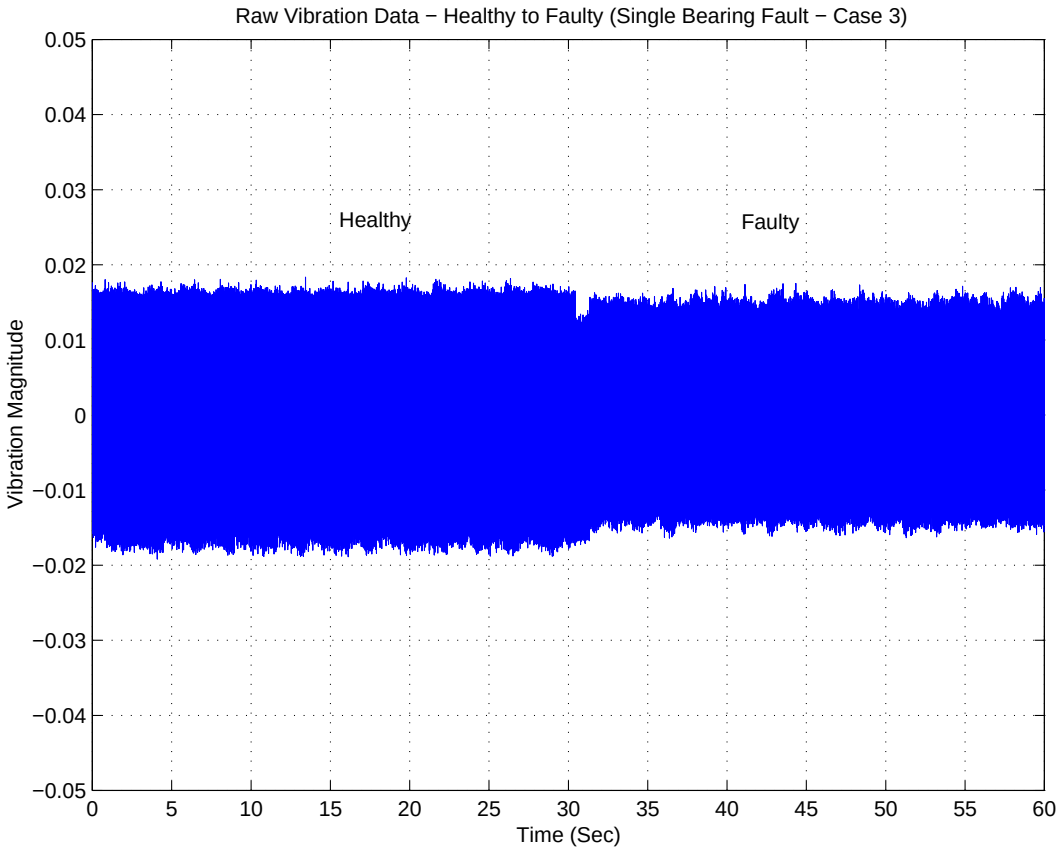

Fig. 19. Raw Vibration Signal - Single Bearing Fault - Case 3

For the Single Bearing Fault Case 3, Figures [19]-[23] show the raw vibration signal, vibration-based indicator, raw current signal, current-based indicator and the comparison chart between the two indicators, respectively. It is interesting to note that there is not a significant increase in the vibration-based indicator magnitude (28.1%). It is in fact lesser than the increase in the current-based indicator magnitude (43.1%). This means that this particular type of fault in the bearing may be easily detectable by processing the current signals.

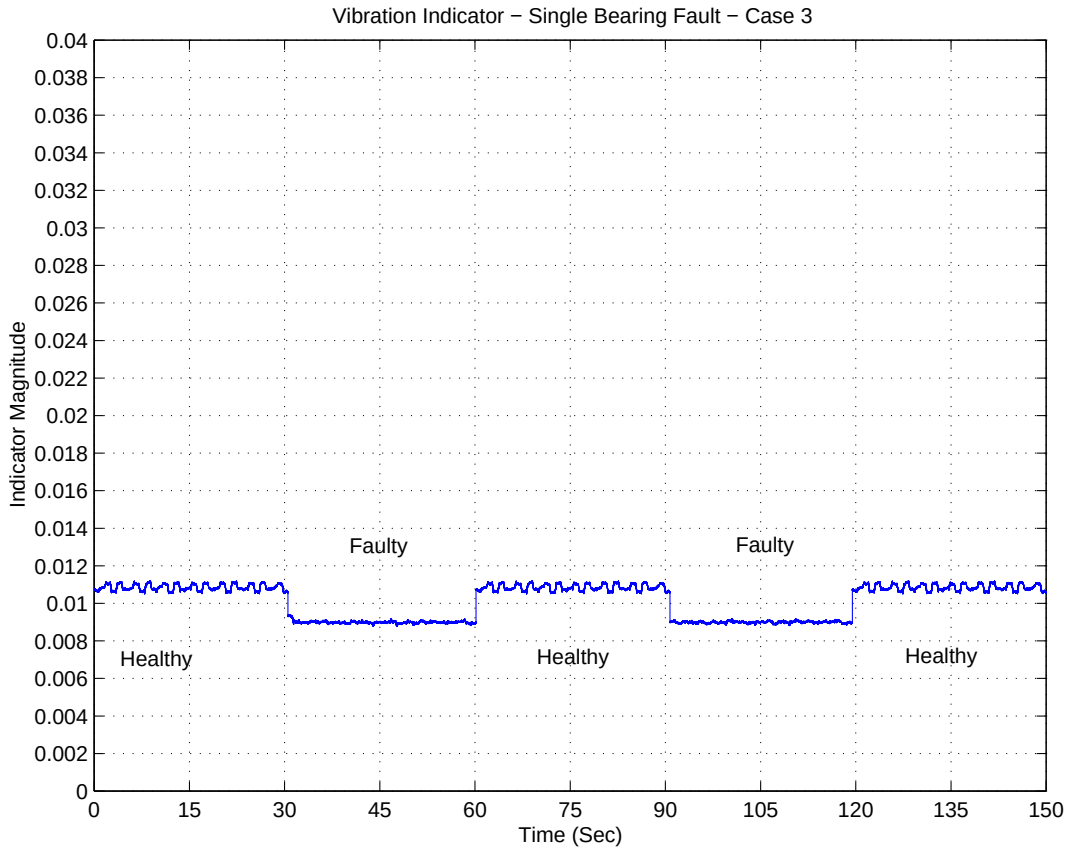

Fig. 20. Vibration-based Mechanical Indicator - Single Bearing Fault - Case 3

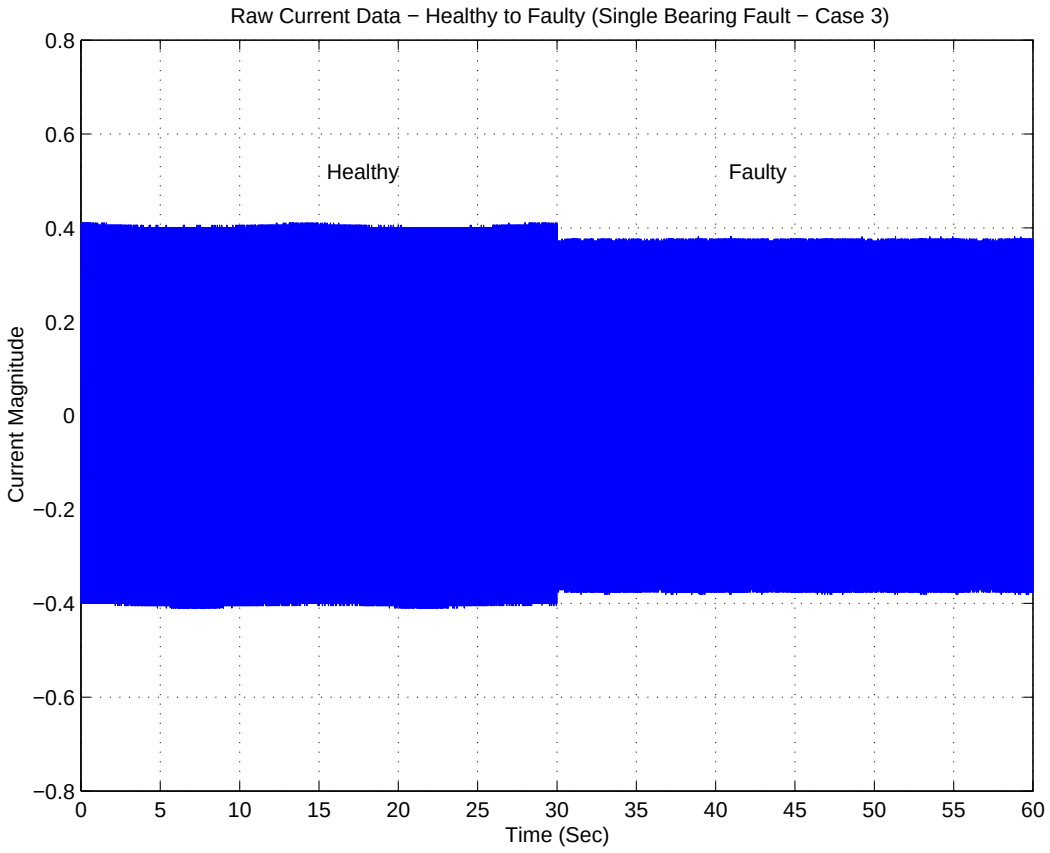

Fig. 21. Raw Current Signal - Single Bearing Fault - Case 3

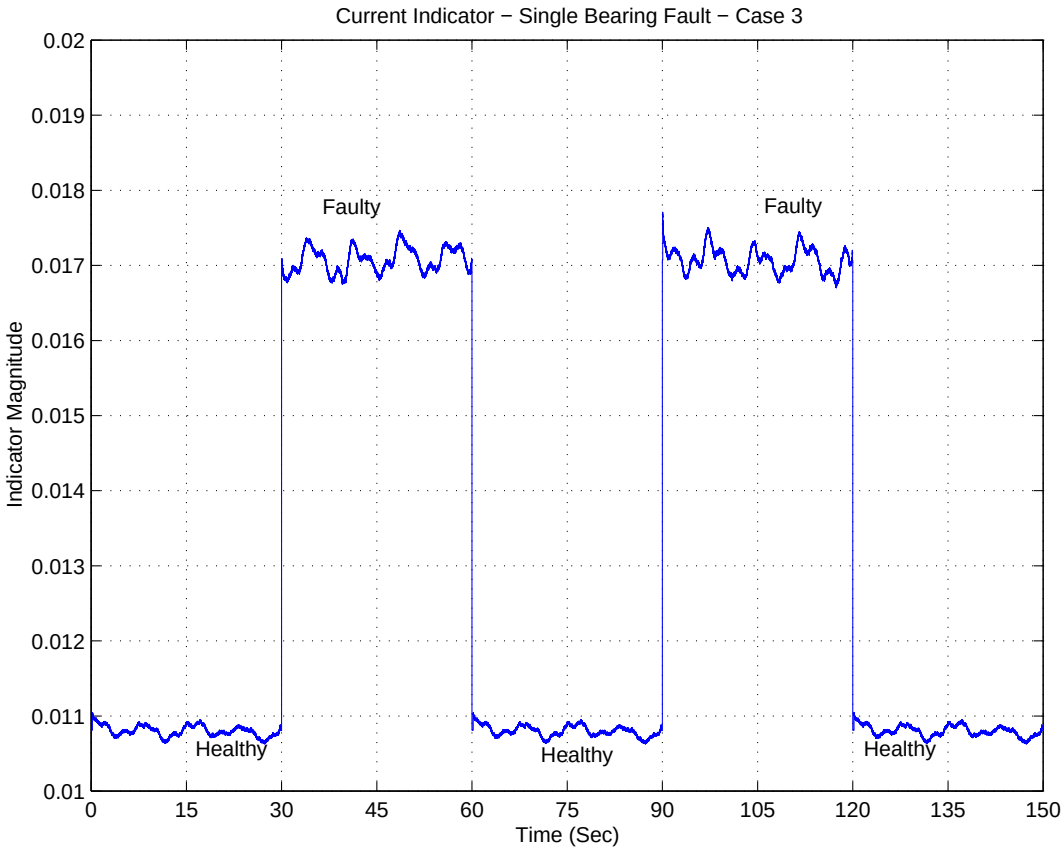

Fig. 22. Current-based Mechanical Indicator - Single Bearing Fault - Case 3

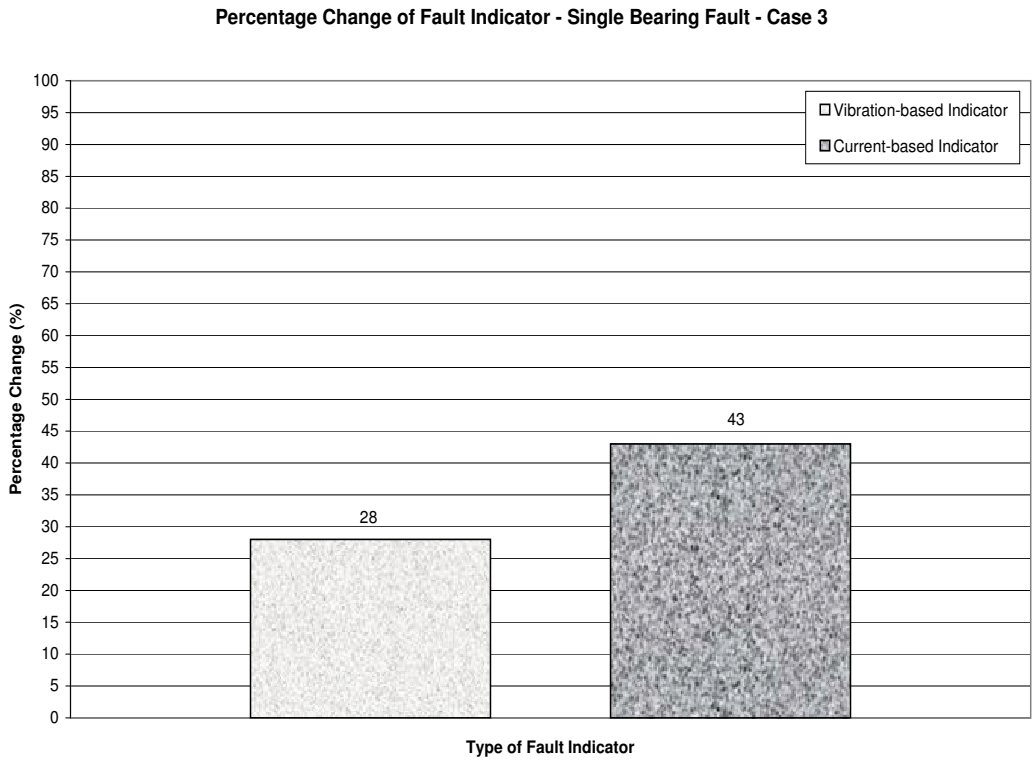

Fig. 23. Comparison of Current-based and Vibration-based Mechanical Fault Indicators - Single Bearing Fault - Case 3

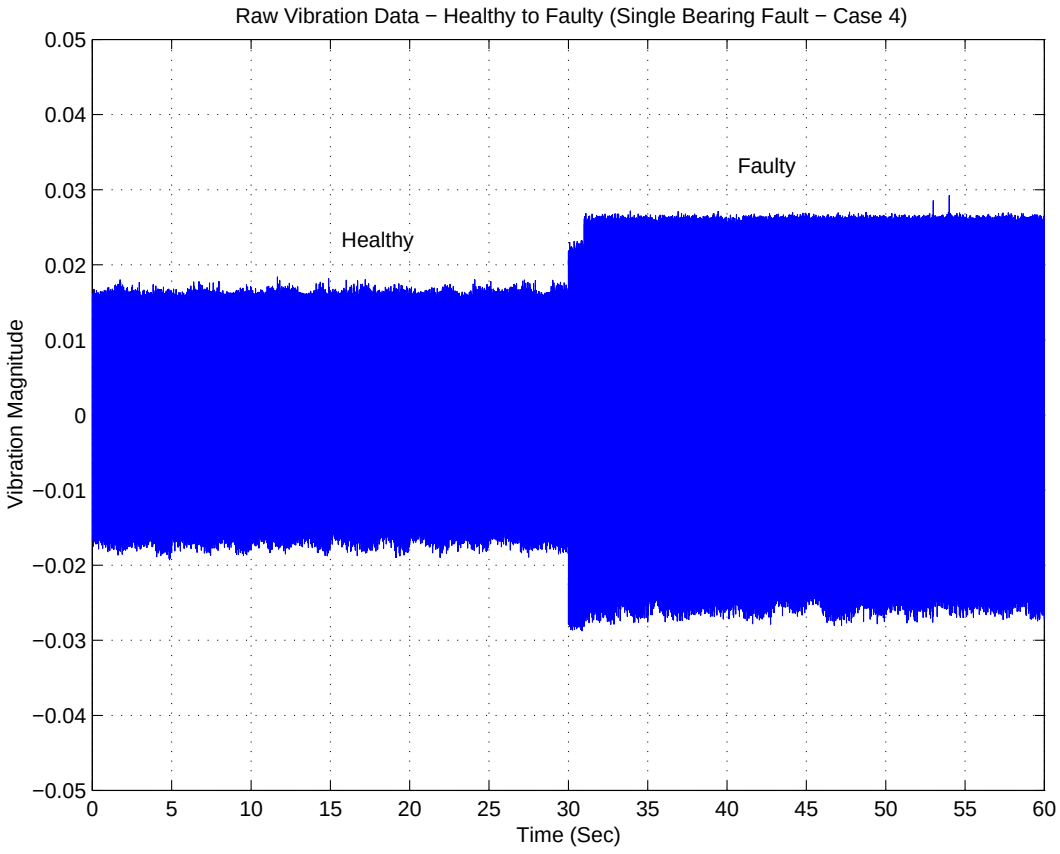

Fig. 24. Raw Vibration Signal - Single Bearing Fault - Case 4

For Case 4, Figures [24]-[28] show the raw vibration signal, vibration-based indicator, raw current signal, current-based indicator and the comparison chart between the two indicators, respectively. We can see a pattern similar to the other cases. The mean percentage increase of the current-based indicator is about 50% in comparison to the mean percentage increase of the vibration-based indicator, which is about 14%.

2. Double Deteriorating Bearing

While the raw vibration signals are being indicative of the mechanical fault, it is difficult to draw any conclusions by merely looking at the raw current signals. The

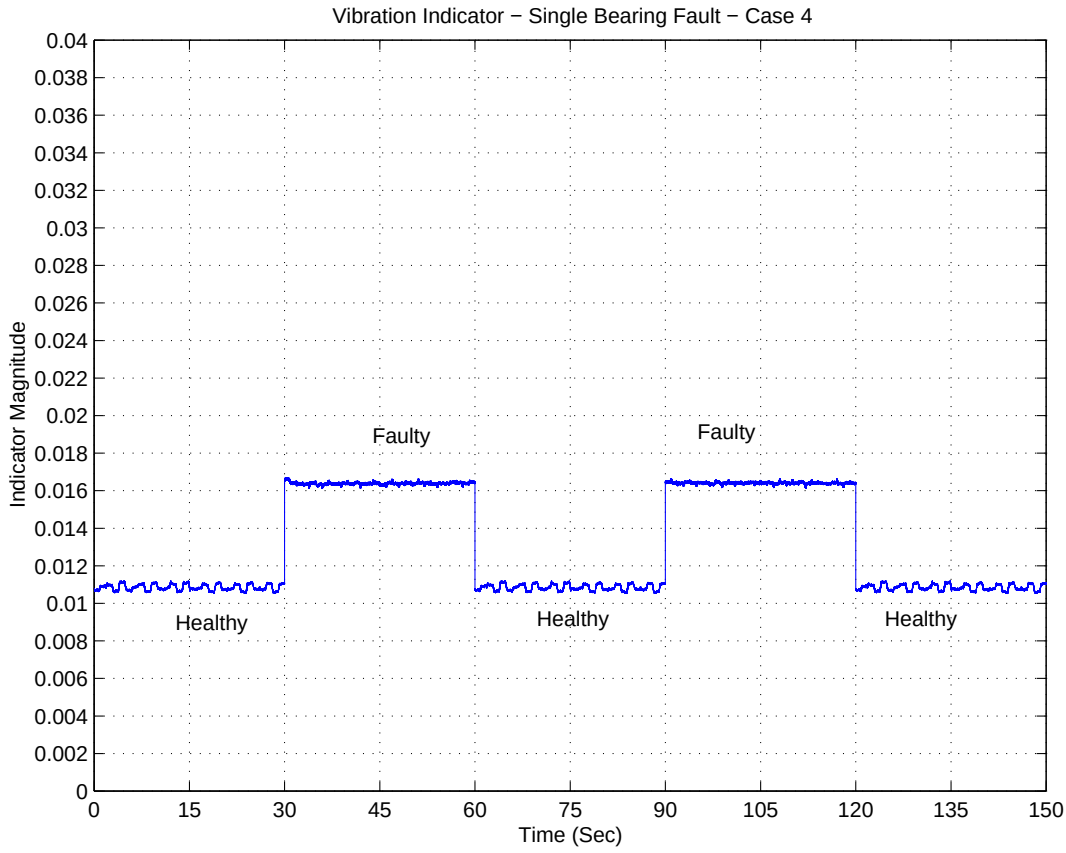

Fig. 25. Vibration-based Mechanical Indicator - Single Bearing Fault - Case 4

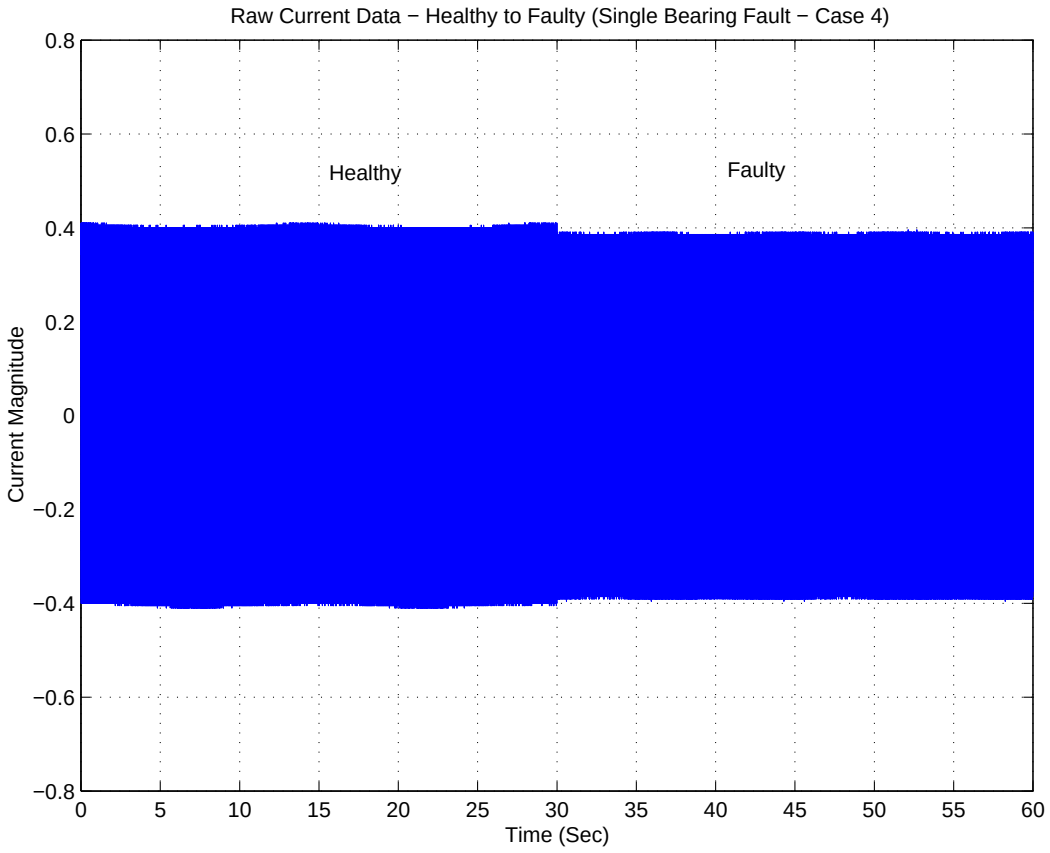

Fig. 26. Raw Current Signal - Single Bearing Fault - Case 4

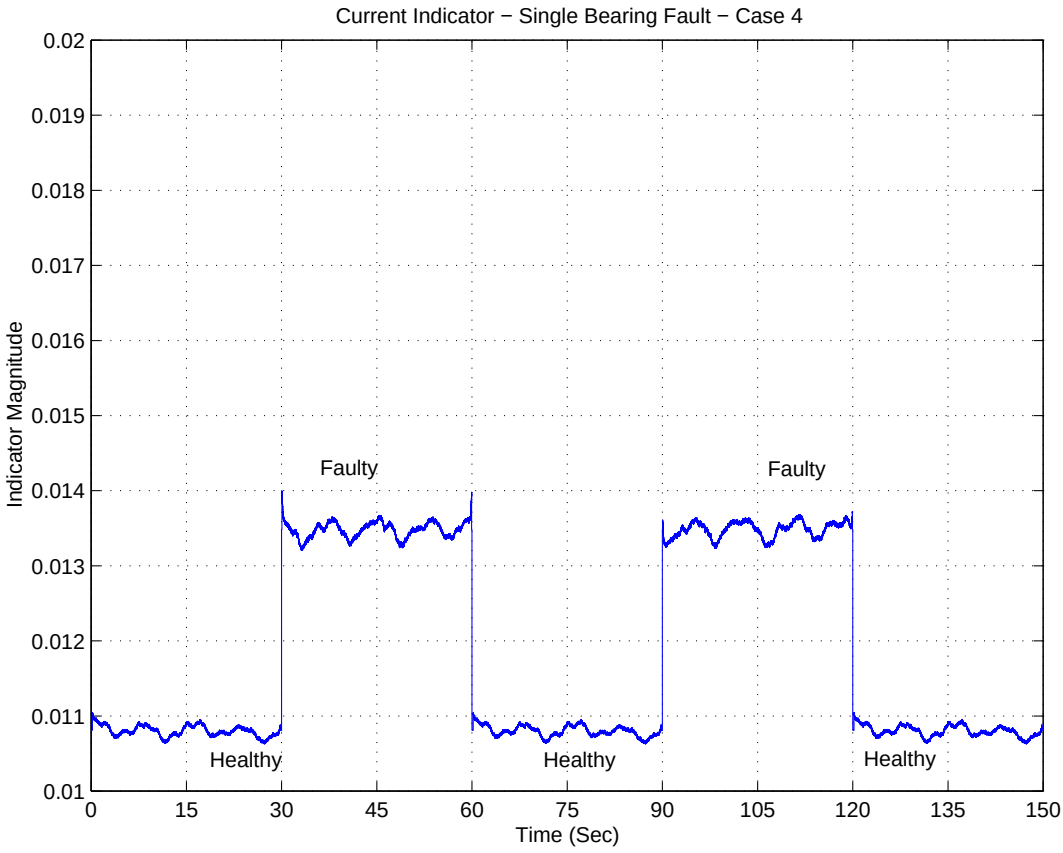

Fig. 27. Current-based Mechanical Indicator - Single Bearing Fault - Case 4

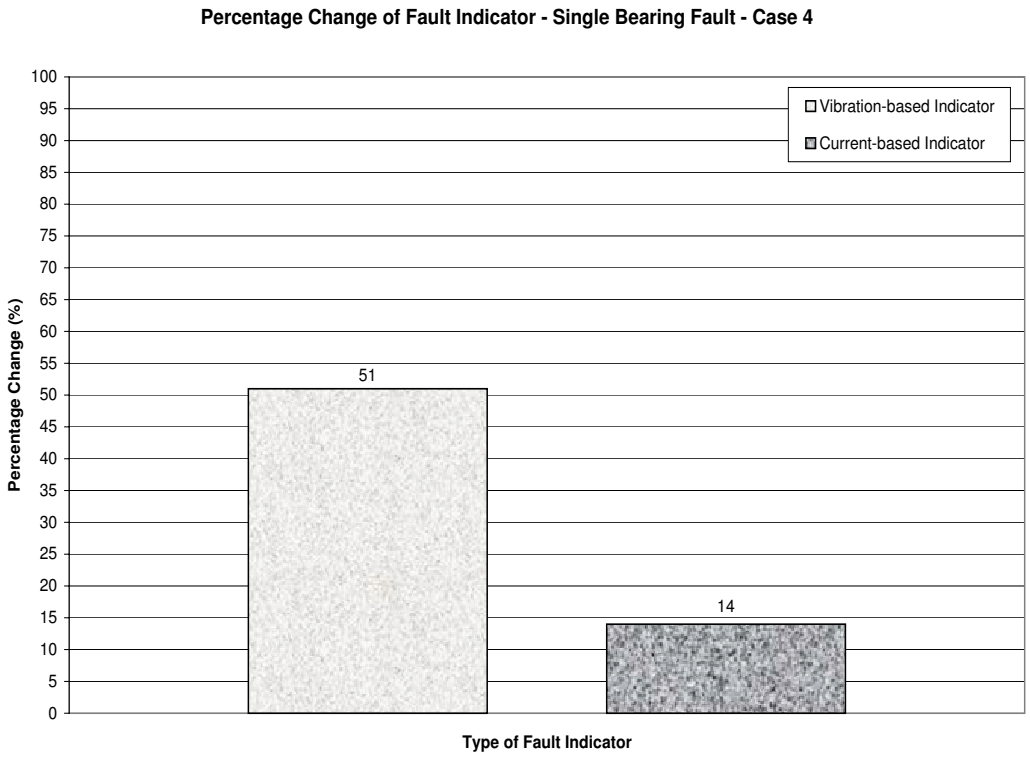

Fig. 28. Comparison of Current-based and Vibration-based Mechanical Fault Indicators - Single Bearing Fault - Case 4

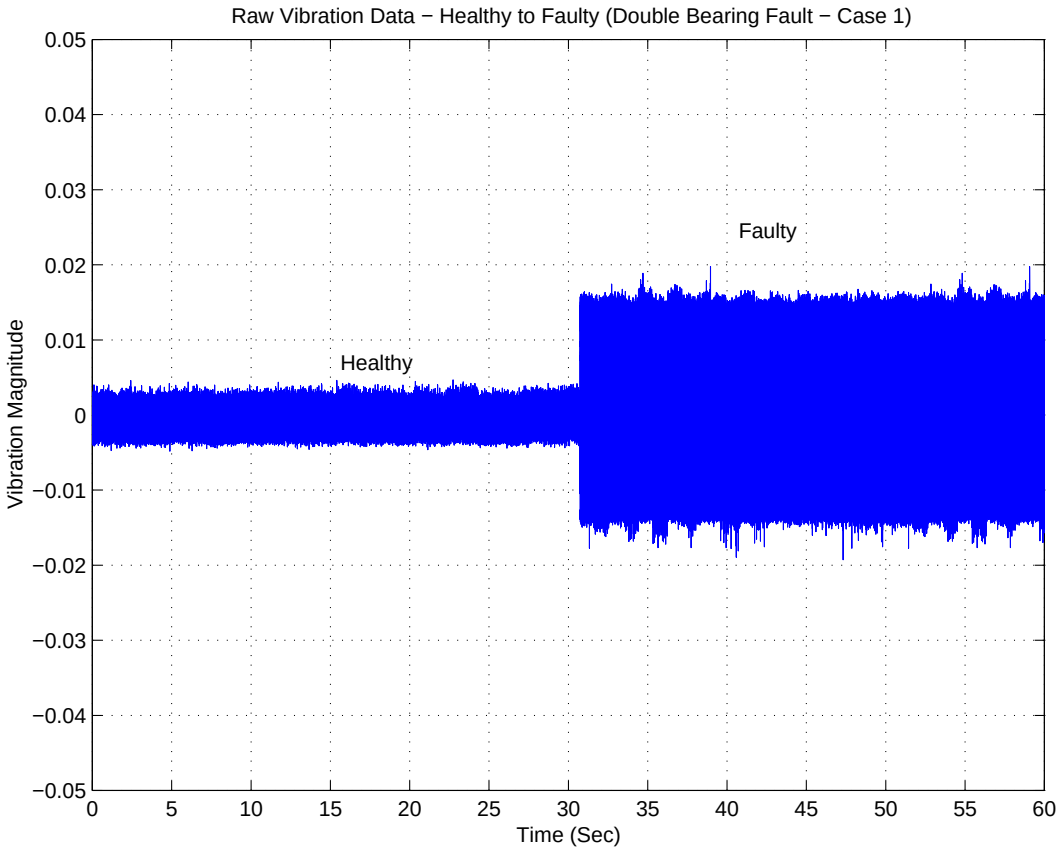

Fig. 29. Raw Vibration Signal - Double Bearing Fault - Case 1

vibration-based fault indicator shows a significant increase from the healthy conditions. We can also note that this increase is a lot more than that observed in the single bearing fault cases. A similar pattern can be seen with the current-based indicators as well, although the magnitudes of the mean percentage increase is a lot lesser in comparison to the vibration-based indicator. This is observed to be consistent for the various double bearing fault cases.

For Double Bearing Fault Case 1, Figures [29]-[33] show the raw vibration signal, vibration-based indicator, raw current signal, current-based indicator and the comparison chart between the two indicators, respectively. The mean increase of the

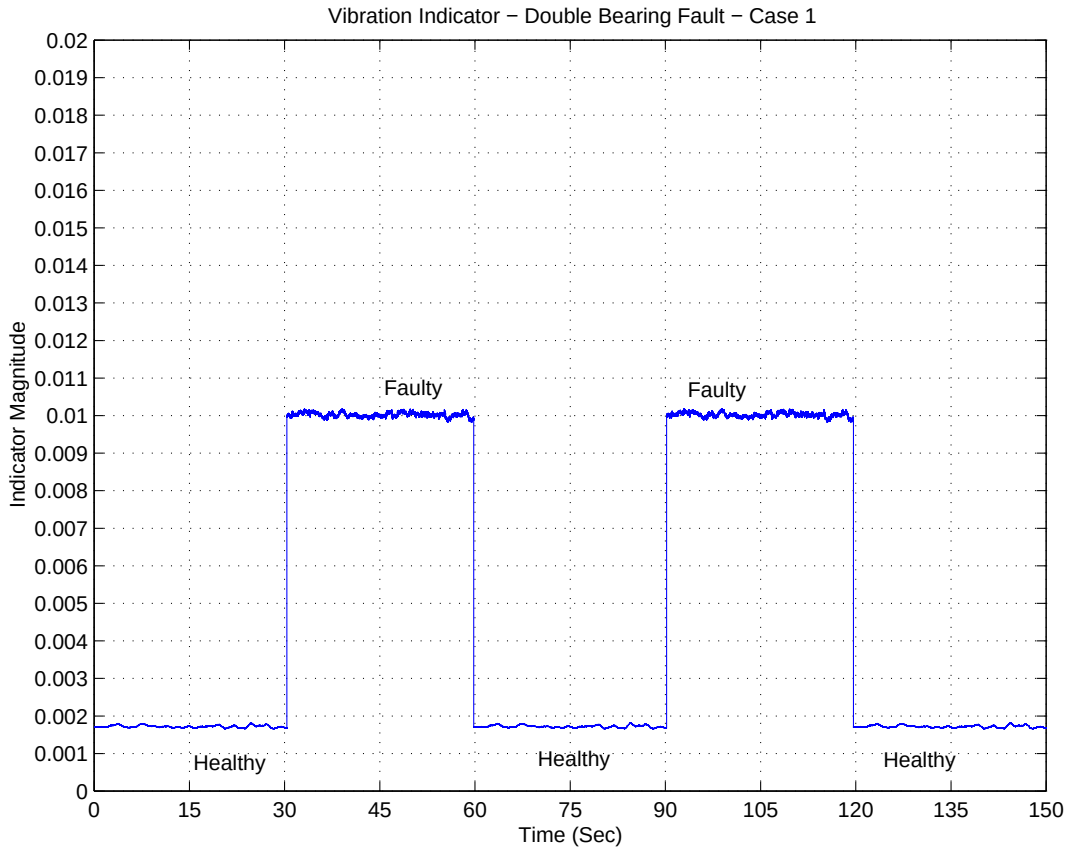

Fig. 30. Vibration-based Mechanical Indicator - Double Bearing Fault - Case 1

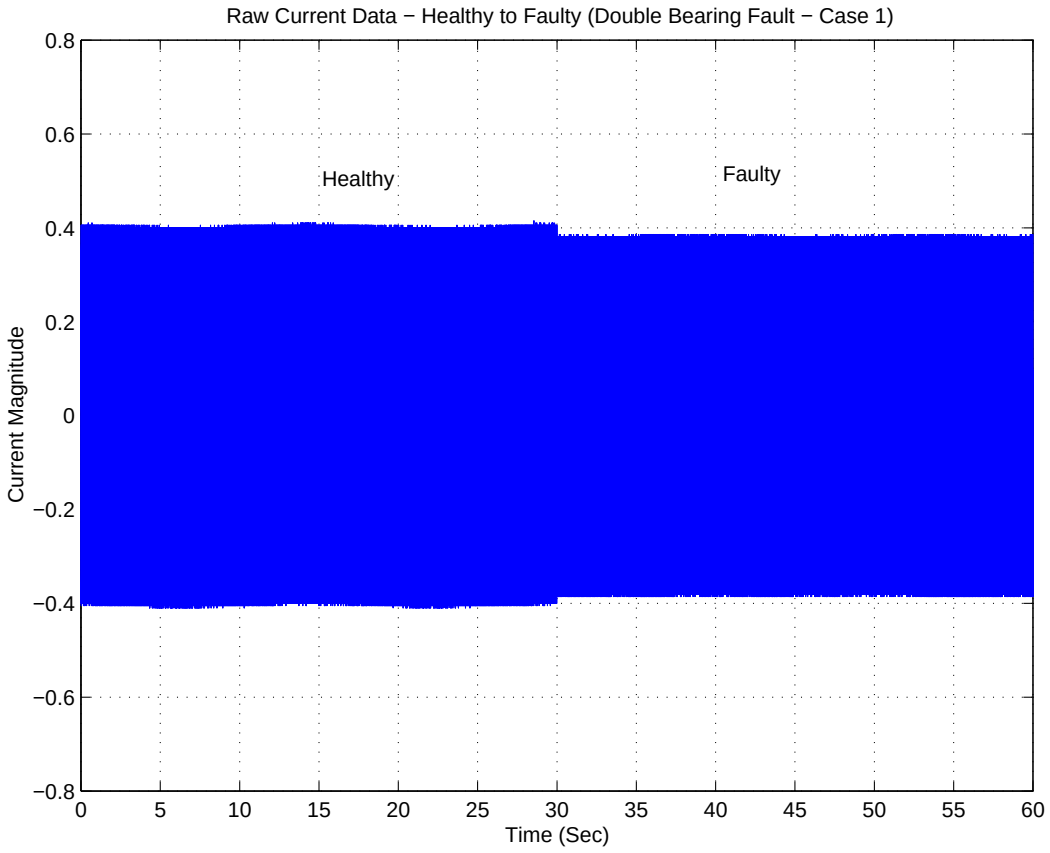

Fig. 31. Raw Current Signal - Double Bearing Fault - Case 1

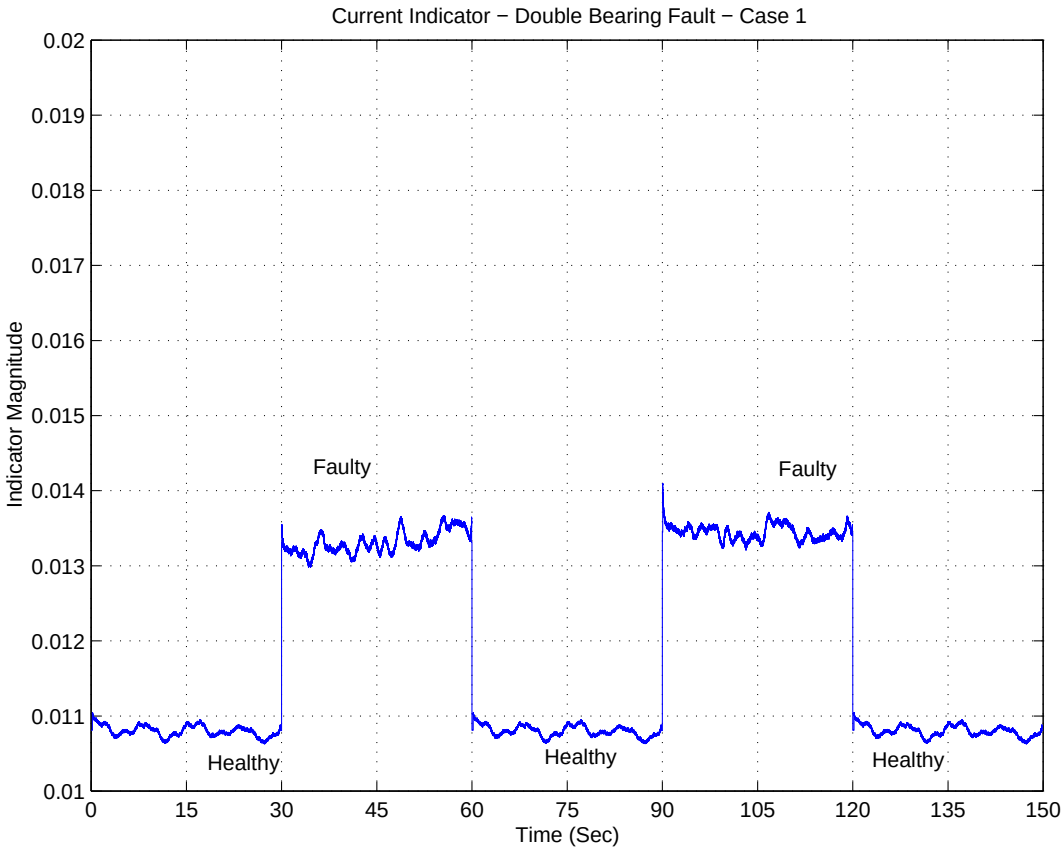

Fig. 32. Current-based Mechanical Indicator - Double Bearing Fault - Case 1

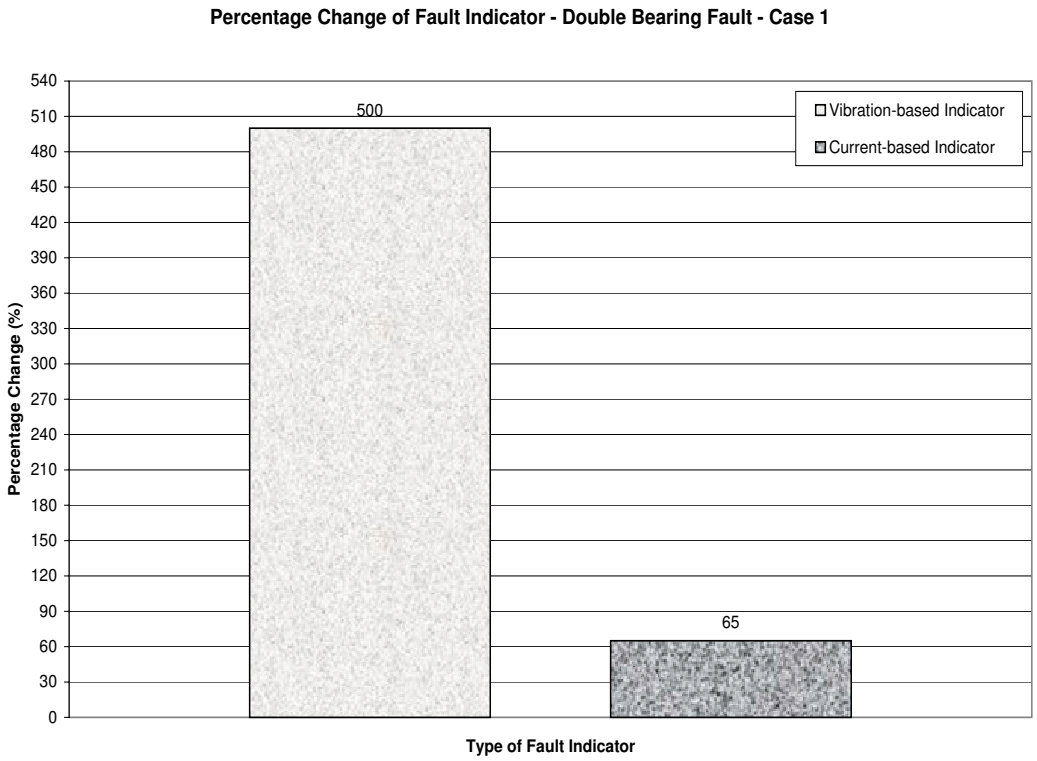

Fig. 33. Comparison of Current-based and Vibration-based Mechanical Fault Indicators - Double Bearing Fault - Case 1

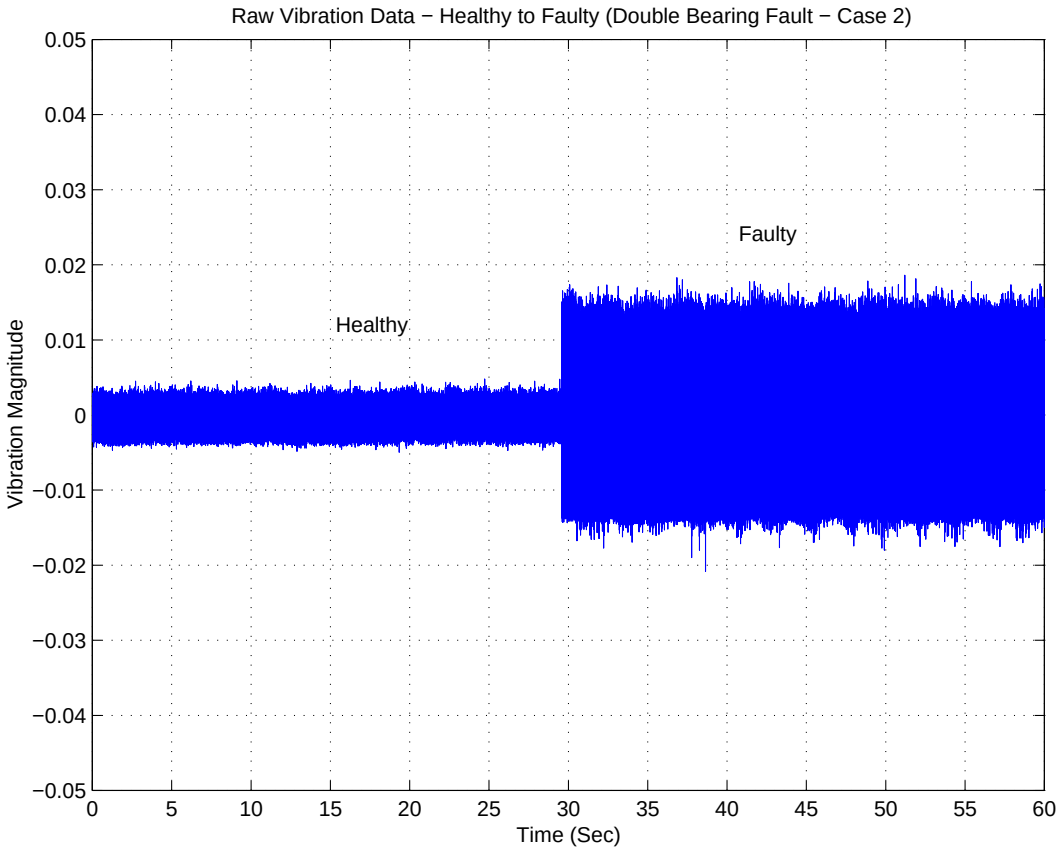

Fig. 34. Raw Vibration Signal - Double Bearing Fault - Case 2

vibration-based fault indicator is almost five times that of the healthy indicator. We can also see a significantly big increase in the current-based indicators compared to the single bearing faulty cases. The mean increase in the current-based indicator is about 65% as compared to the mean increase of the vibration-based indicator, which is about 500%.

For Double Bearing Fault Case 2, Figures [34]-[38] show the raw vibration signal, vibration-based indicator, raw current signal, current-based indicator and the comparison chart between the two indicators, respectively. We can see a pattern similar to Case 1. However, the increase in the current-based indicator is higher (91.7%).

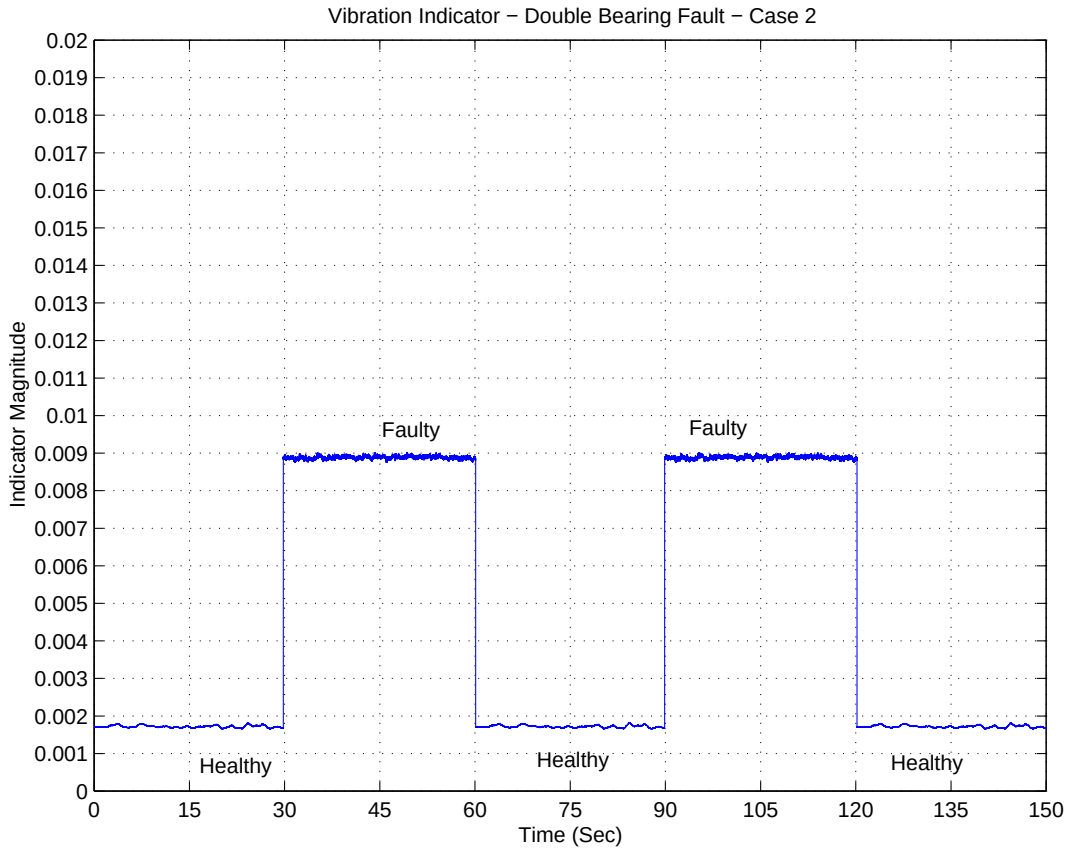

Fig. 35. Vibration-based Mechanical Indicator - Double Bearing Fault - Case 2

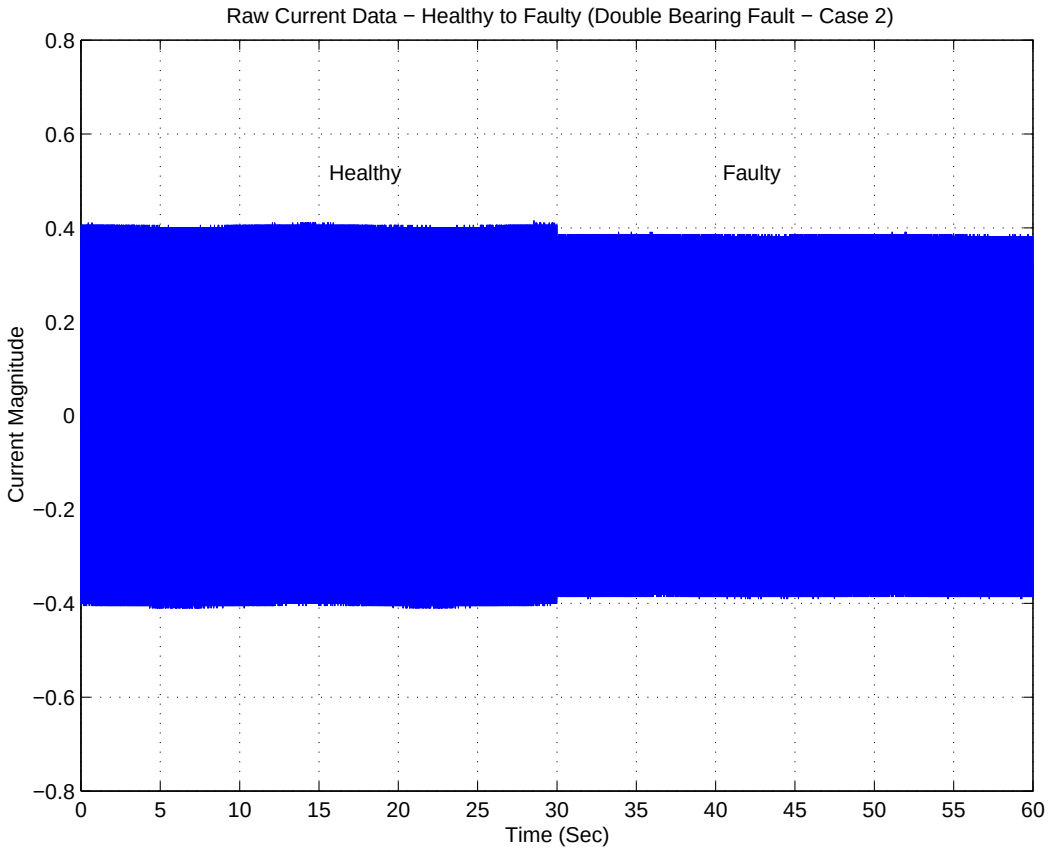

Fig. 36. Raw Current Signal - Double Bearing Fault - Case 2

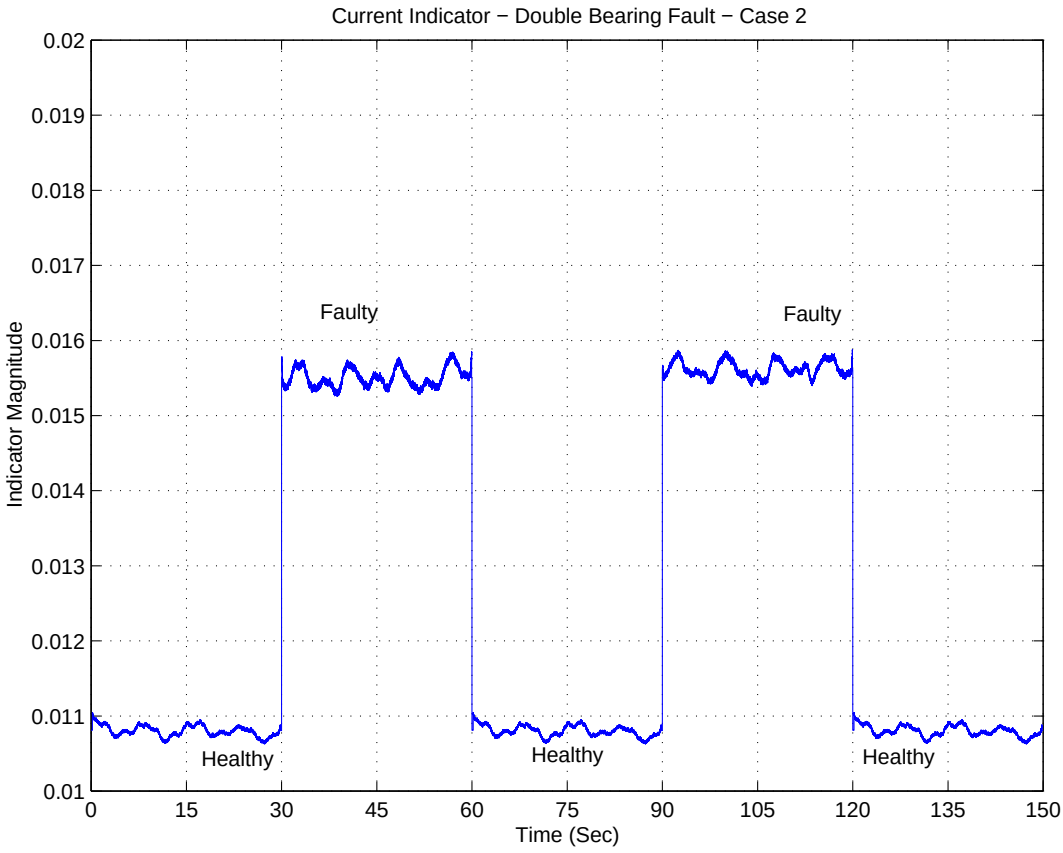

Fig. 37. Current-based Mechanical Indicator - Double Bearing Fault - Case 2

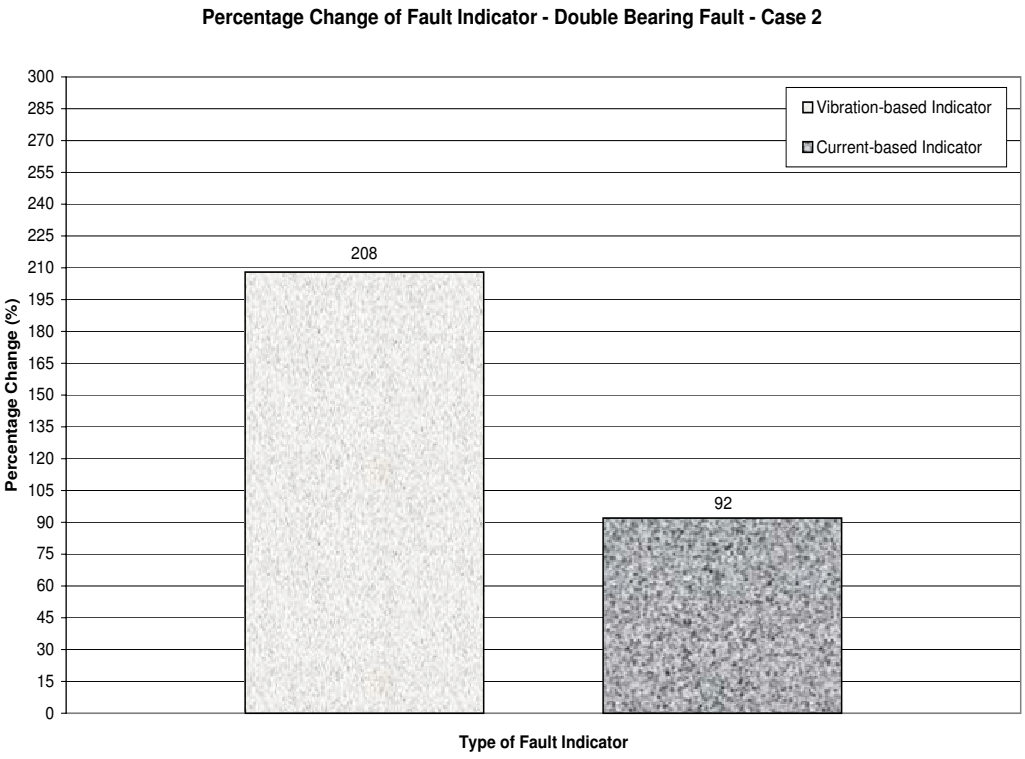

Fig. 38. Comparison of Current-based and Vibration-based Mechanical Fault Indicators - Double Bearing Fault - Case 2

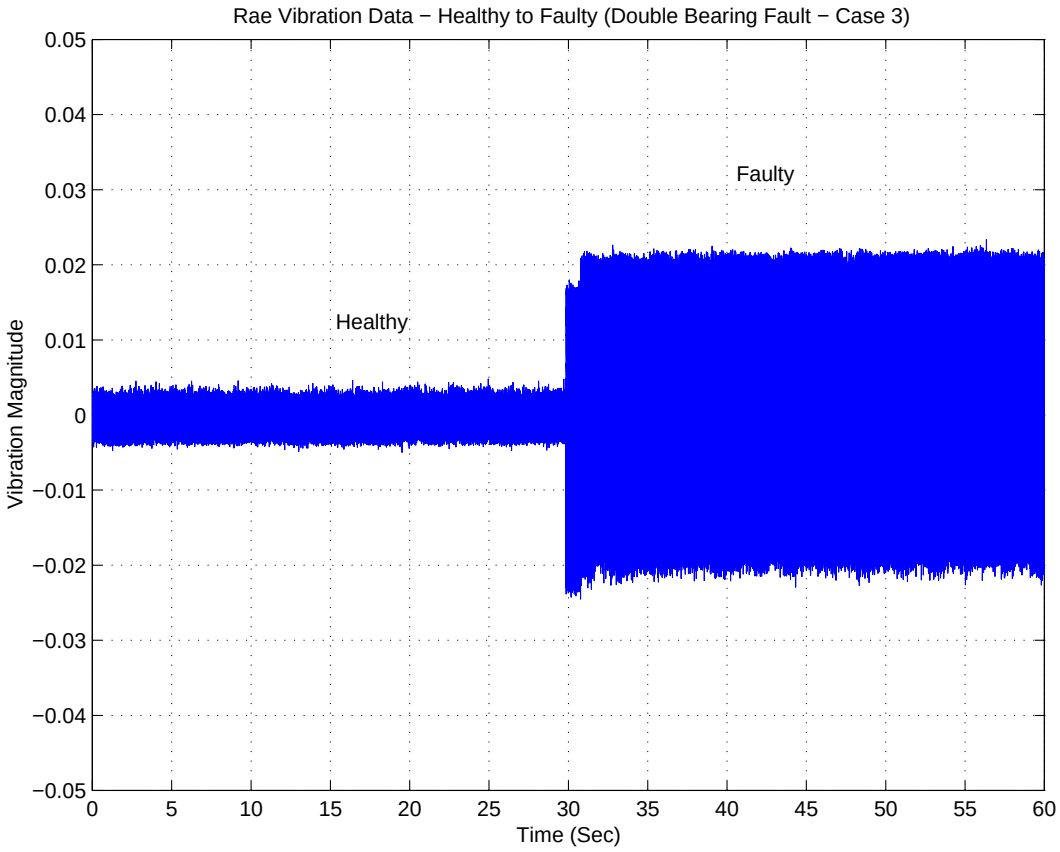

Fig. 39. Raw Vibration Signal - Double Bearing Fault - Case 3

For Double Bearing Fault Case 3, Figures [39]-[43] show the raw vibration signal, vibration-based indicator, raw current signal, current-based indicator and the comparison chart between the two indicators, respectively. The increase in the current-based indicator is about 83.7% as compared to that of the increase in the vibration-based indicator, which is about 315.2%.

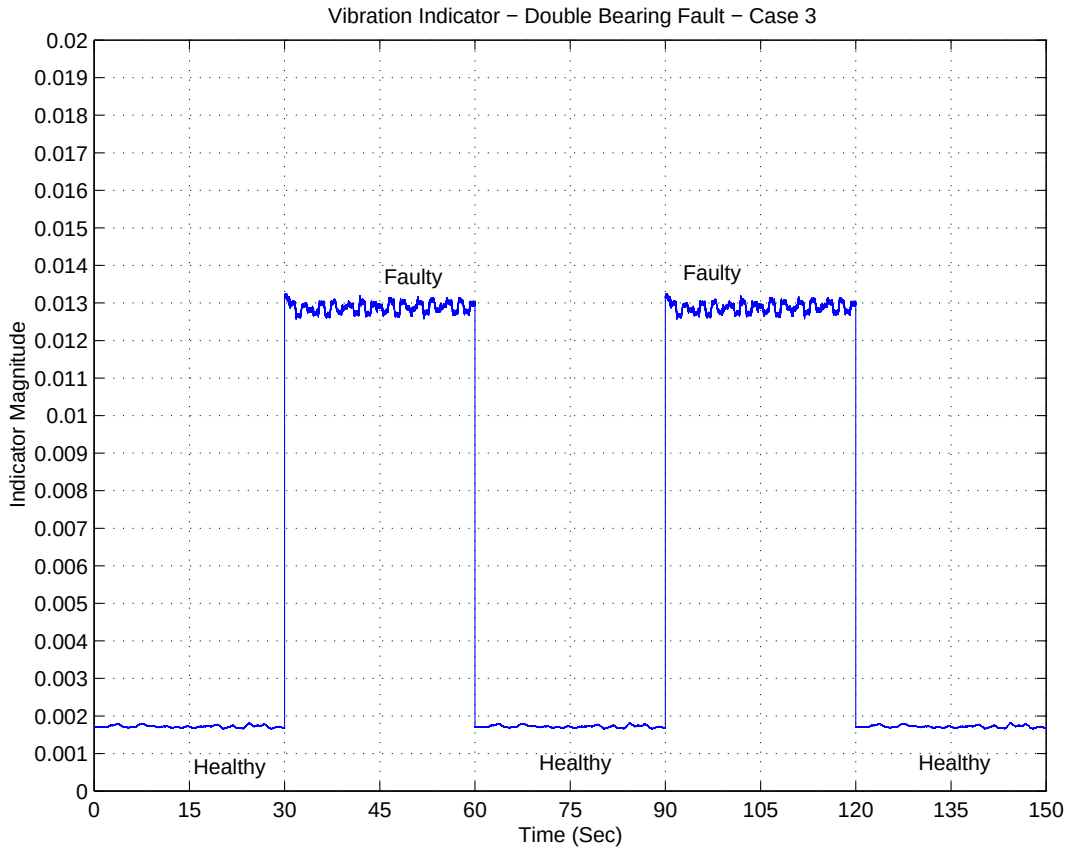

Fig. 40. Vibration-based Mechanical Indicator - Double Bearing Fault - Case 3

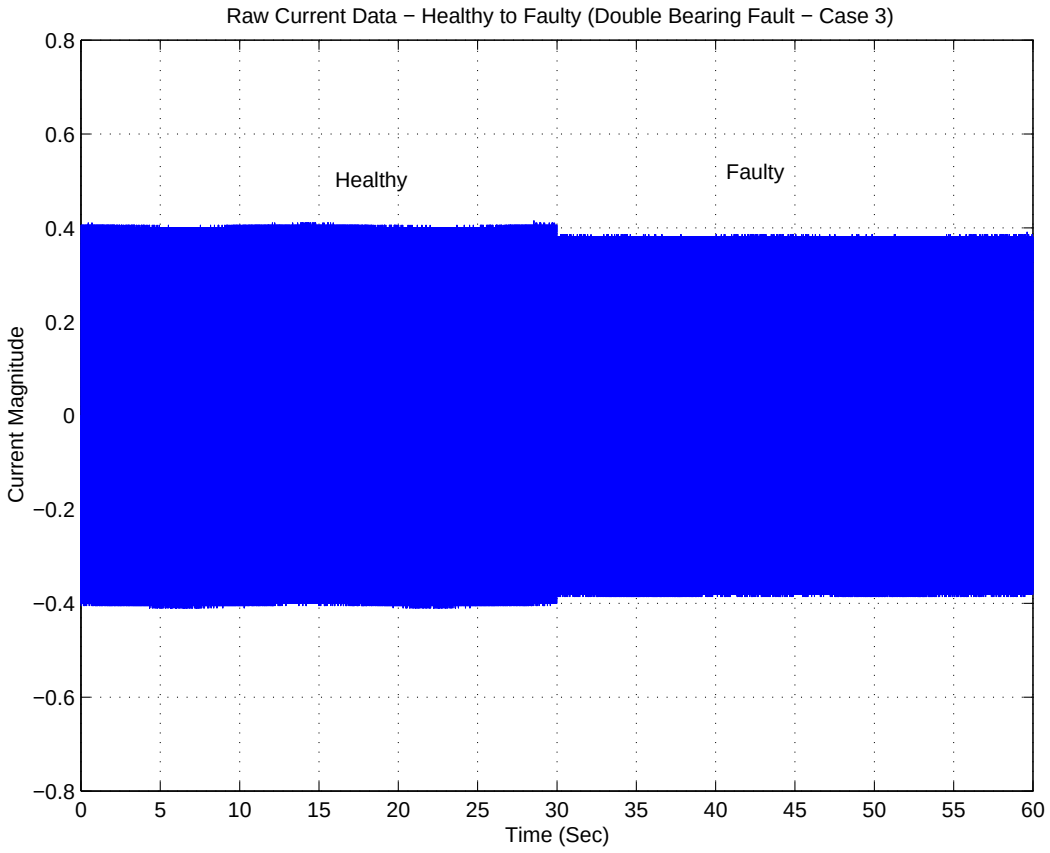

Fig. 41. Raw Current Signal - Double Bearing Fault - Case 3

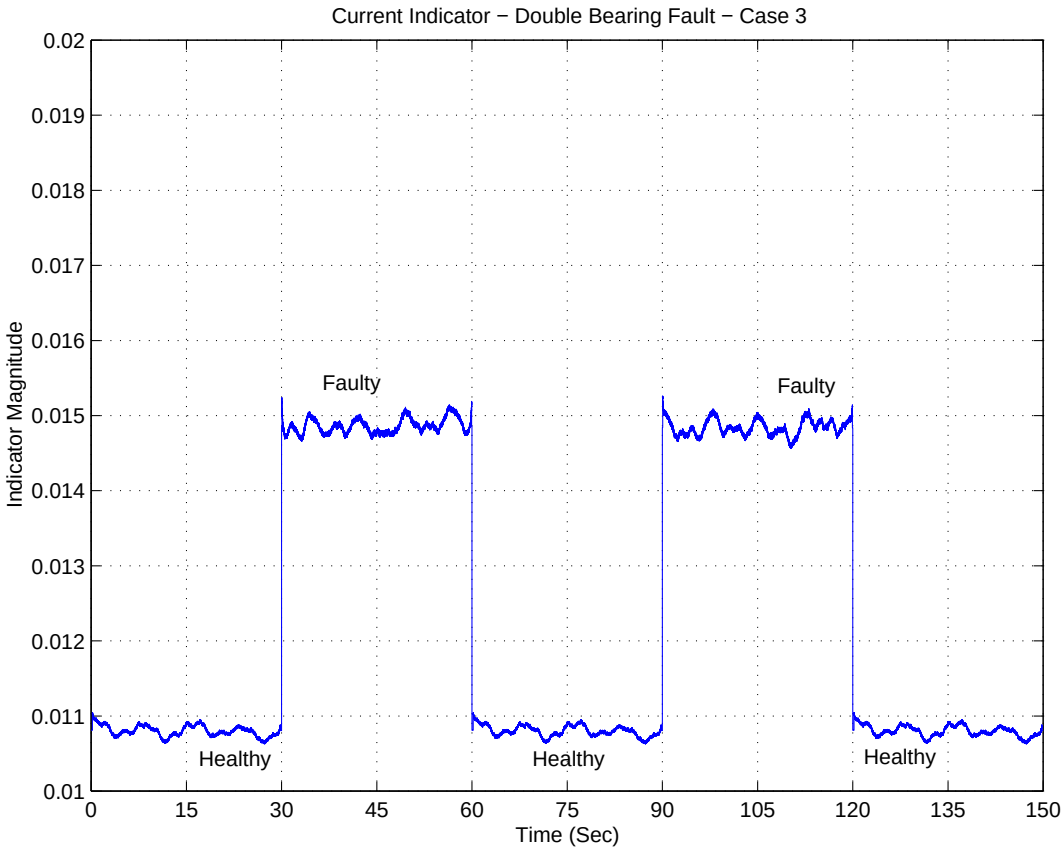

Fig. 42. Current-based Mechanical Indicator - Double Bearing Fault - Case 3

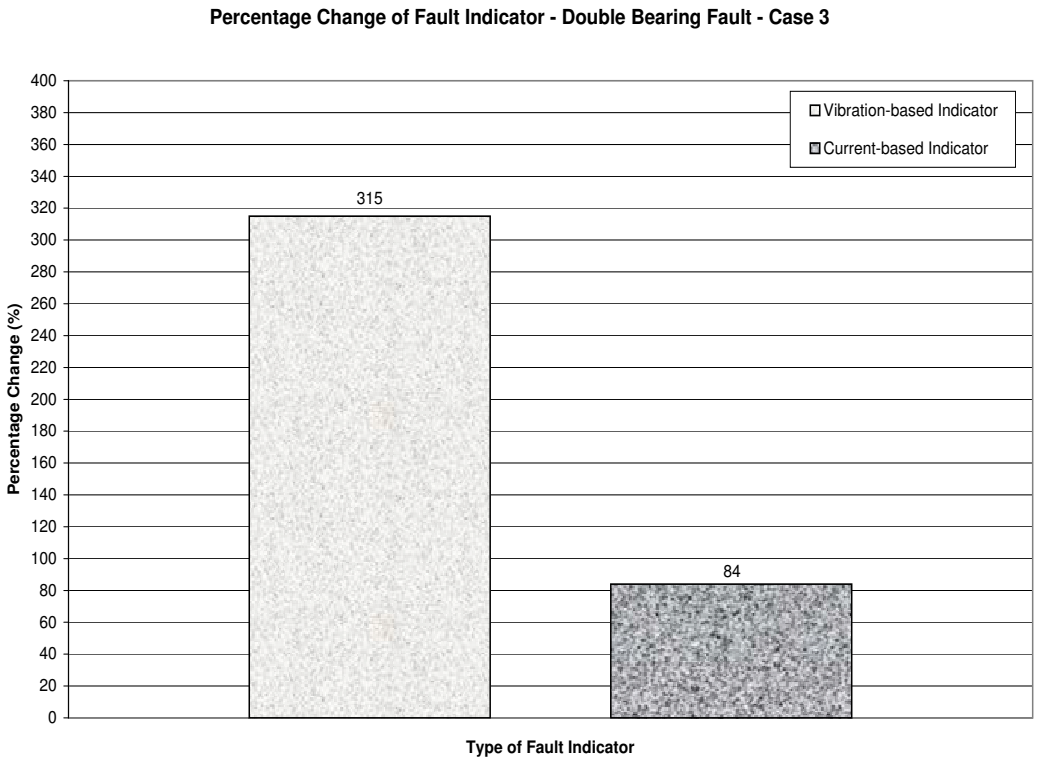

Fig. 43. Comparison of Current-based and Vibration-based Mechanical Fault Indicators - Double Bearing Fault - Case 3

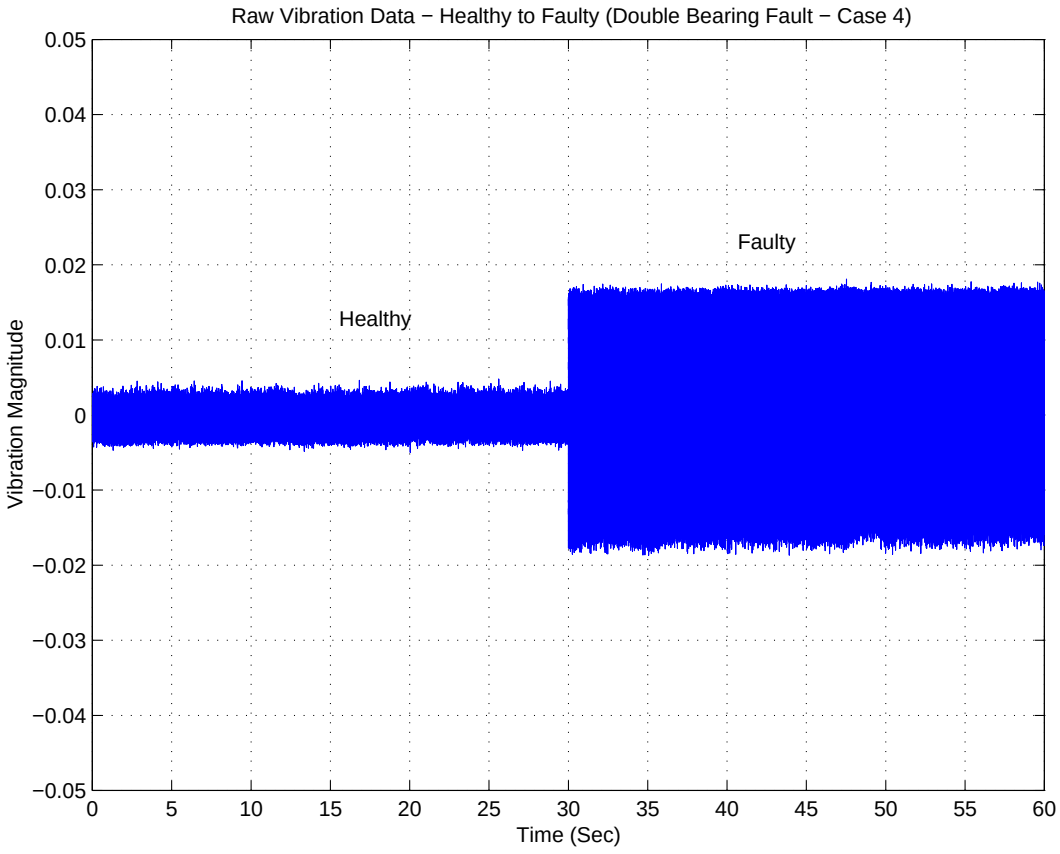

Fig. 44. Raw Vibration Signal - Double Bearing Fault - Case 4

For the Double Bearing Fault Case 4, Figures [44]-[48] show the raw vibration signal, vibration-based indicator, raw current signal, current-based indicator and the comparison chart between the two indicators, respectively. The current-based indicator increases 33% as much as the vibration-based indicator. This is similar to the values obtained for the other cases of double bearing faults.

In the Double Bearing Fault Case 5, Figures [49]-[53] show the raw vibration signal, vibration-based indicator, raw current signal, current-based indicator and the comparison chart between the two indicators, respectively. The motor was loaded to 25% of its rated capacity. This was done by coupling the motor to a set of friction

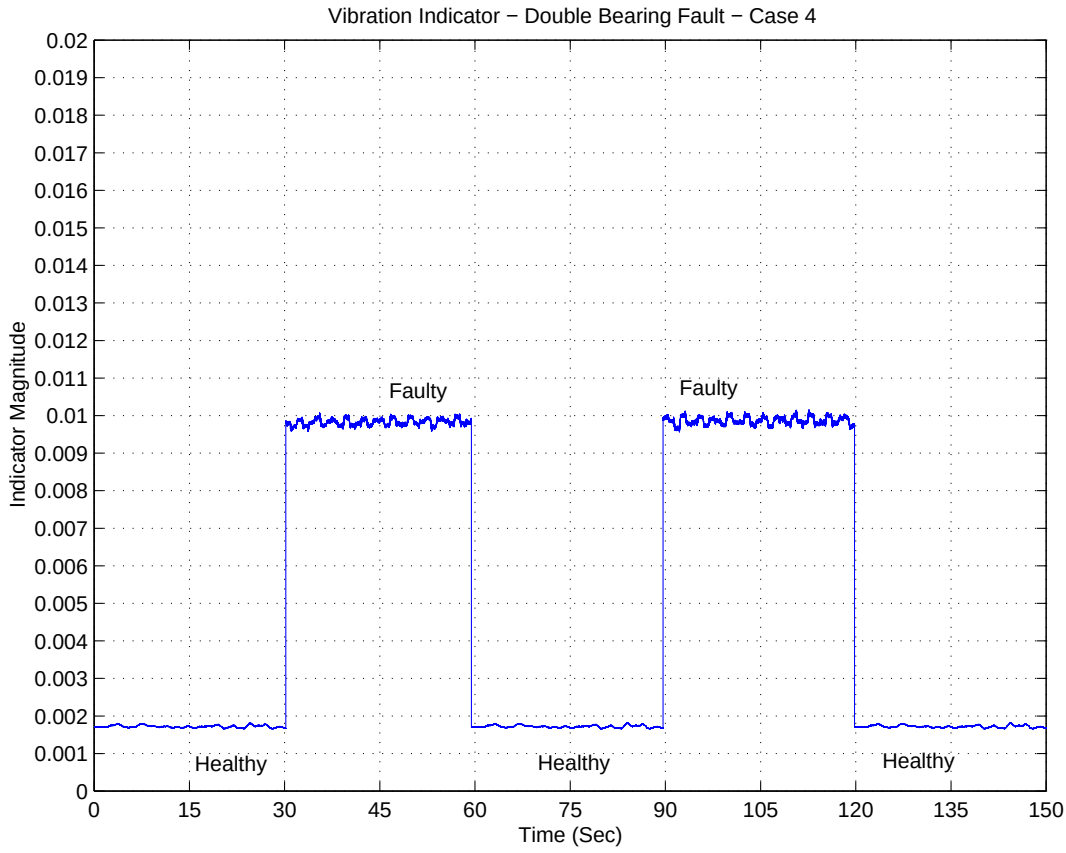

Fig. 45. Vibration-based Mechanical Indicator - Double Bearing Fault - Case 4

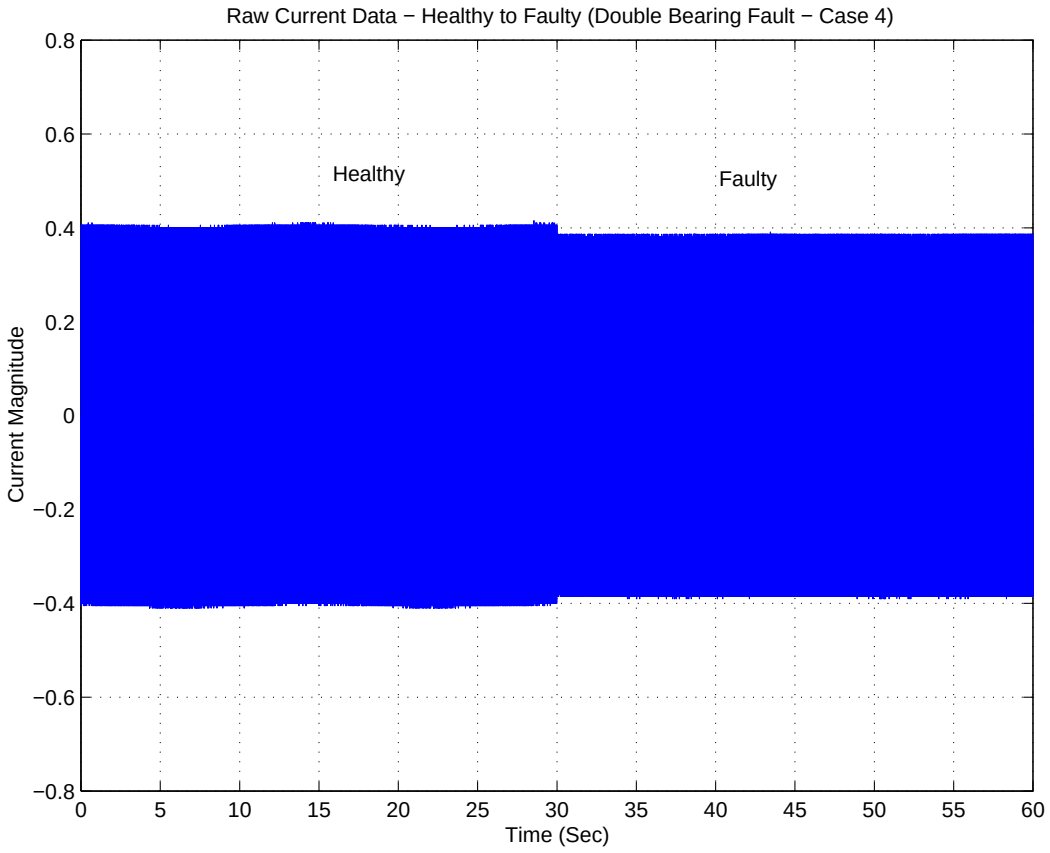

Fig. 46. Raw Current Signal - Double Bearing Fault - Case 4

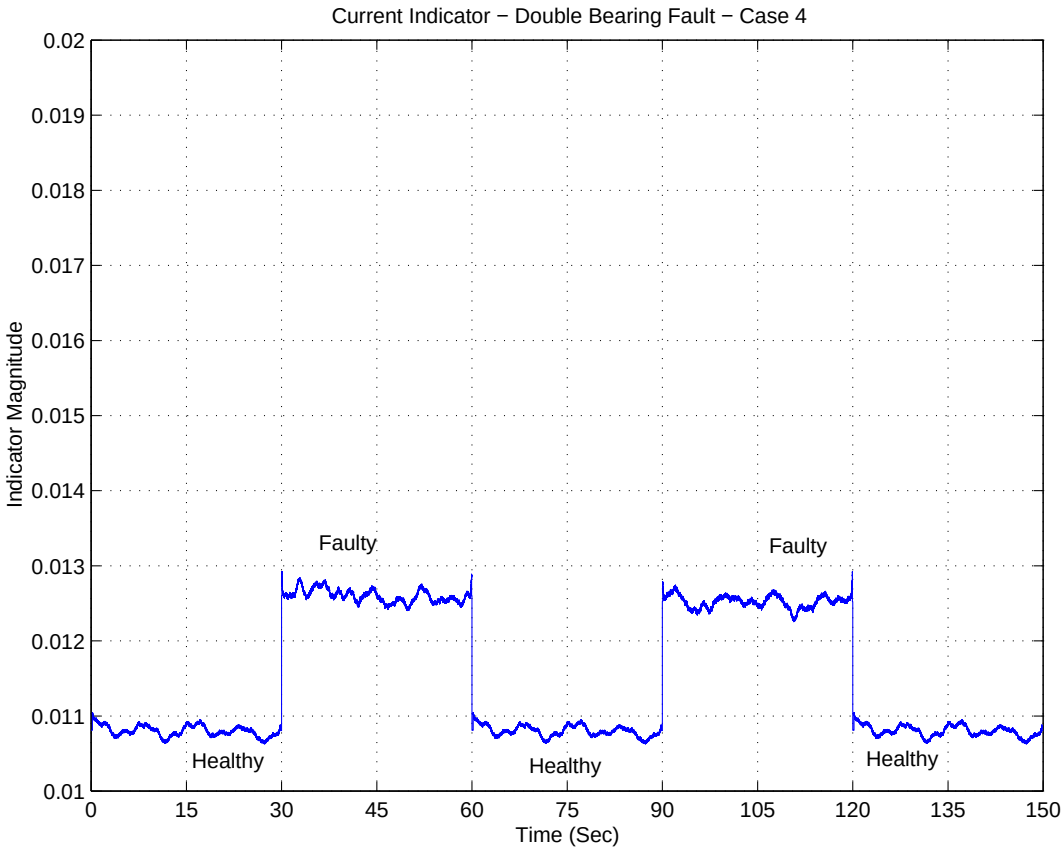

Fig. 47. Current-based Mechanical Indicator - Double Bearing Fault - Case 4

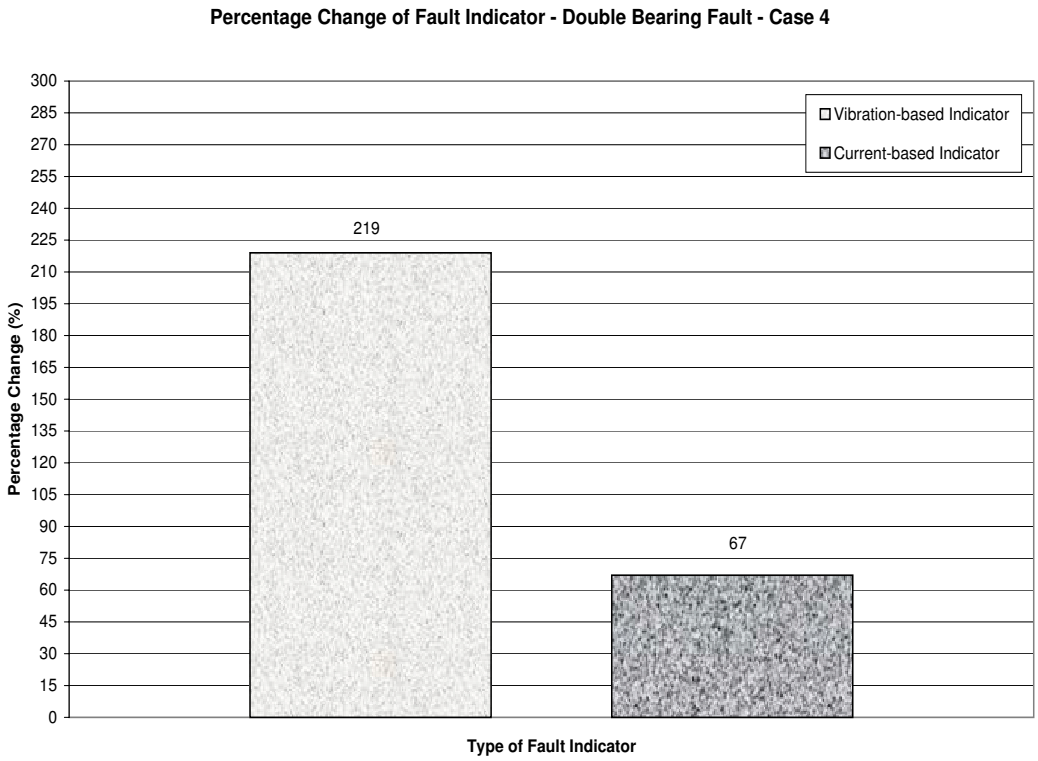

Fig. 48. Comparison of Current-based and Vibration-based Mechanical Fault Indicators - Double Bearing Fault - Case 4

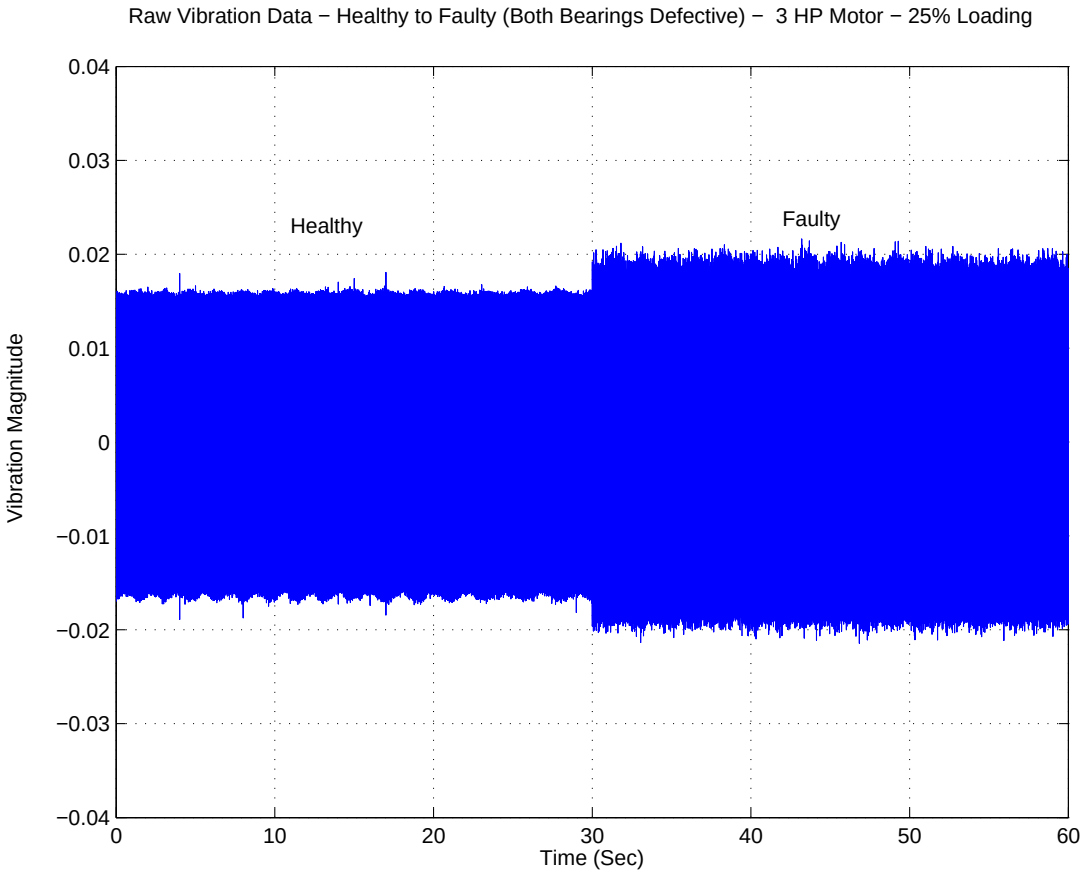

Fig. 49. Raw Vibration Signal - Double Bearing Fault - Case 5

loads (circular discs attached to the shaft) and a gearbox. We can observe that for this case, the current-based indicator increases almost as much as the vibration-based indicator. The reduction in the vibration-based fault indicator magnitude itself may be attributed to the increase in the baseline vibration due to the gearbox setup.

To summarize the bearing faults, we can say that there is a consistency in the way the current-based indicators compare to the vibration-based indicators and it also relates to the severity of the fault.

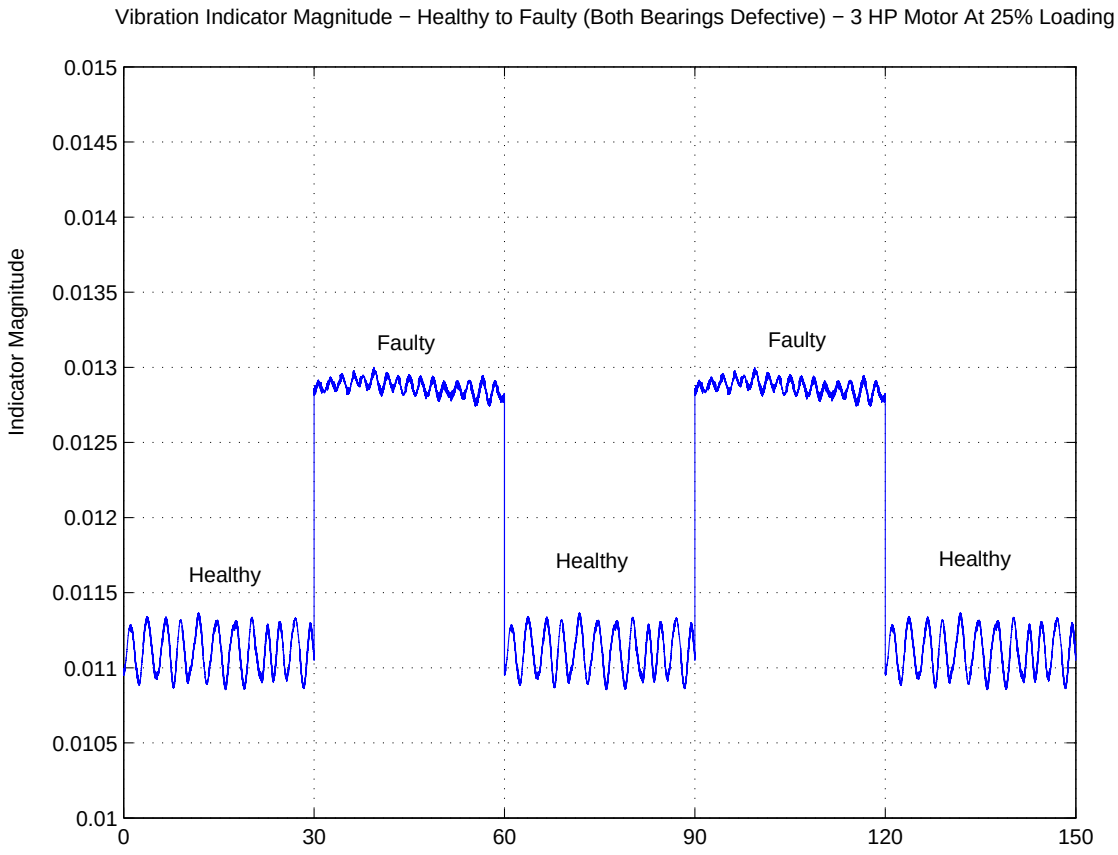

Fig. 50. Vibration-based Mechanical Indicator - Double Bearing Fault - Case 5

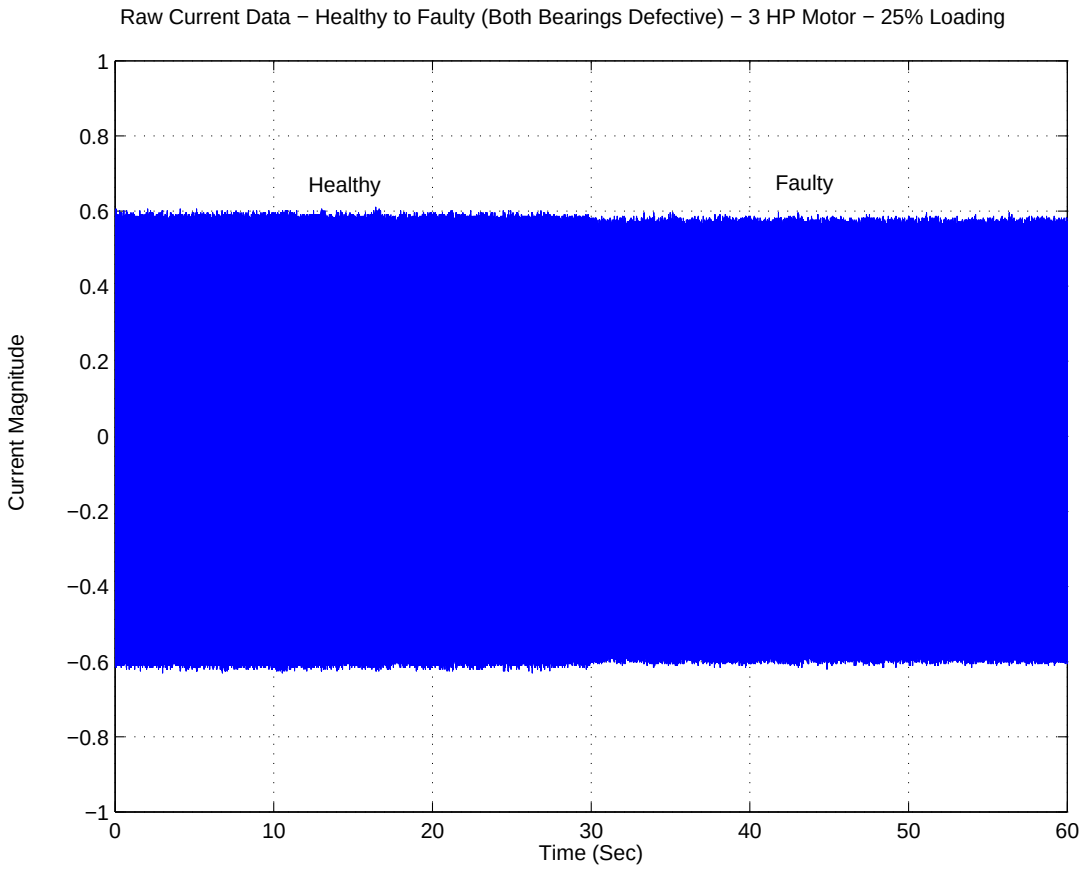

Fig. 51. Raw Current Signal - Double Bearing Fault - Case 5

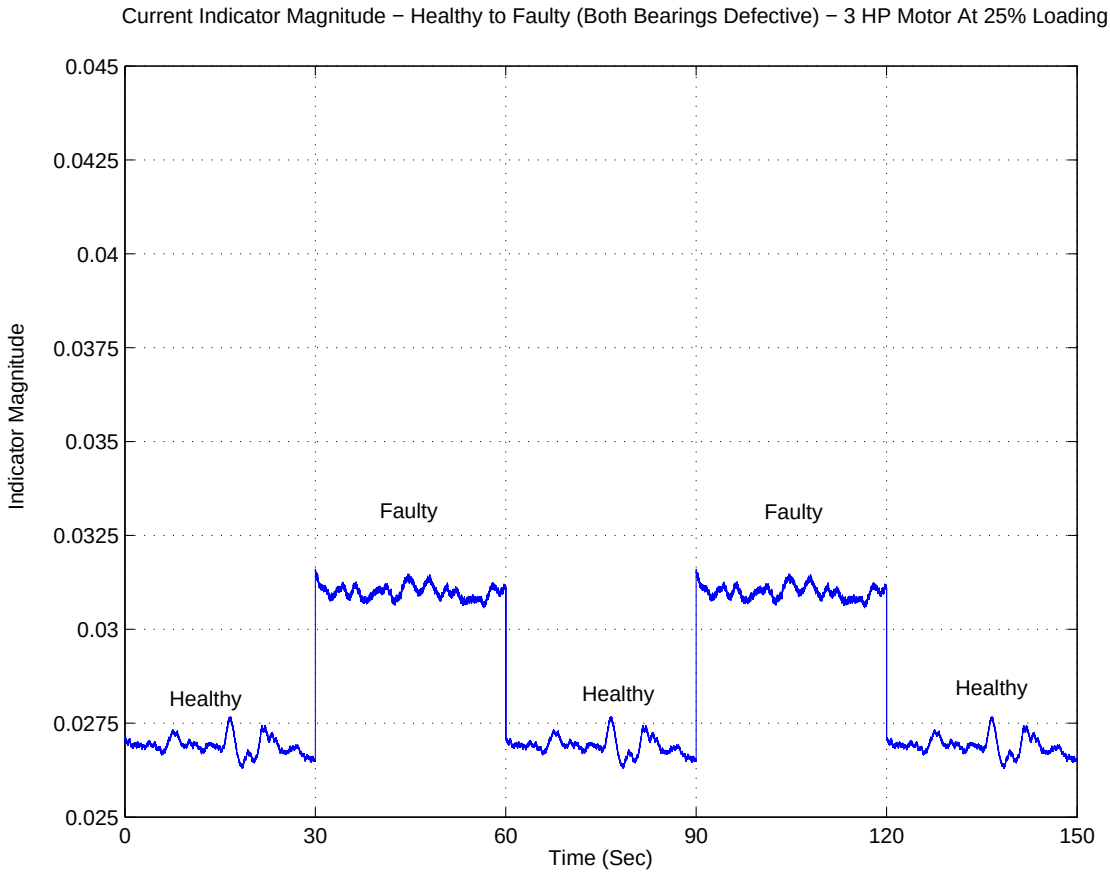

Fig. 52. Current-based Mechanical Indicator - Double Bearing Fault - Case 5

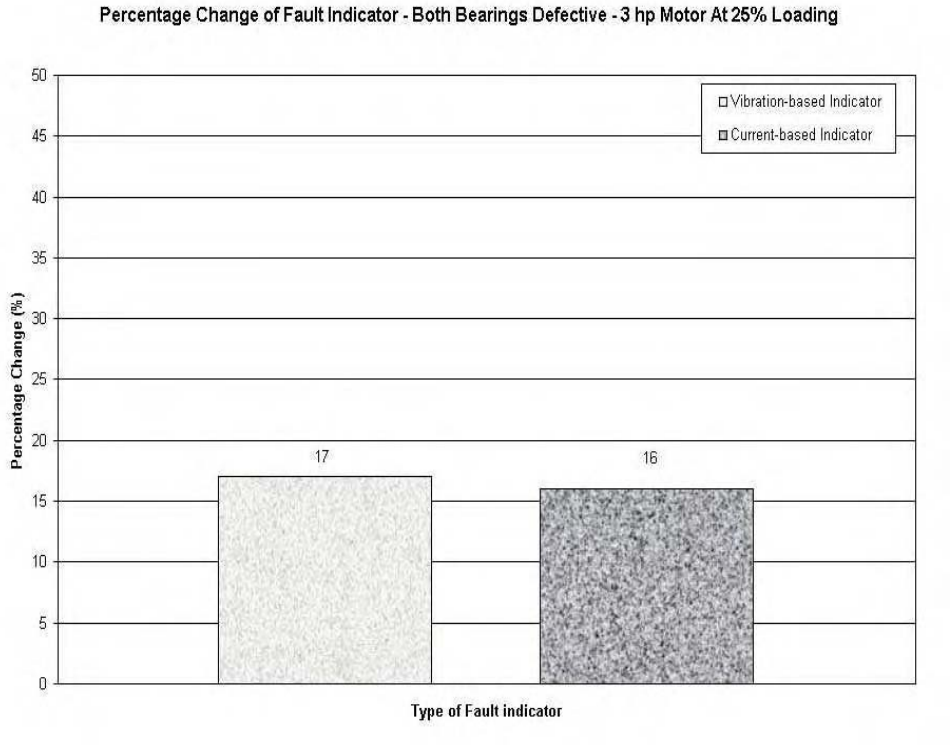

Fig. 53. Comparison of Current-based and Vibration-based Mechanical Fault Indicators - Double Bearing Fault - Case 5

B. Fault II: Broken Rotor Bars

Baseline data sets were obtained using a motor operating under healthy conditions. Keeping in mind the fact that the severity of the fault affects the magnitude of the fault indicators obtained, the experiments were conducted using an increasing number of broken rotor bars. Experiments were conducted with half broken rotor bar, one broken rotor bar, two broken rotor bars and four broken rotor bars. In each case, data was collected for different load levels. For the present research, only steady state data obtained at 50% loading and 100% loading levels were used. While the pattern obtained through the fault indicators allow for the detection of faults, the identification of the type of fault through the developed fault indicators is not considered for this research.

1. Half Broken Rotor Bar

At 100% loading for 1/2 Broken Bar, Figures [54]-[58] show the raw vibration signal, vibration-based indicator, raw current signal, current-based indicator and the comparison chart between the two indicators, respectively. The raw vibration signals do not clearly indicate a significant increase from healthy to faulty condition. However the mean increase of the computed vibration-based indicator is about 16.4%. The current-based indicator is only about 4.3%, and is hence little indicative of the fault condition.

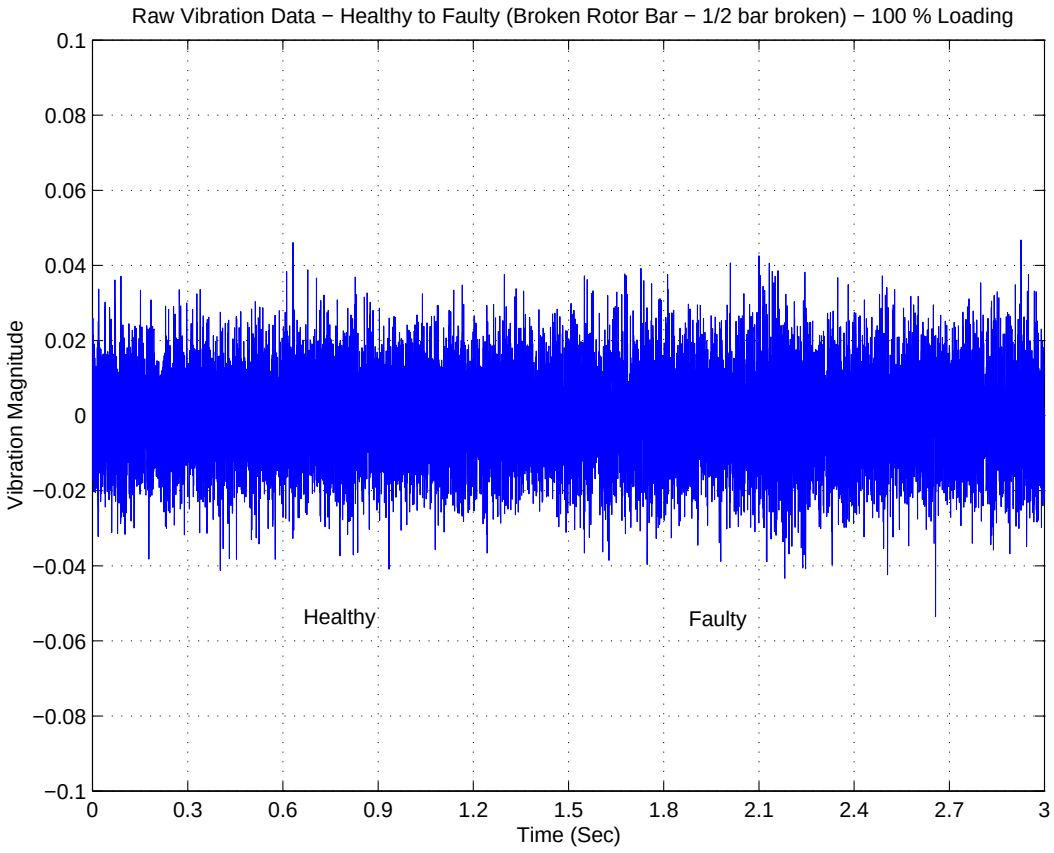

Fig. 54. Raw Vibration Signal - Half Broken Rotor Bar at 100% Loading

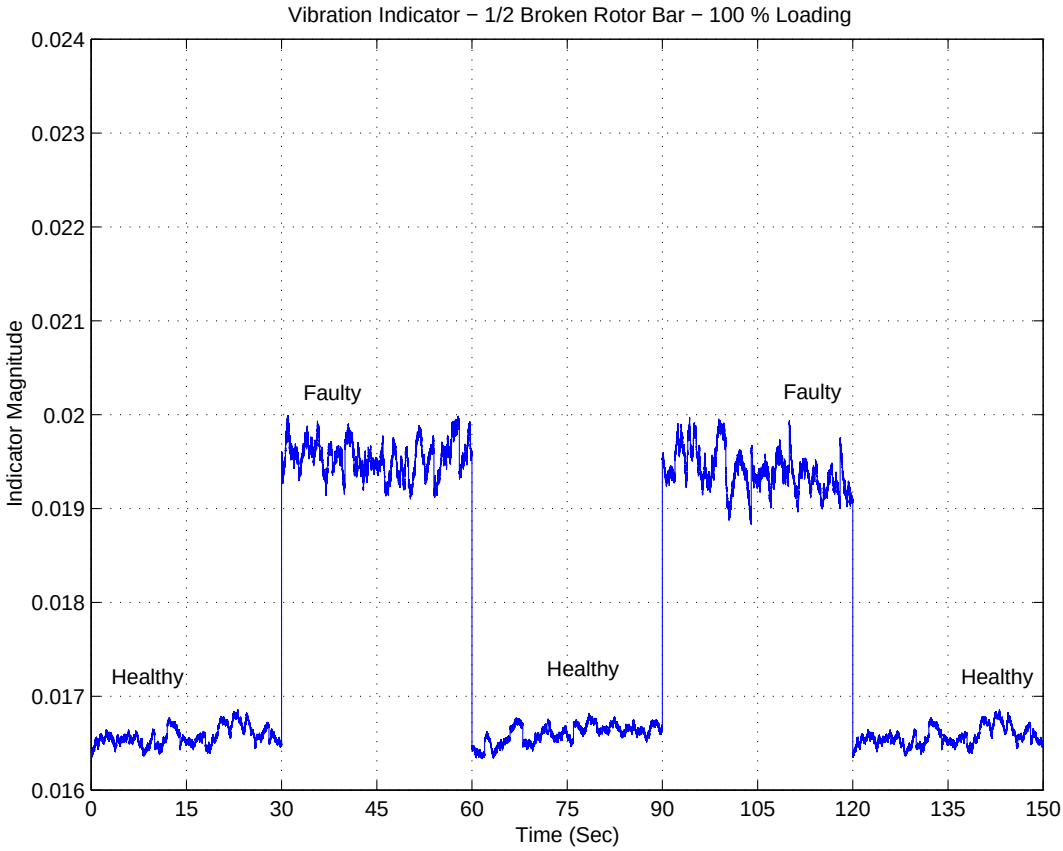

Fig. 55. Vibration-based Mechanical Indicator - Half Broken Rotor Bar at 100% Loading

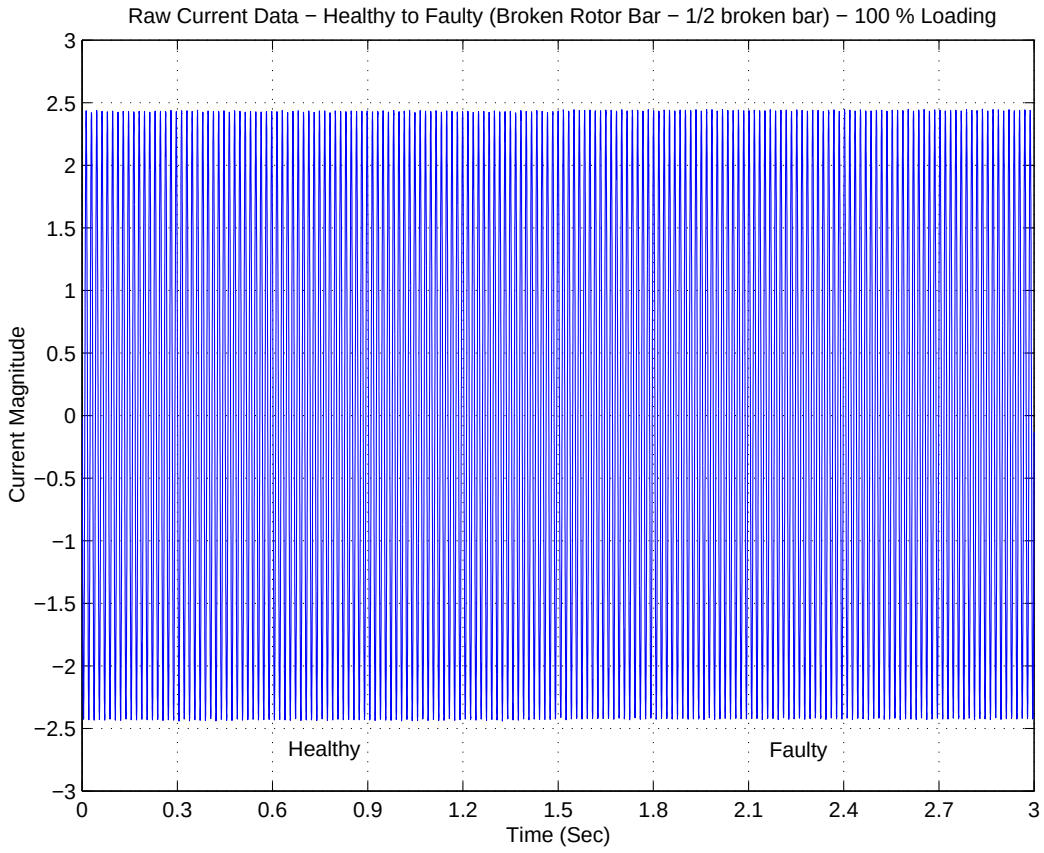

Fig. 56. Raw Current Signal - Half Broken Rotor Bar at 100% Loading

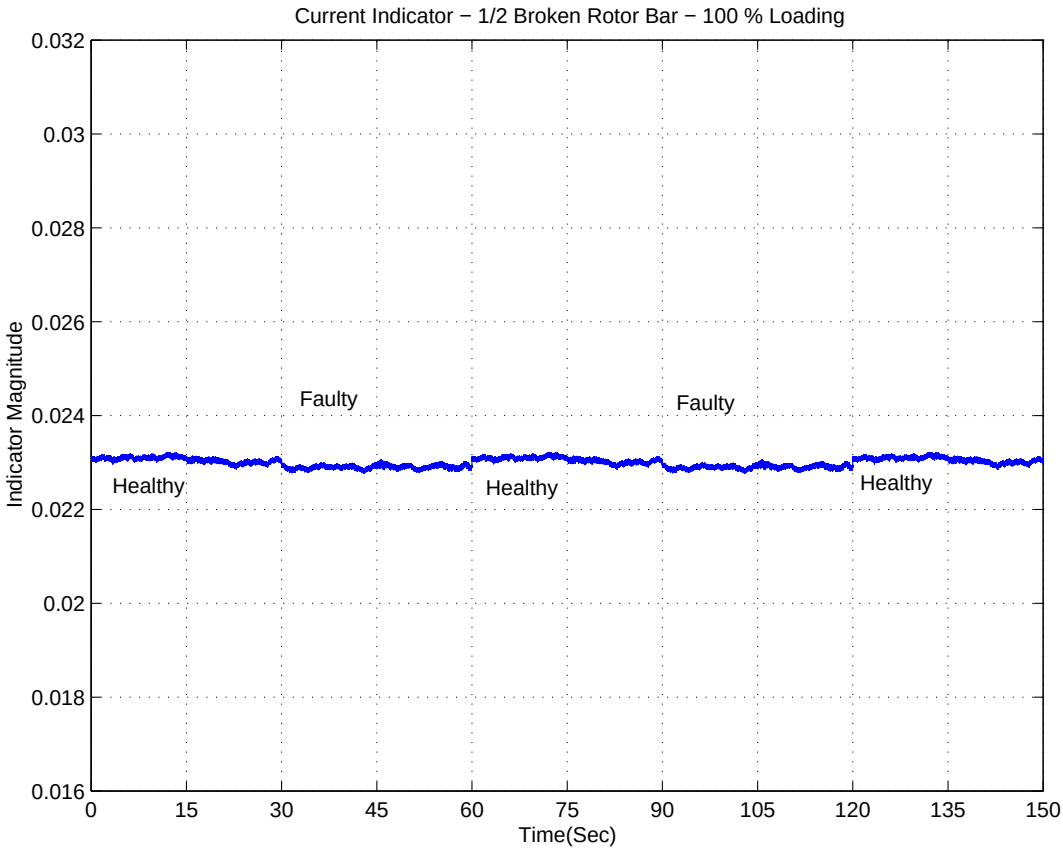

Fig. 57. Current-based Mechanical Indicator - Half Broken Rotor Bar at 100% Loading

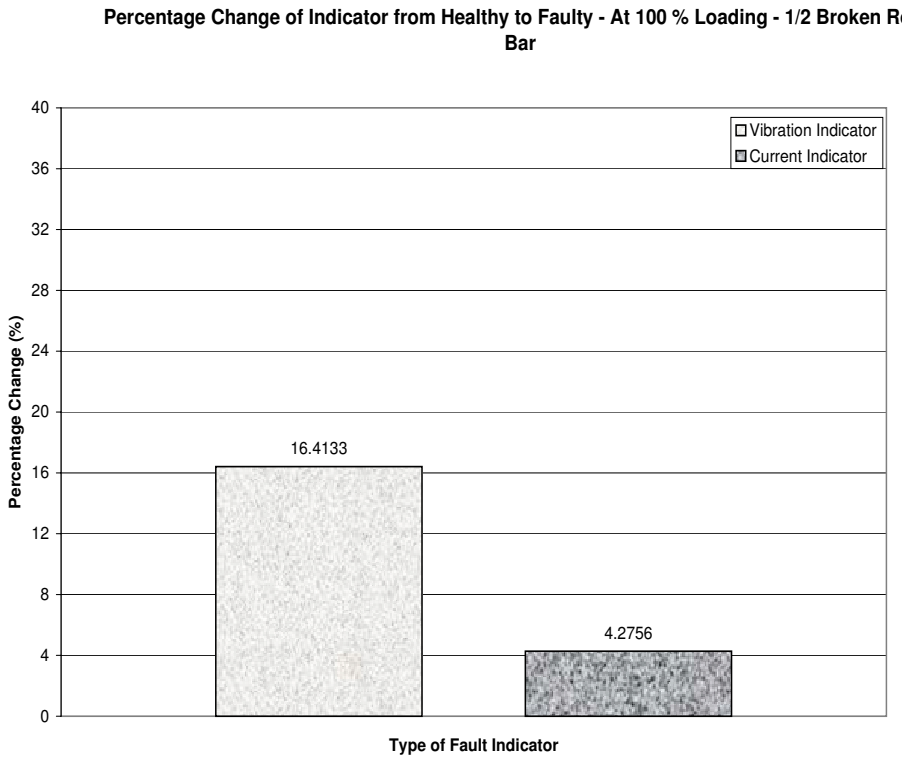

Fig. 58. Comparison of Current-based and Vibration-based Mechanical Fault Indicators - Half Broken Rotor Bar at 100% Loading

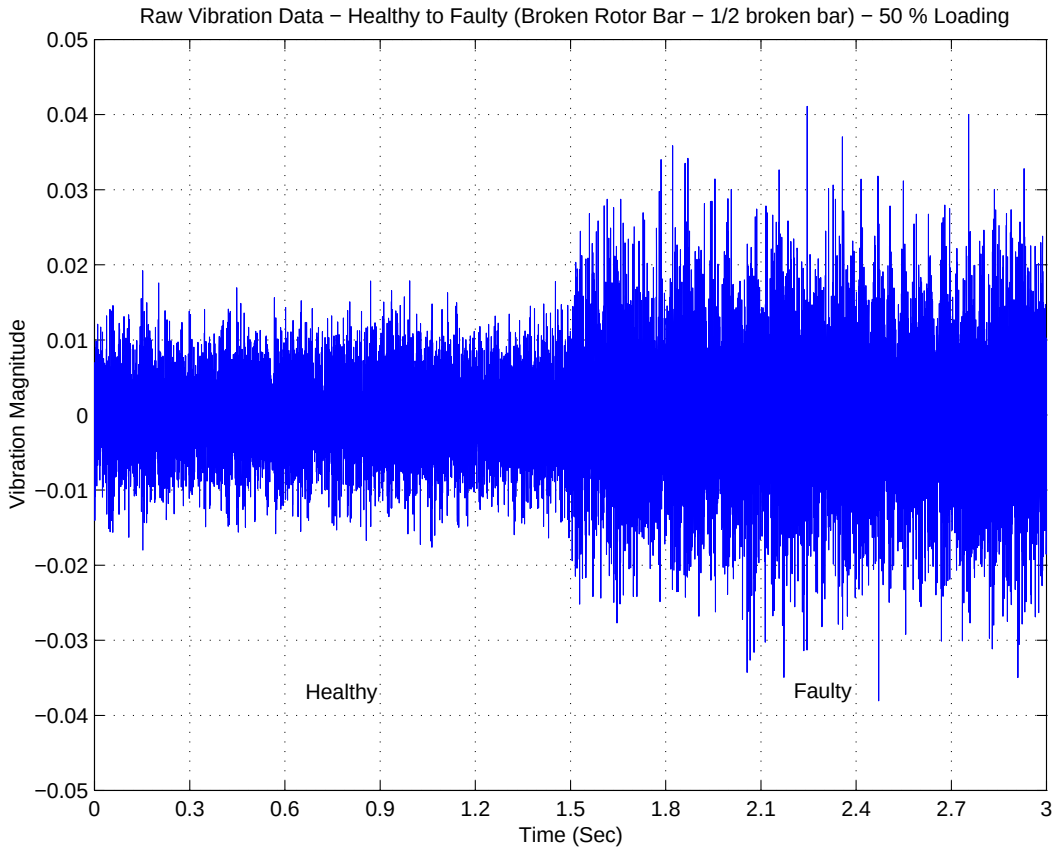

Fig. 59. Raw Vibration Signal - Half Broken Rotor Bar at 50% Loading

At 50% loading for 1/2 Broken Bar, Figures [59]-[63] show the raw vibration signal, vibration-based indicator, raw current signal, current-based indicator and the comparison chart between the two indicators, respectively. The increases in the fault indicator percentages is much larger as compared to the corresponding increases at 100% loading. At 50% loading, surprisingly, for this case, the vibration is a lot higher than expected (this being the one with the minimum severity in the family of broken rotor bar faults). The relative increase of the current-based indicator with respect to the vibration-based indicator is about 33% in magnitude.

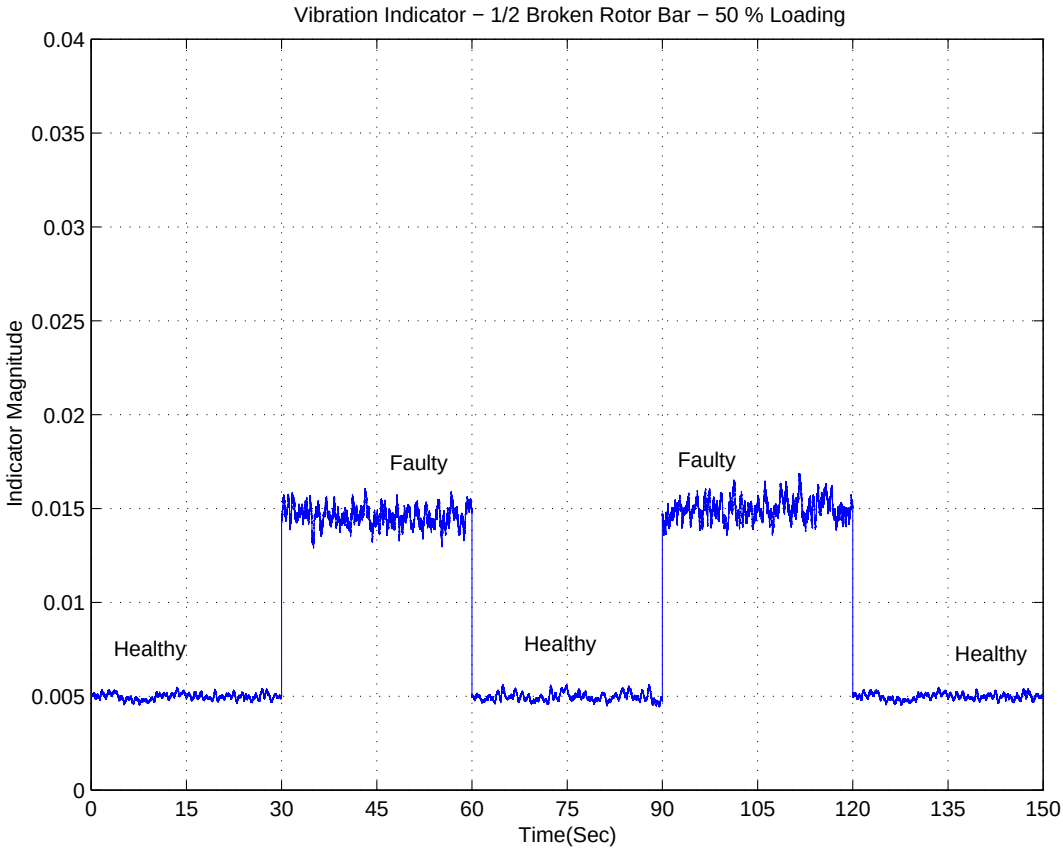

Fig. 60. Vibration-based Mechanical Indicator - Half Broken Rotor Bar at 50% Loading

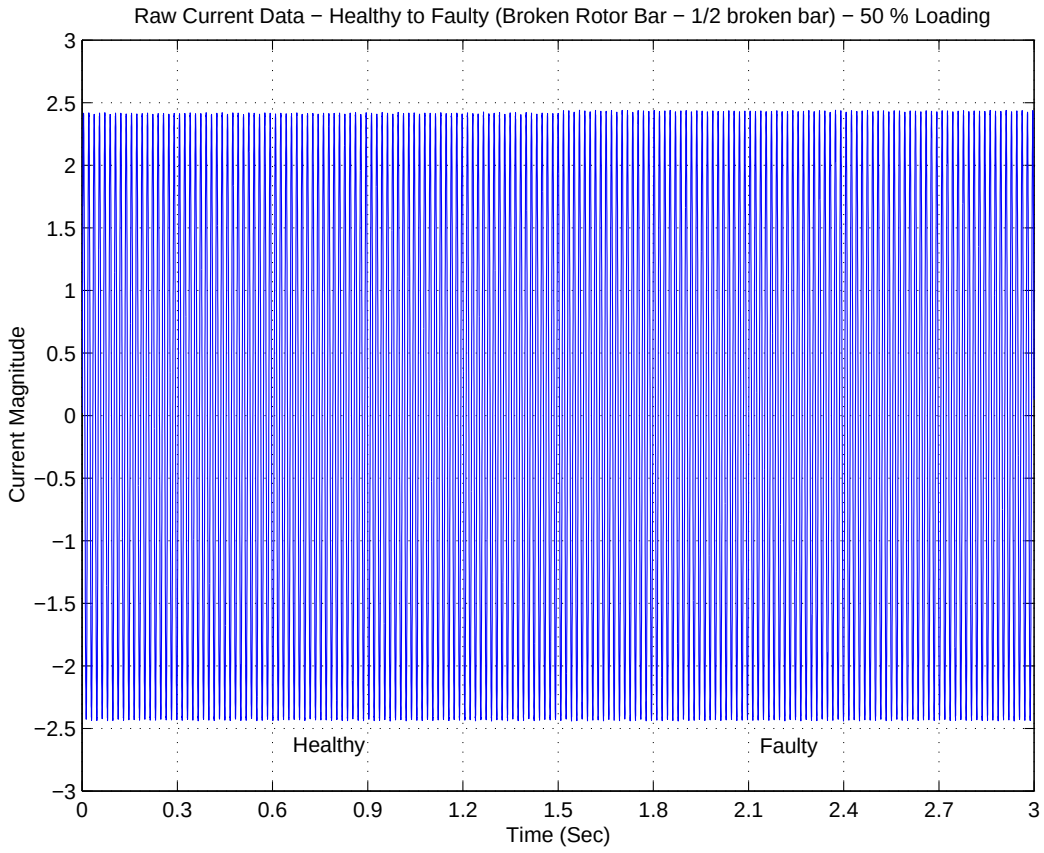

Fig. 61. Raw Current Signal - Half Broken Rotor Bar at 50% Loading

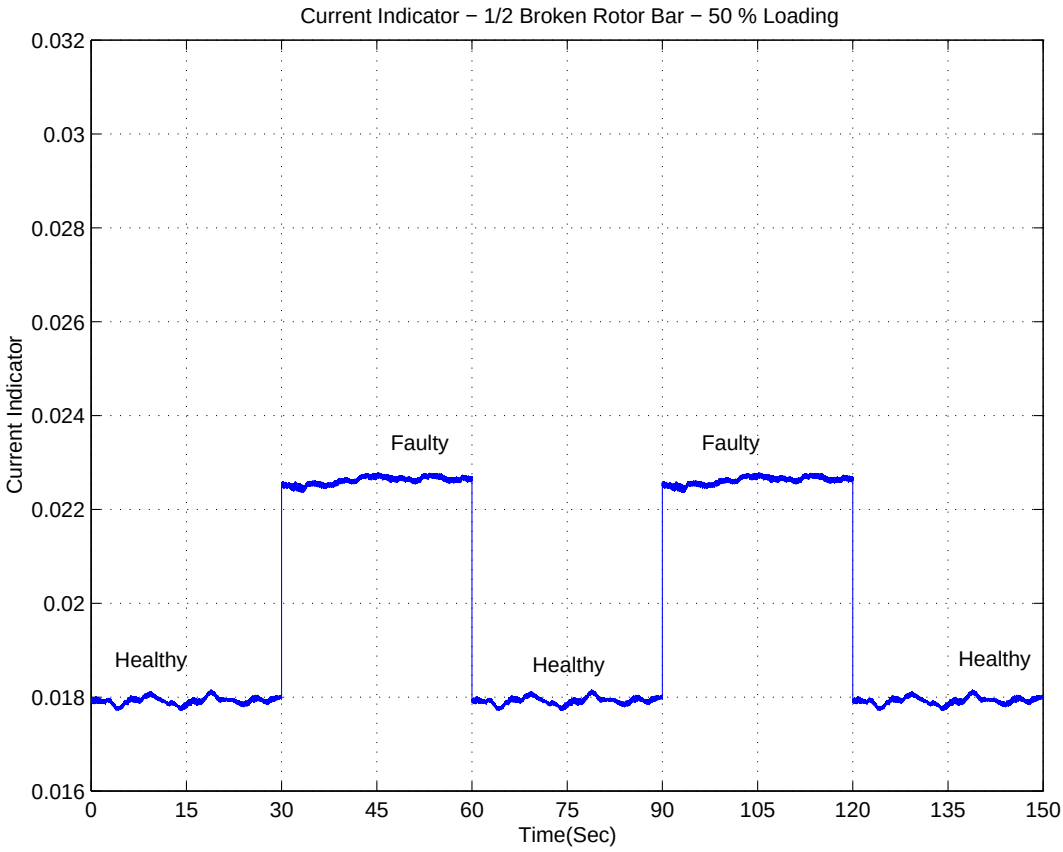

Fig. 62. Current-based Mechanical Indicator - Half Broken Rotor Bar at 50% Loading

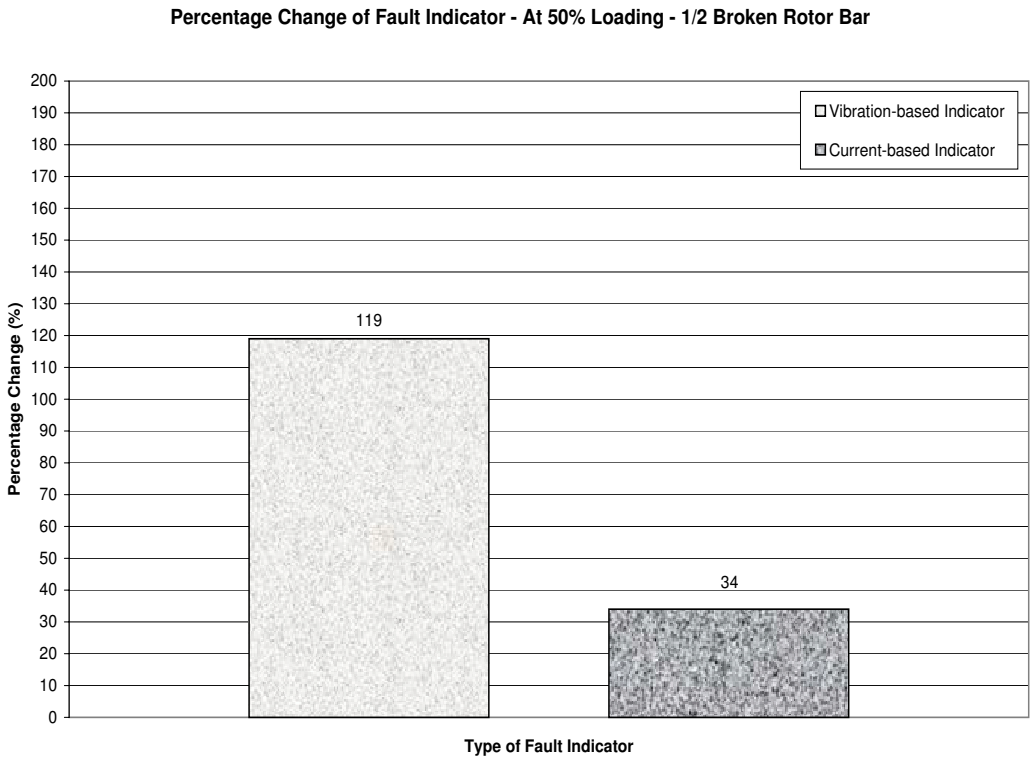

Fig. 63. Comparison of Current-based and Vibration-based Mechanical Fault Indicators - Half Broken Rotor Bar at 50% Loading

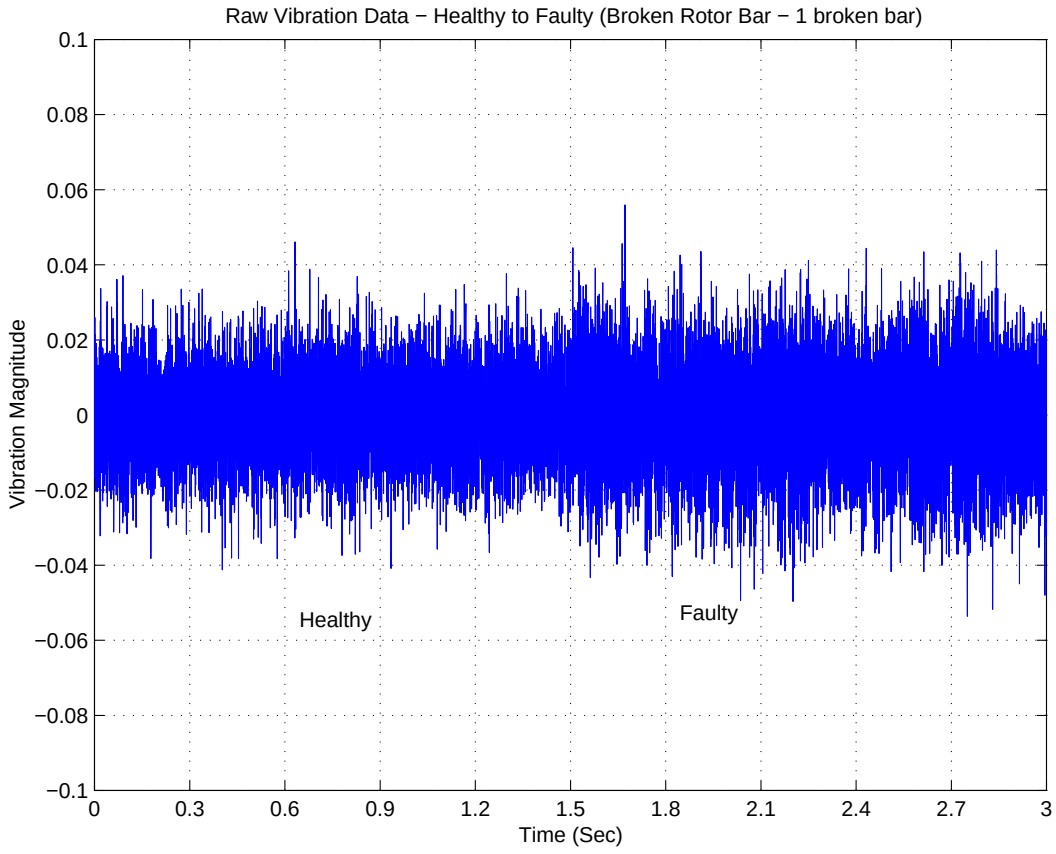

Fig. 64. Raw Vibration Signal - One Broken Rotor Bar at 100% Loading

2. One Broken Rotor Bar

At 100% loading level for 1 Broken Bar, Figures [64]-[68] show the raw vibration signal, vibration-based indicator, raw current signal, current-based indicator and the comparison chart between the two indicators, respectively. We can observe that the mean increase in the fault indicators is higher than the Half broken rotor bar case. The mean increase in the current-based indicator levels is about 33% of the increase found in the vibration-based indicator levels.

At 50% loading for 1 Broken Bar, Figures [69]-[73] show the raw vibration signal, vibration-based indicator, raw current signal, current-based indicator and the

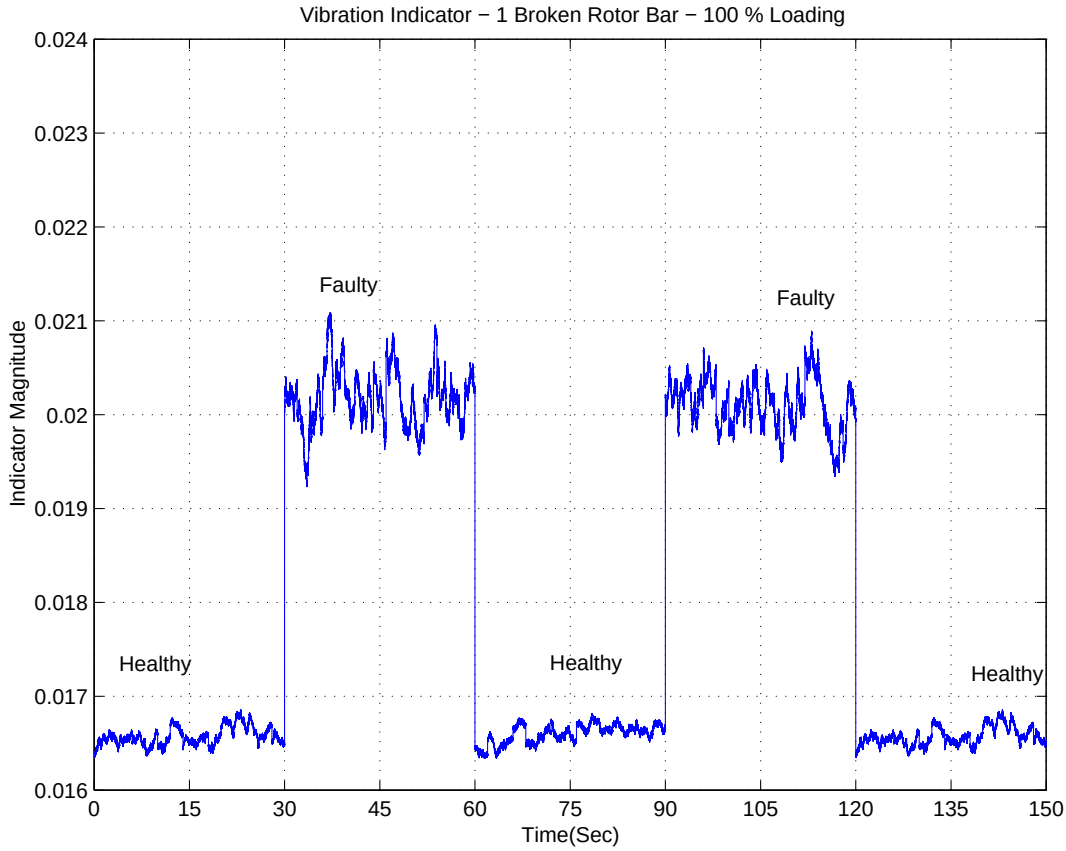

Fig. 65. Vibration-based Mechanical Indicator - One Broken Rotor Bar at 100% Loading

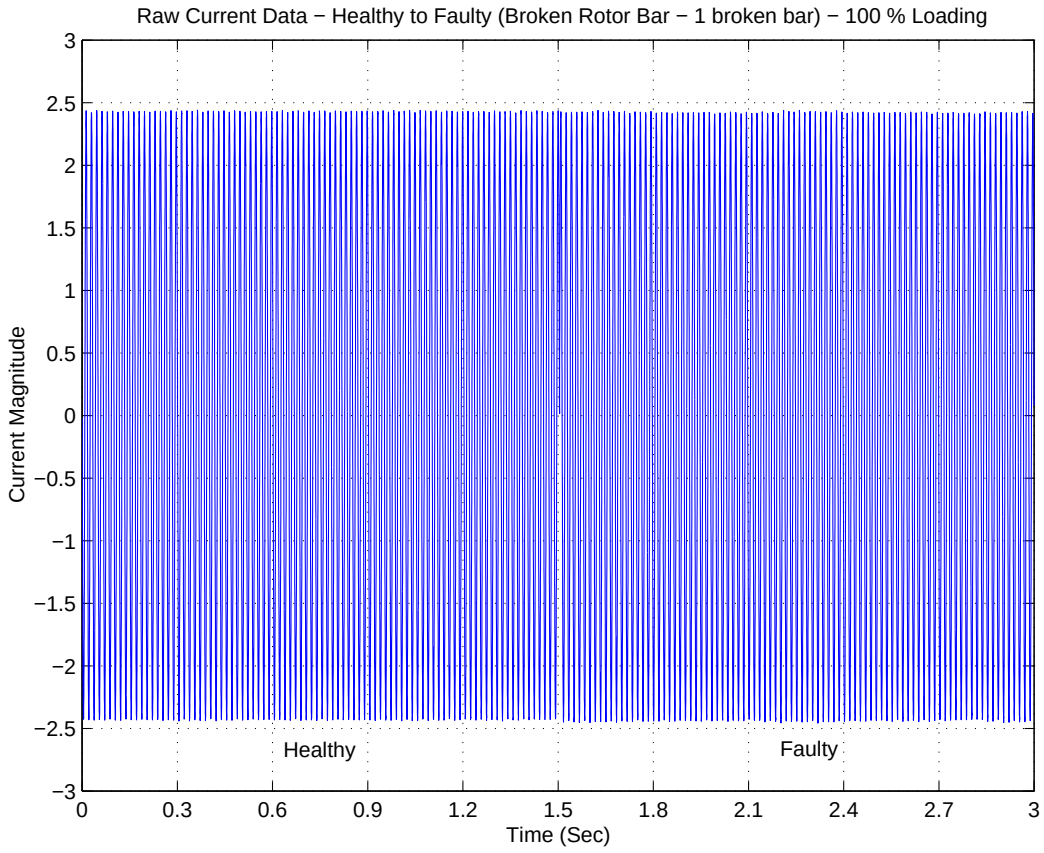

Fig. 66. Raw Current Signal - One Broken Rotor Bar at 100% Loading

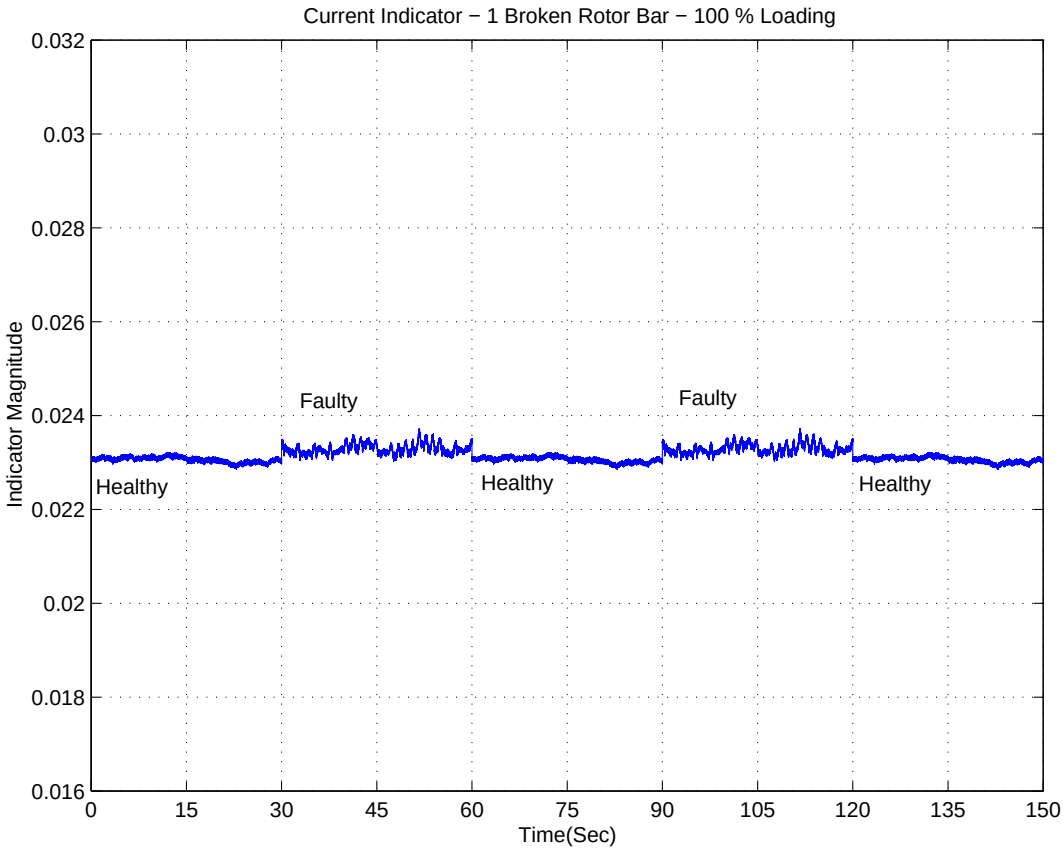

Fig. 67. Current-based Mechanical Indicator - One Broken Rotor Bar at 100% Loading

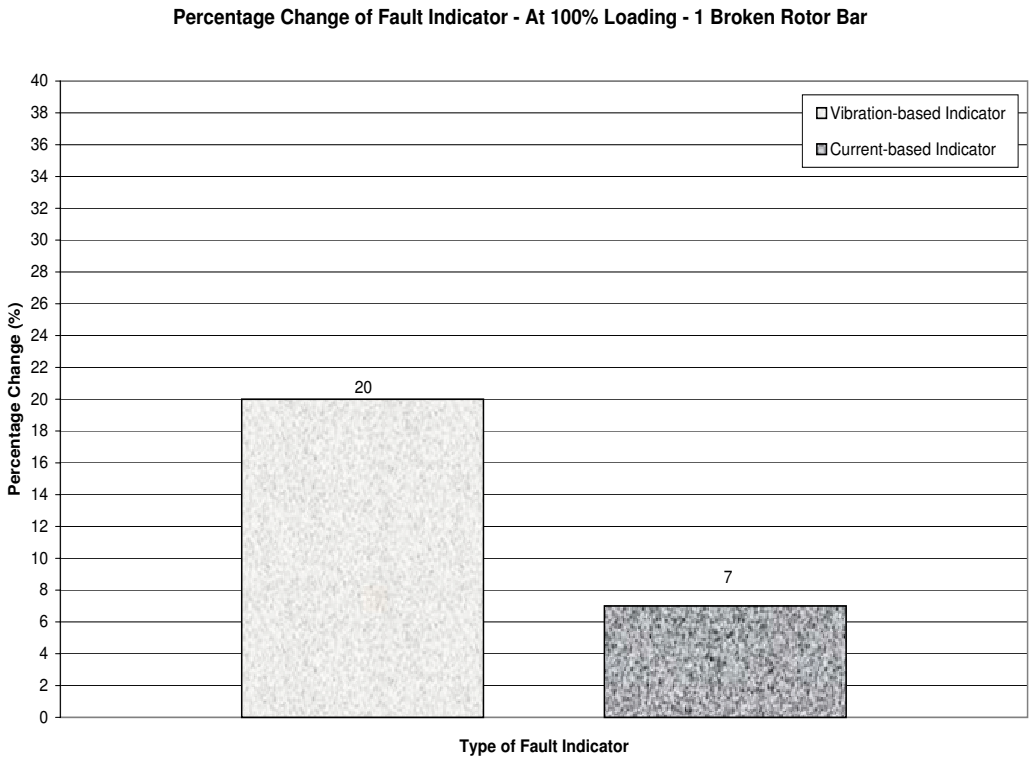

Fig. 68. Comparison of Current-based and Vibration-based Mechanical Fault Indicators - One Broken Rotor Bar at 100% Loading

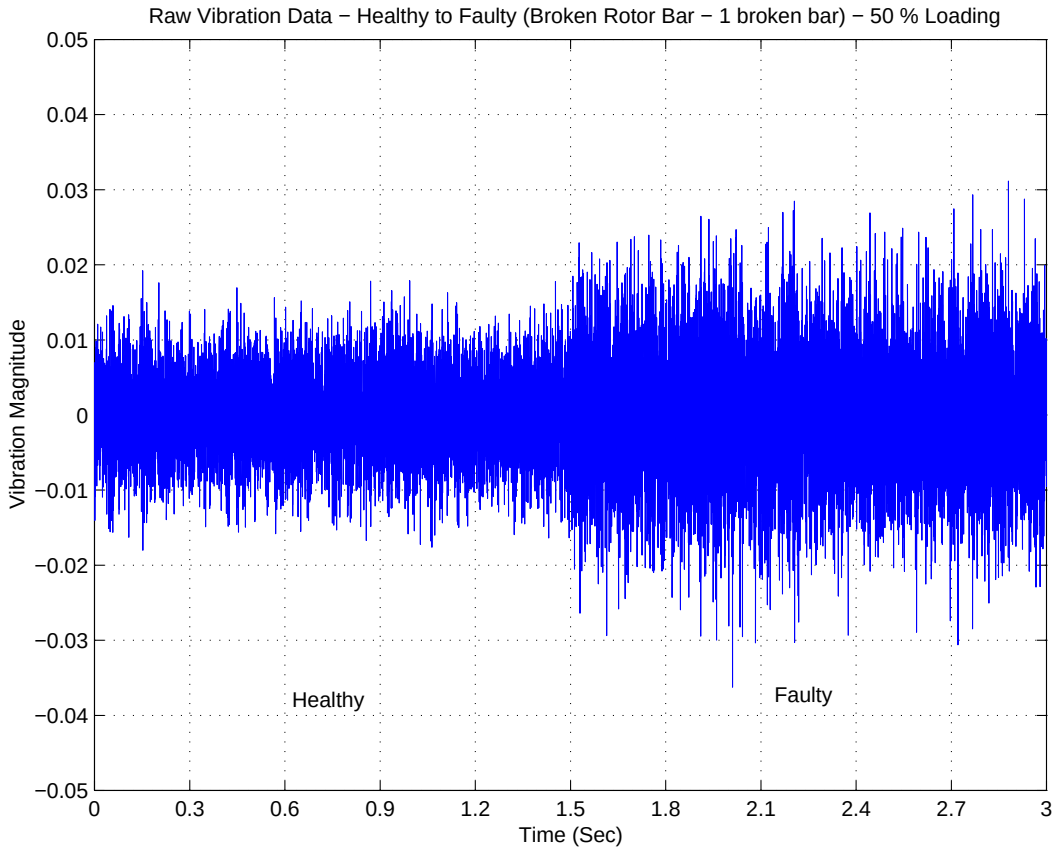

Fig. 69. Raw Vibration Signal - One Broken Rotor Bar at 50% Loading

comparison chart between the two indicators, respectively. This value is a lot higher. Also, the magnitudes of the mean increases are much more than that obtained while operating at 100% loading conditions.

3. Two Broken Rotor Bars

For this case we can observe a significant increase in the magnitude of the raw vibration signals. However, the raw current signals continue to be non-indicative of the mechanical fault. At 100% loading for 2 Broken Bars, Figures [74]-[78] show the raw vibration signal, vibration-based indicator, raw current signal, current-based in-

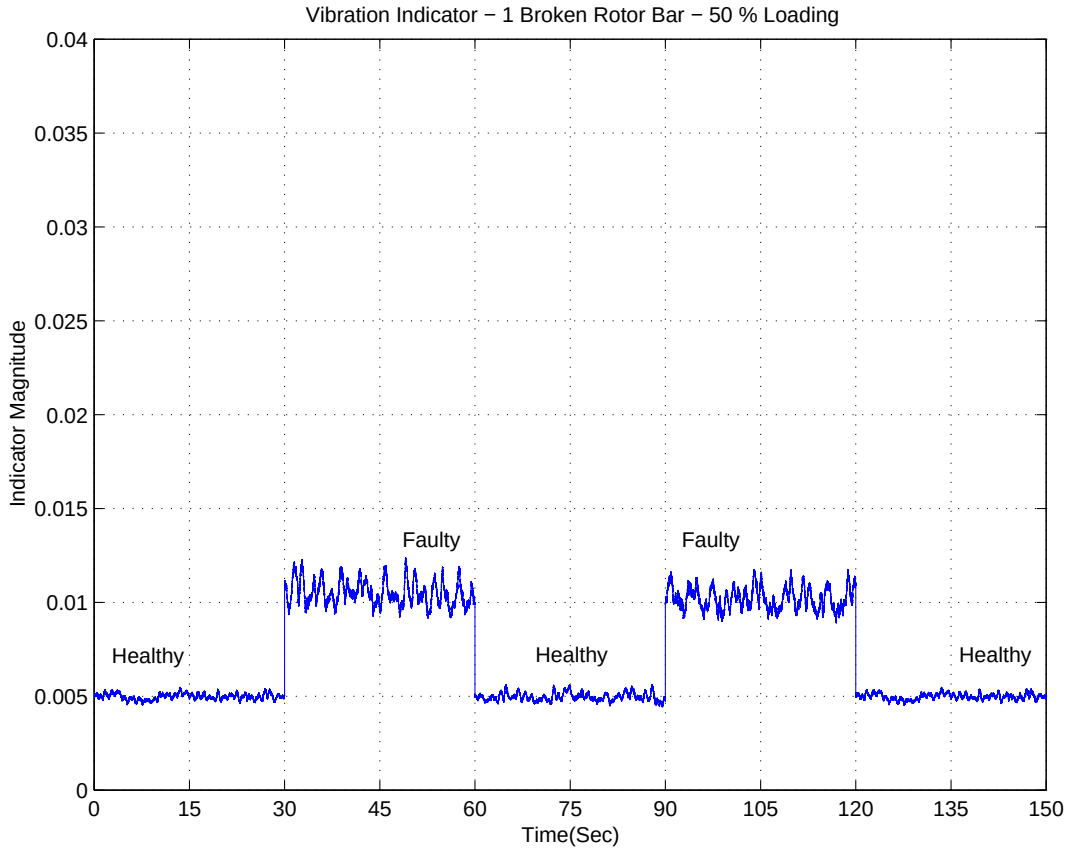

Fig. 70. Vibration-based Mechanical Indicator - One Broken Rotor Bar at 50% Loading

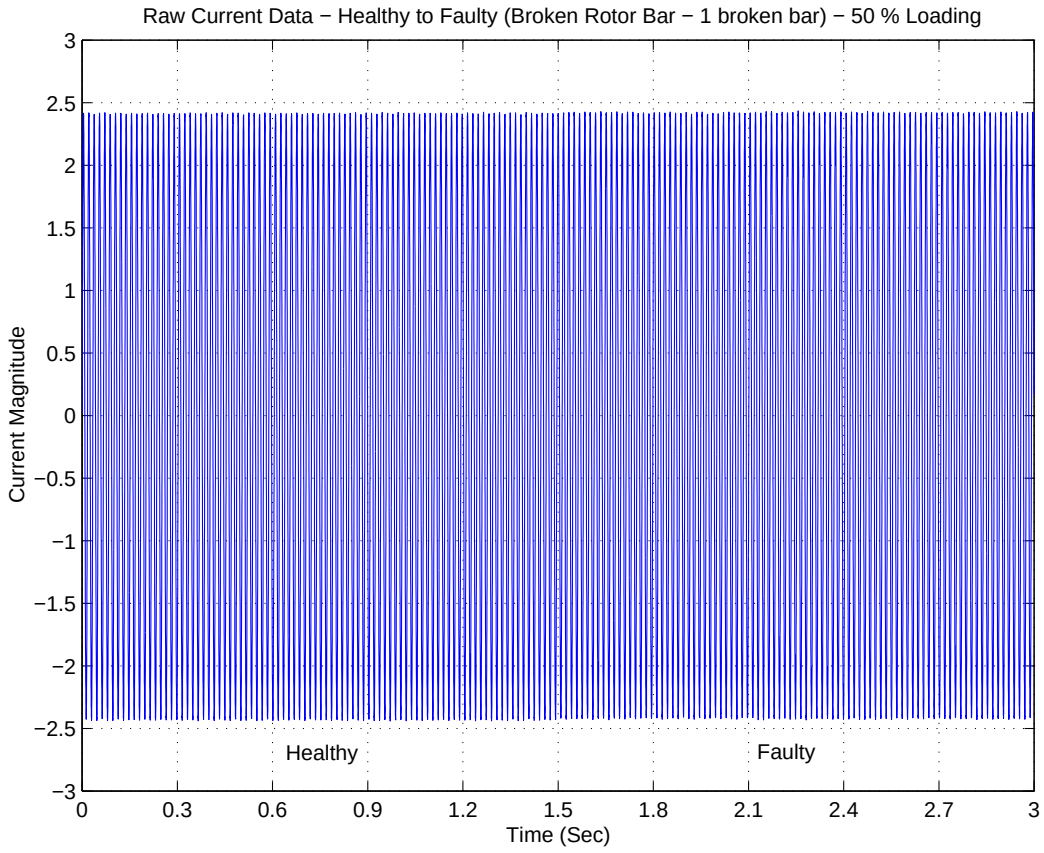

Fig. 71. Raw Current Signal - One Broken Rotor Bar at 50% Loading

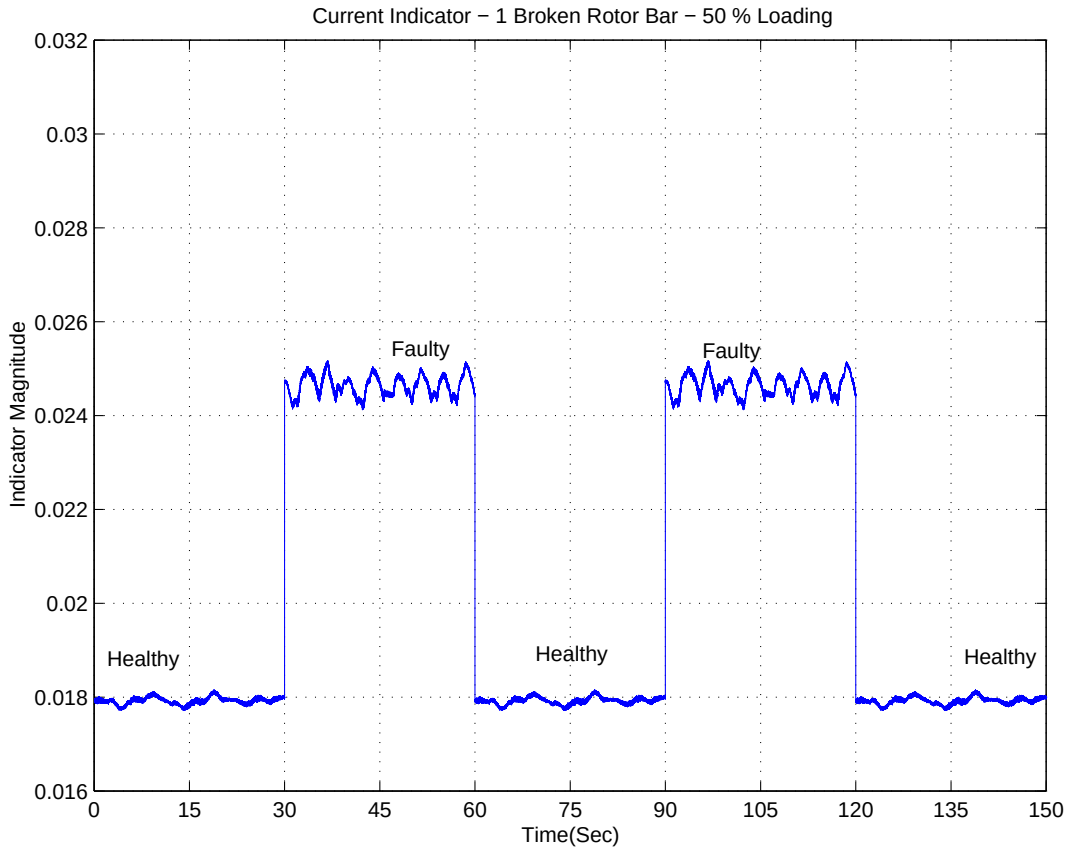

Fig. 72. Current-based Mechanical Indicator - One Broken Rotor Bar at 50% Loading

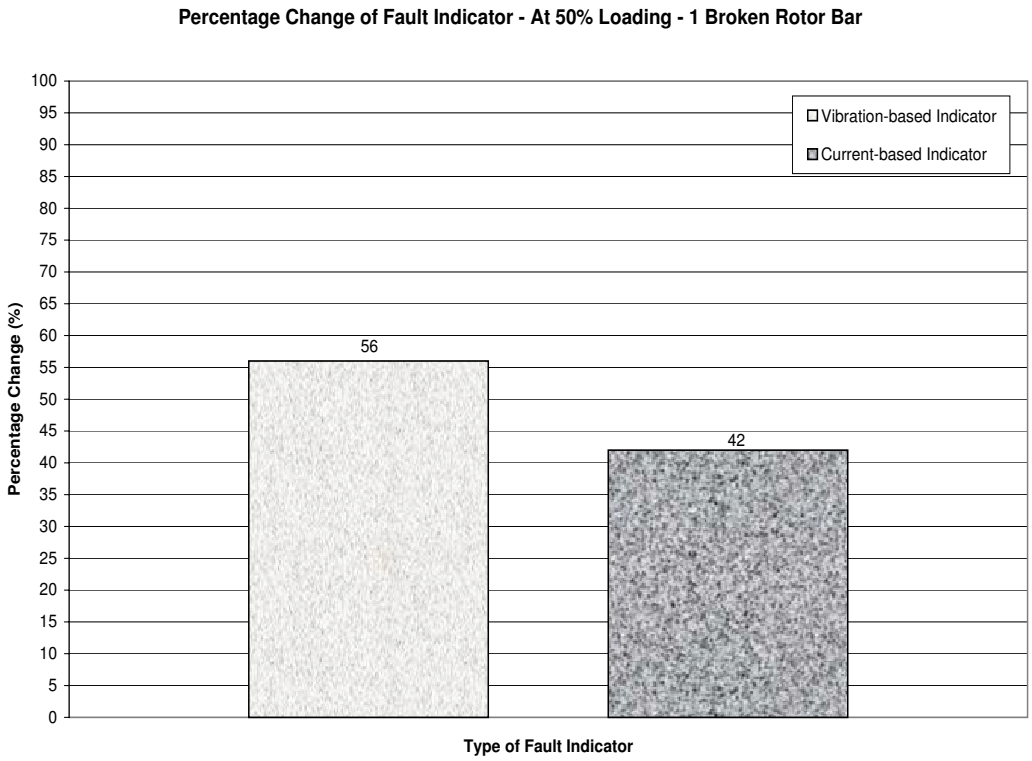

Fig. 73. Comparison of Current-based and Vibration-based Mechanical Fault Indicators - One Broken Rotor Bar at 50% Loading

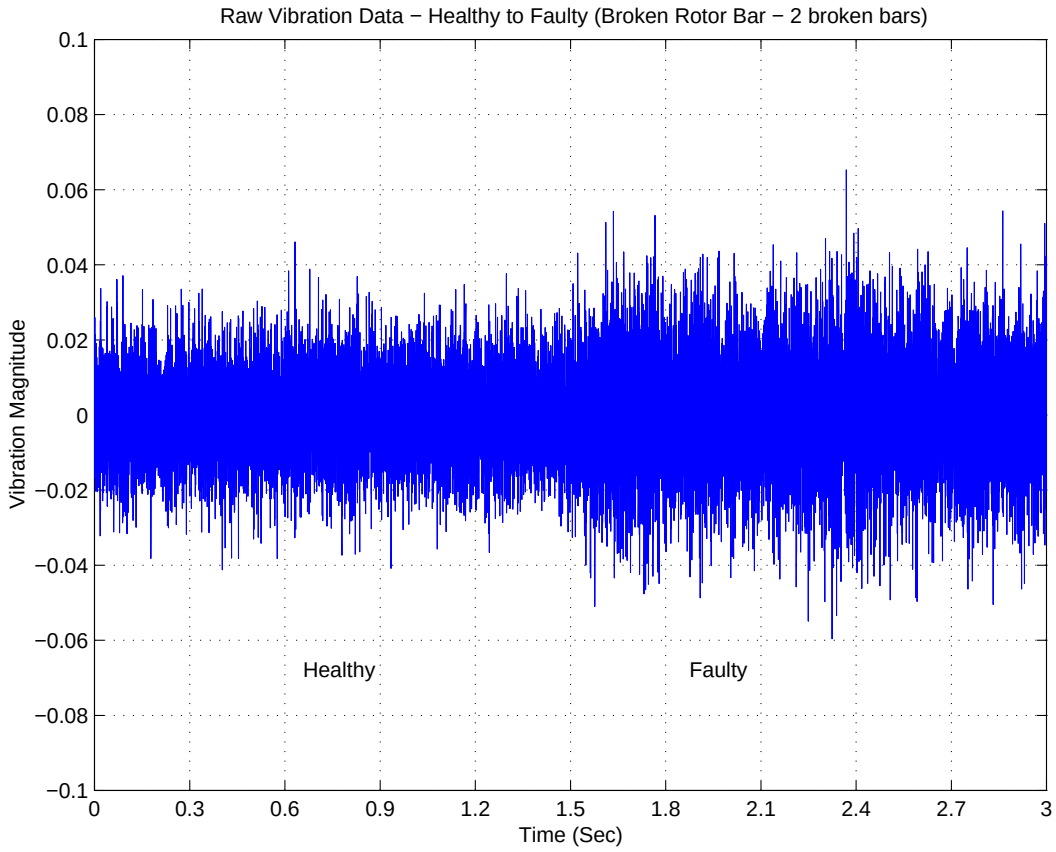

Fig. 74. Raw Vibration Signal - Two Broken Rotor Bars at 100% Loading

dicator and the comparison chart between the two indicators, respectively. There is about 26.3% increase in the vibration-based indicator level and about 9.2% increase in the current-based indicator level. These are much higher than those observed for the Half broken rotor bar and the One broken rotor bar cases. This is the expected pattern due to the fact that it is a more severe fault than the previous two cases.

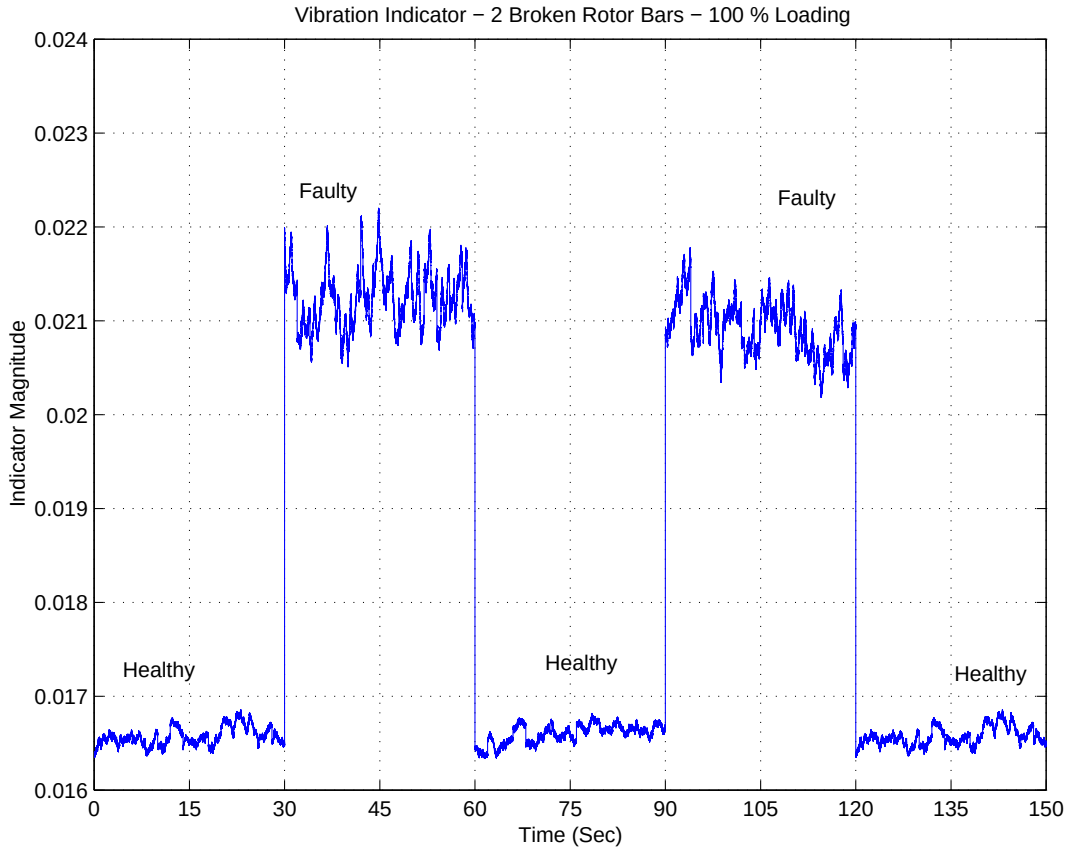

Fig. 75. Vibration-based Mechanical Indicator - Two Broken Rotor Bars at 100% Loading

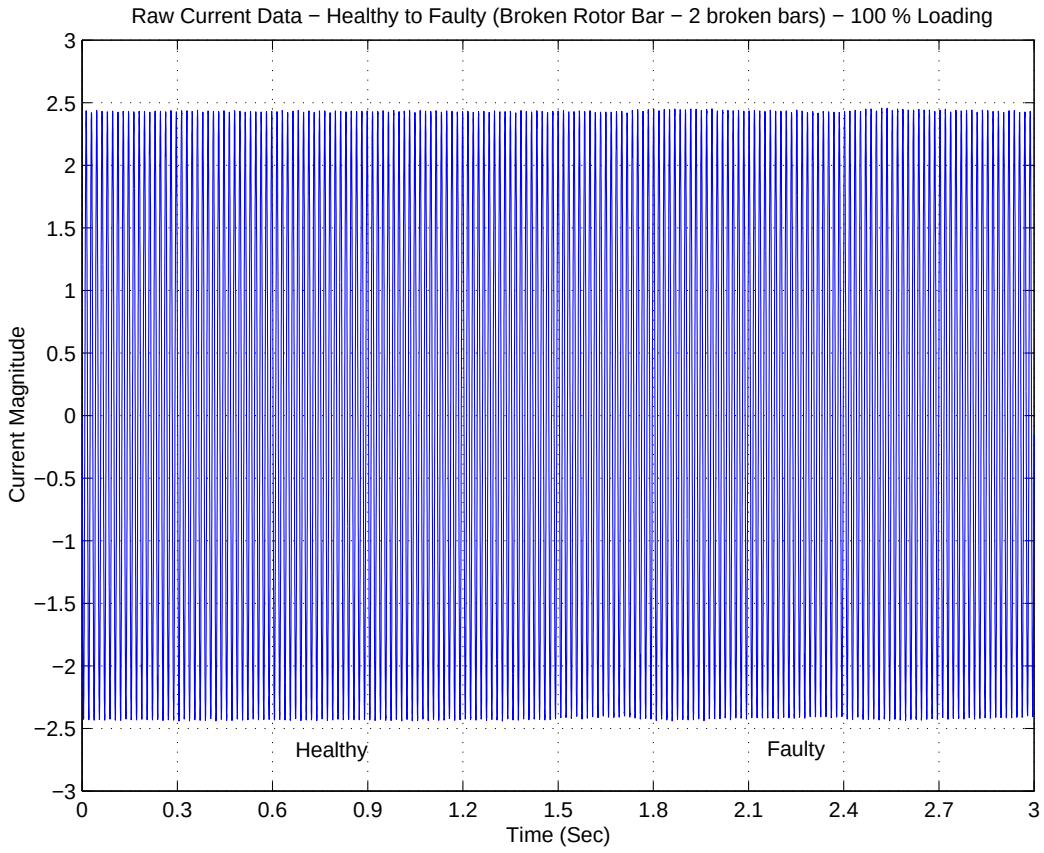

Fig. 76. Raw Current Signal - Two Broken Rotor Bars at 100% Loading

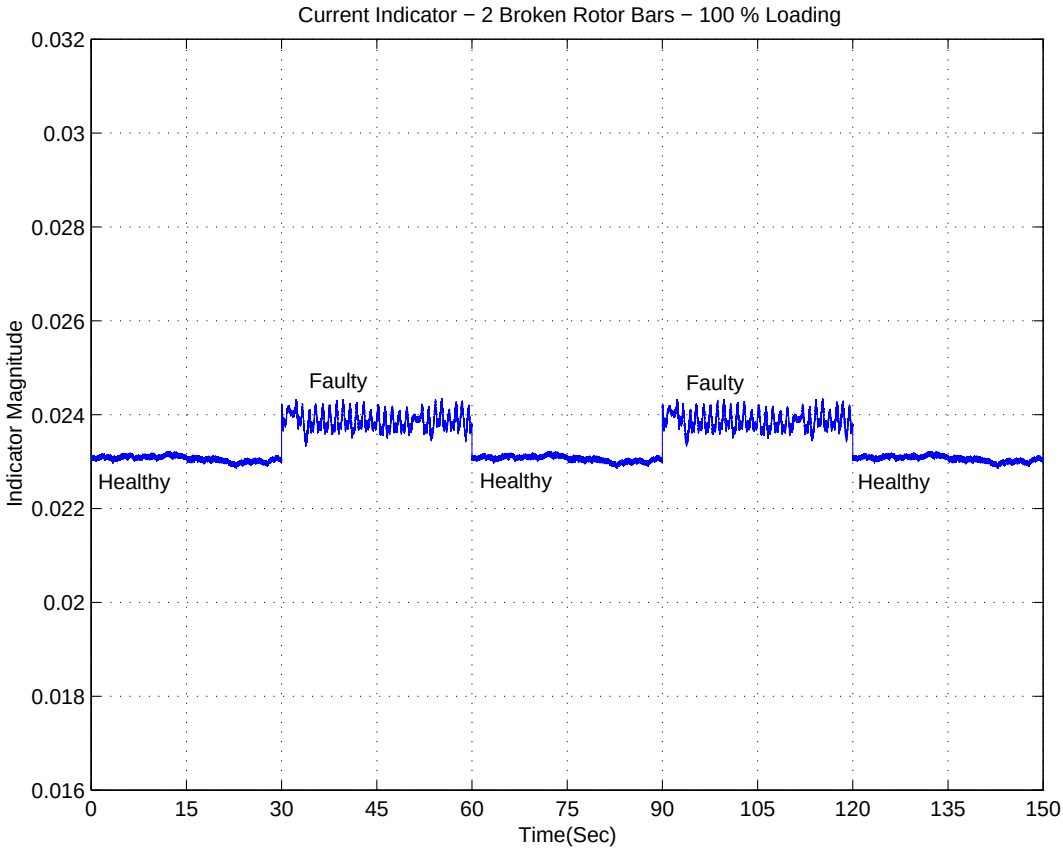

Fig. 77. Current-based Mechanical Indicator - Two Broken Rotor Bars at 100% Loading

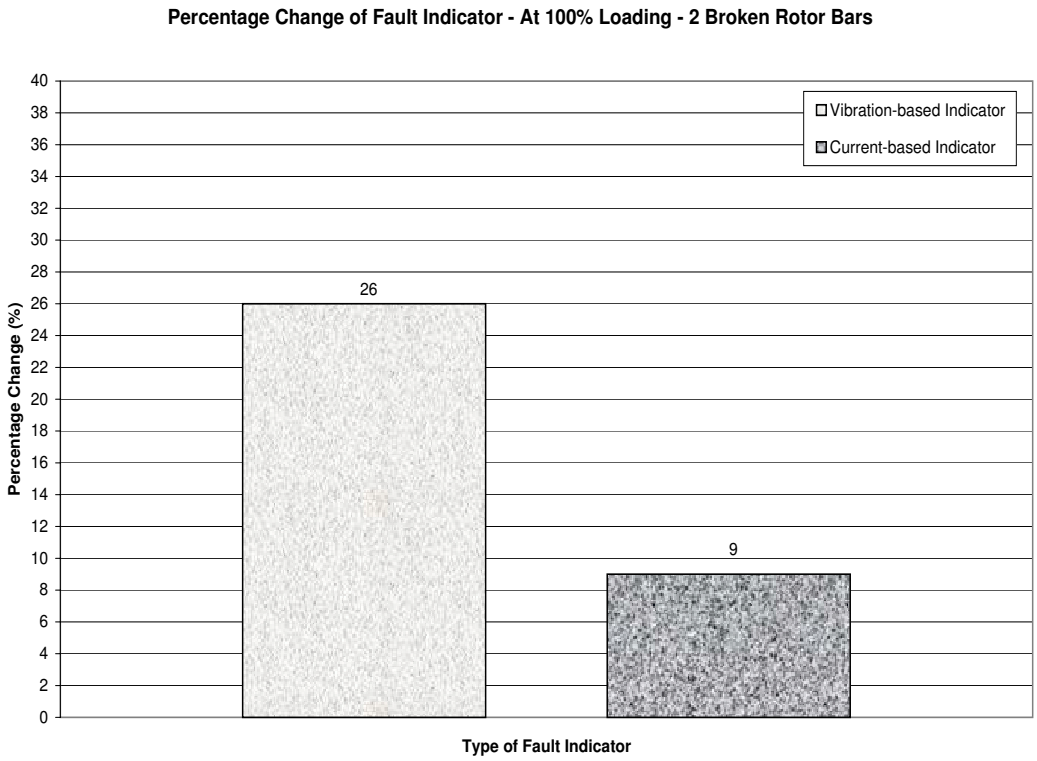

Fig. 78. Comparison of Current-based and Vibration-based Mechanical Fault Indicators - Two Broken Rotor Bars at 100% Loading

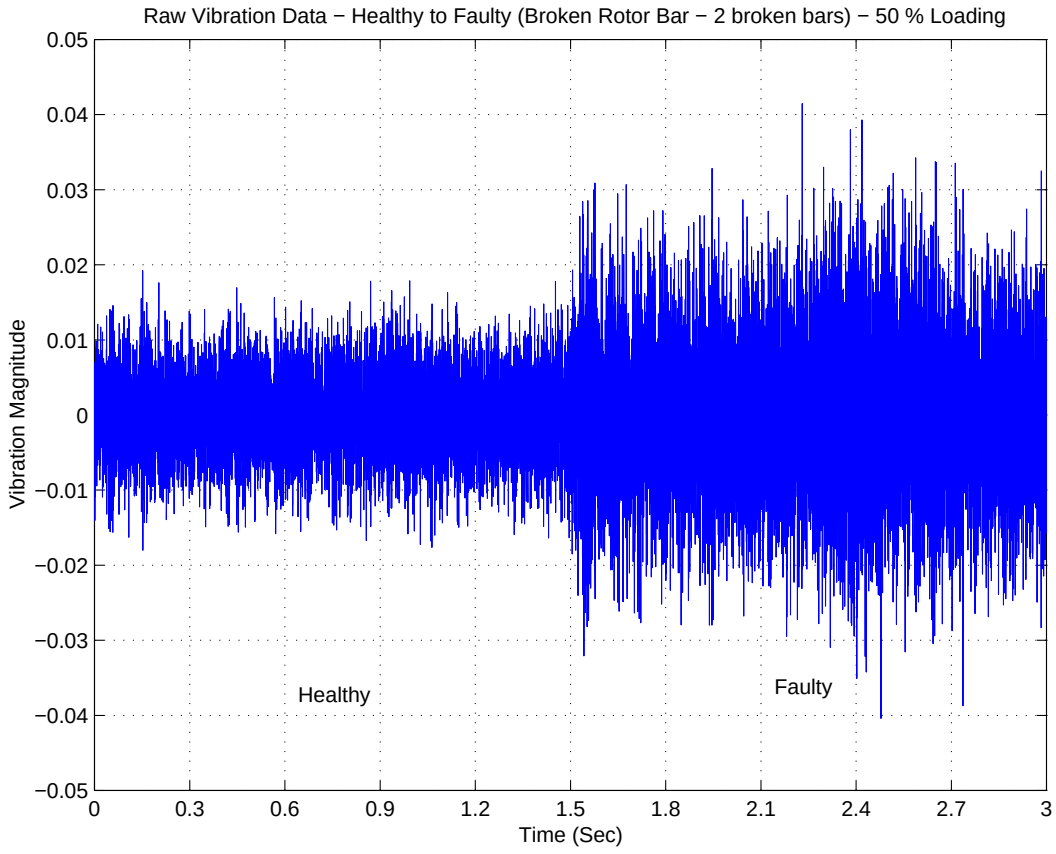

Fig. 79. Raw Vibration Signal - Two Broken Rotor Bars at 50% Loading

The fault indicators are much larger when the motor is operating at 50% as compared to 100% loading conditions. At 50% loading for the 2 Broken Bars, Figures [79]-[83] show the raw vibration signal, vibration-based indicator, raw current signal, current-based indicator and the comparison chart between the two indicators, respectively. The mean increase of the current-based indicator in comparison to the mean increase of the vibration-based indicator, is observed to be about twice as much as at 100% loading.

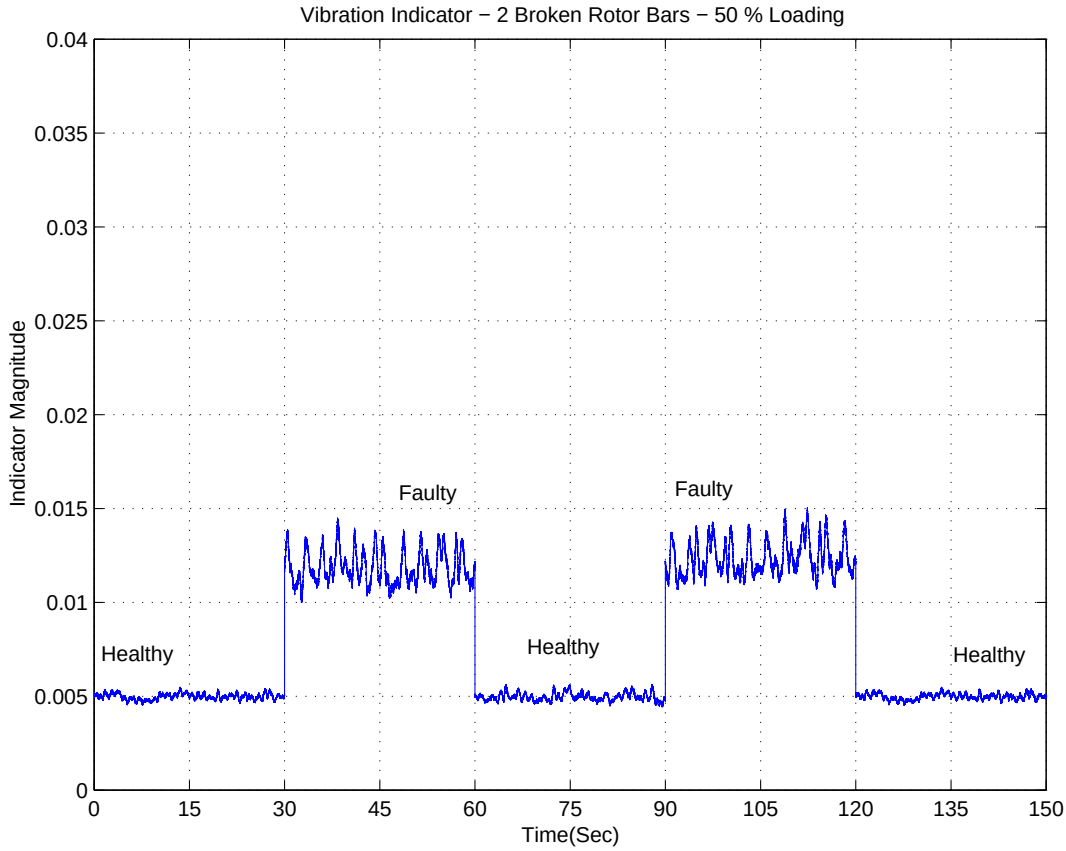

Fig. 80. Vibration-based Mechanical Indicator - Two Broken Rotor Bars at 50% Loading

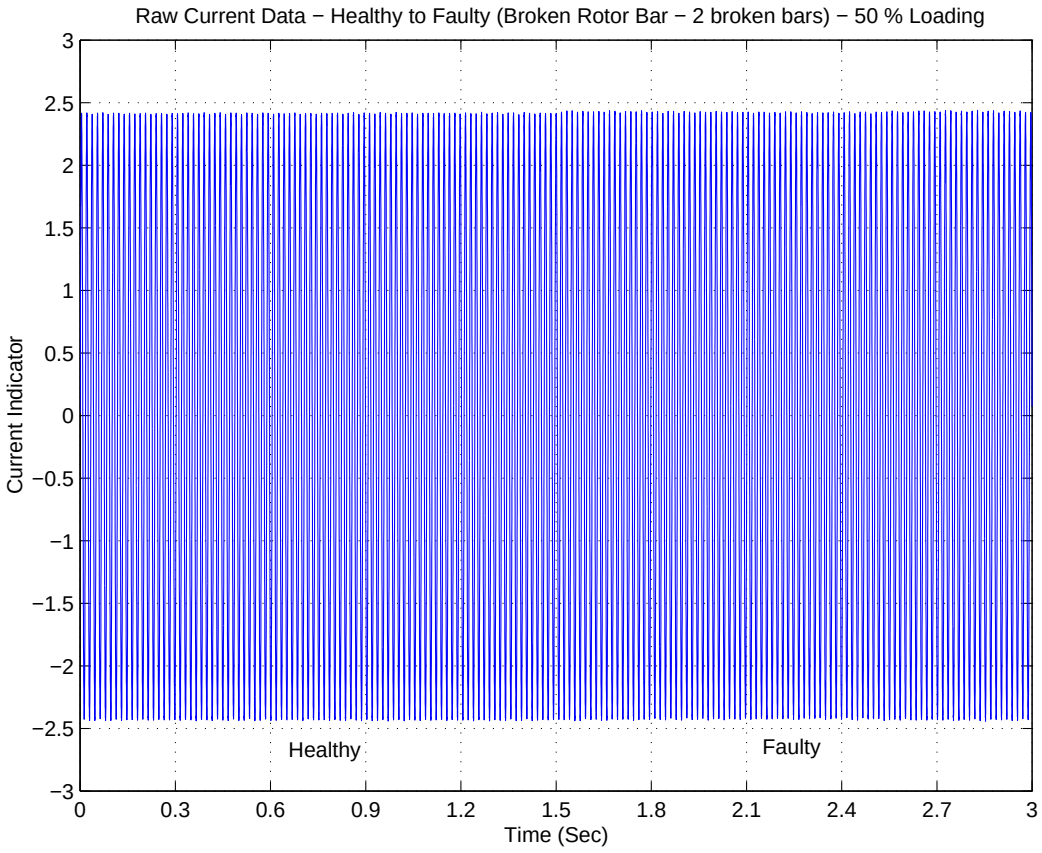

Fig. 81. Raw Current Signal - Two Broken Rotor Bars at 50% Loading

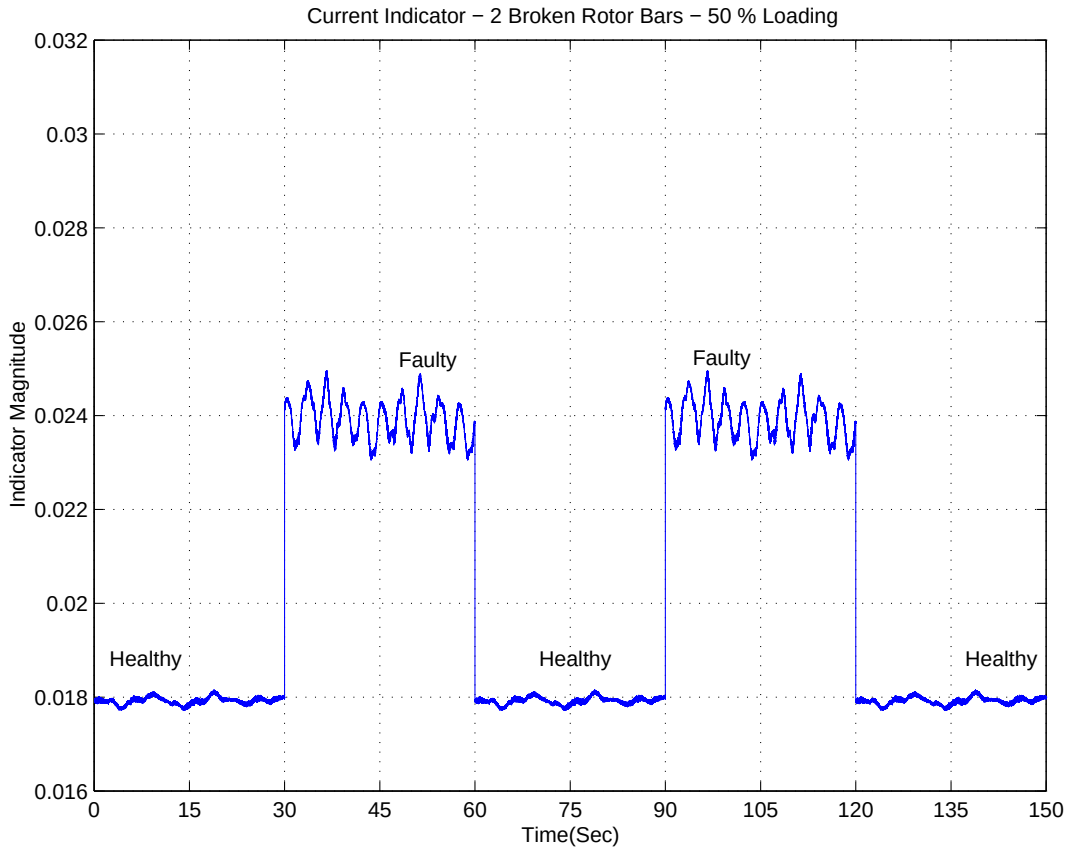

Fig. 82. Current-based Mechanical Indicator - Two Broken Rotor Bars at 50% Loading

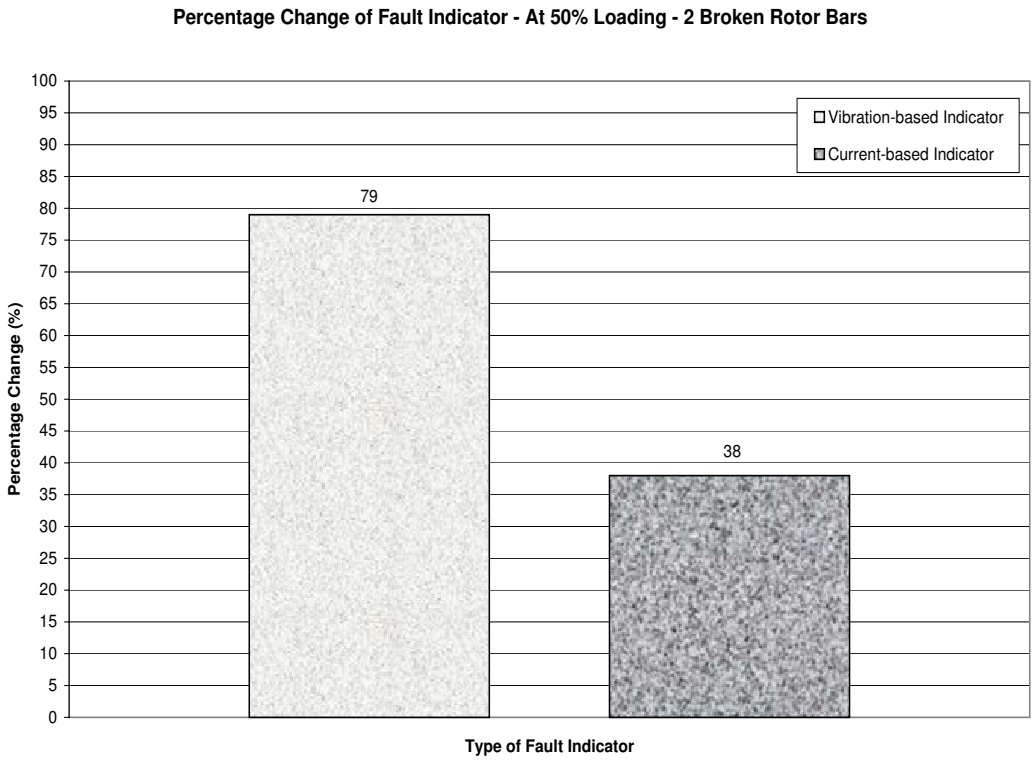

Fig. 83. Comparison of Current-based and Vibration-based Mechanical Fault Indicators - Two Broken Rotor Bars at 50% Loading

4. Four Broken Rotor Bars

The four broken rotor bar case shows the maximum increases in the indicator magnitudes as compared to the other cases. This applies to both types of indicators. At 100% loading for 4 Broken Bars, Figures [84]-[88] show the raw vibration signal, vibration-based indicator, raw current signal, current-based indicator and the comparison chart between the two indicators, respectively. There is about 33% increase in the vibration-based indicator levels, while there is about 20.4% increase in the current-based indicator levels. This means that the relative increase of the current-based indicator compared to the increase of the vibration-based indicator is about 60%.

At 50% loading for 4 Broken Bars, Figures [89]-[93] show the raw vibration signal, vibration-based indicator, raw current signal, current-based indicator and the comparison chart between the two indicators, respectively. The increase from the mean healthy vibration indicator levels is close to 100%, while that of the current indicator levels is about 50%. This means that the relative increase in the current-based indicator is about 50% compared to the increase of the vibration-based indicator.

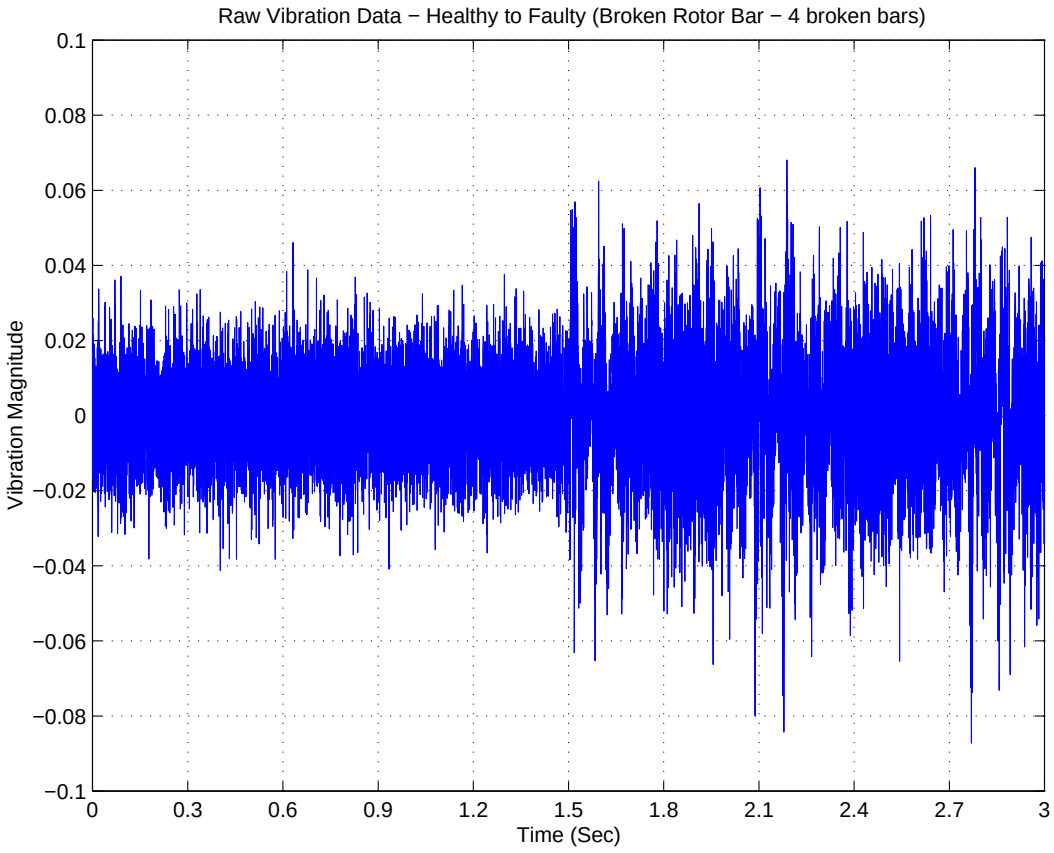

Fig. 84. Raw Vibration Signal - Four Broken Rotor Bars at 100% Loading

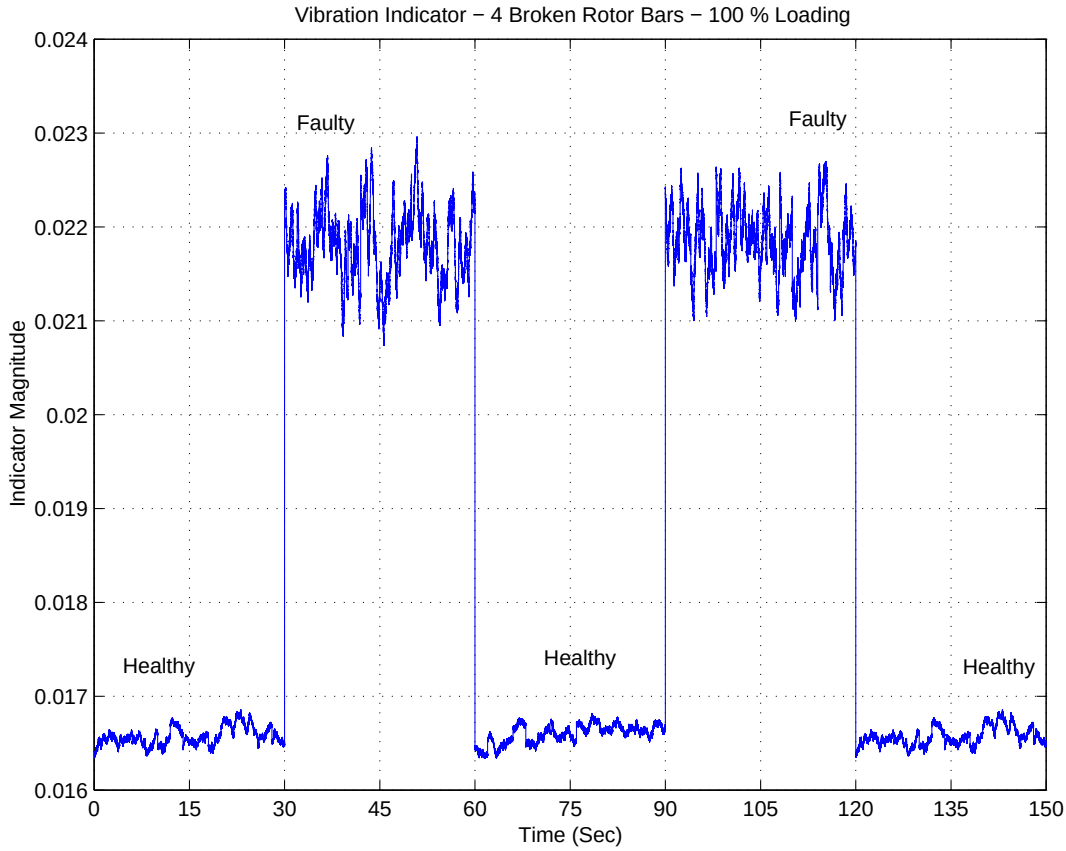

Fig. 85. Vibration-based Mechanical Indicator - Four Broken Rotor Bars at 100% Loading

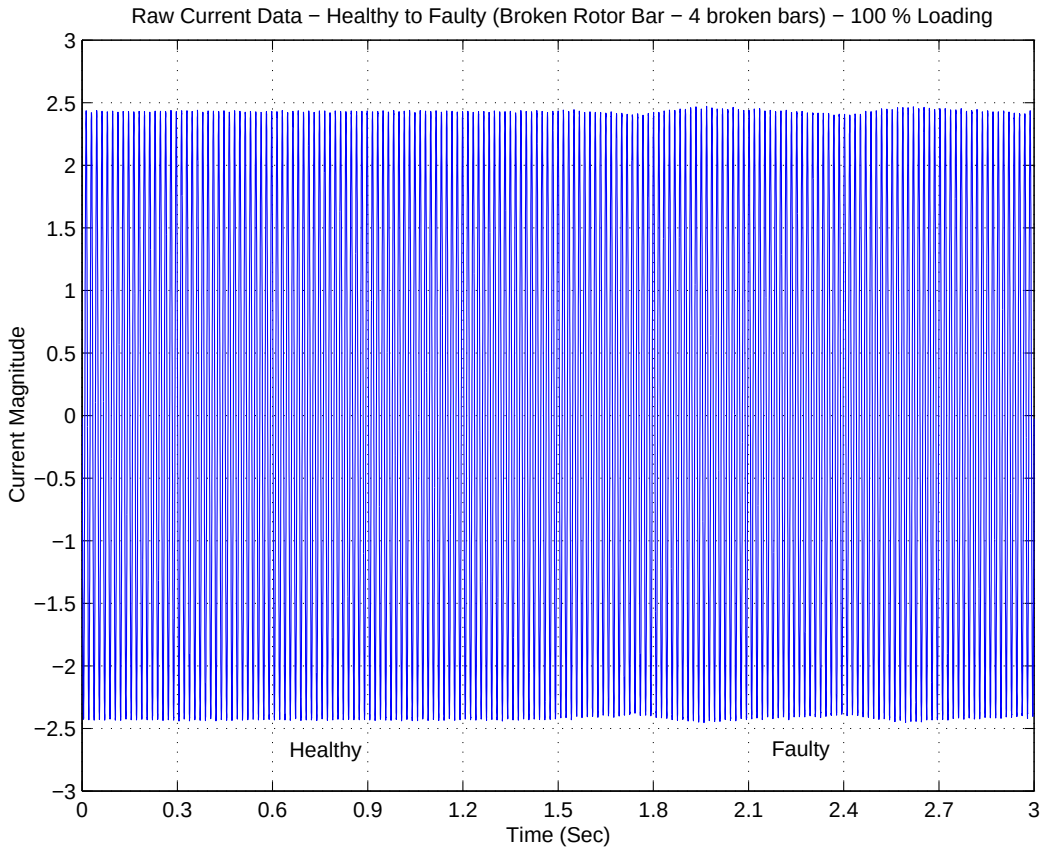

Fig. 86. Raw Current Signal - Four Broken Rotor Bars at 100% Loading

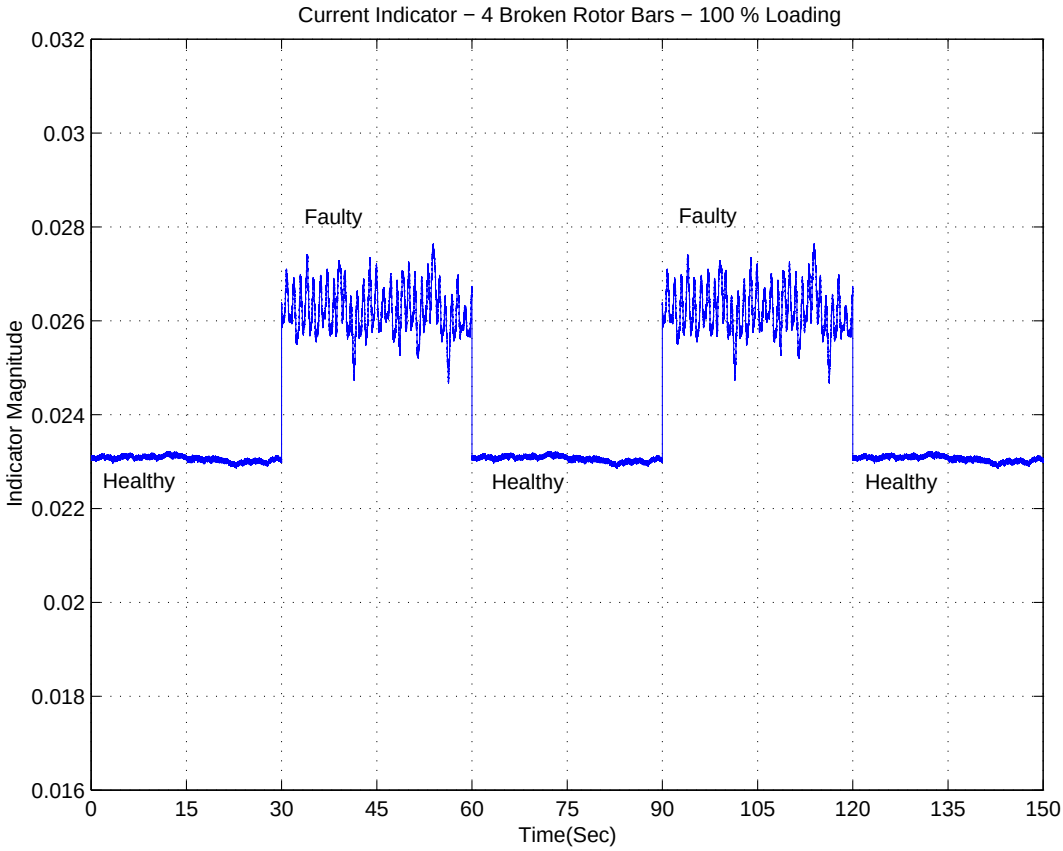

Fig. 87. Current-based Mechanical Indicator - Four Broken Rotor Bars at 100% Loading

Fig. 88. Comparison of Current-based and Vibration-based Mechanical Fault Indicators - Four Broken Rotor Bars at 100% Loading

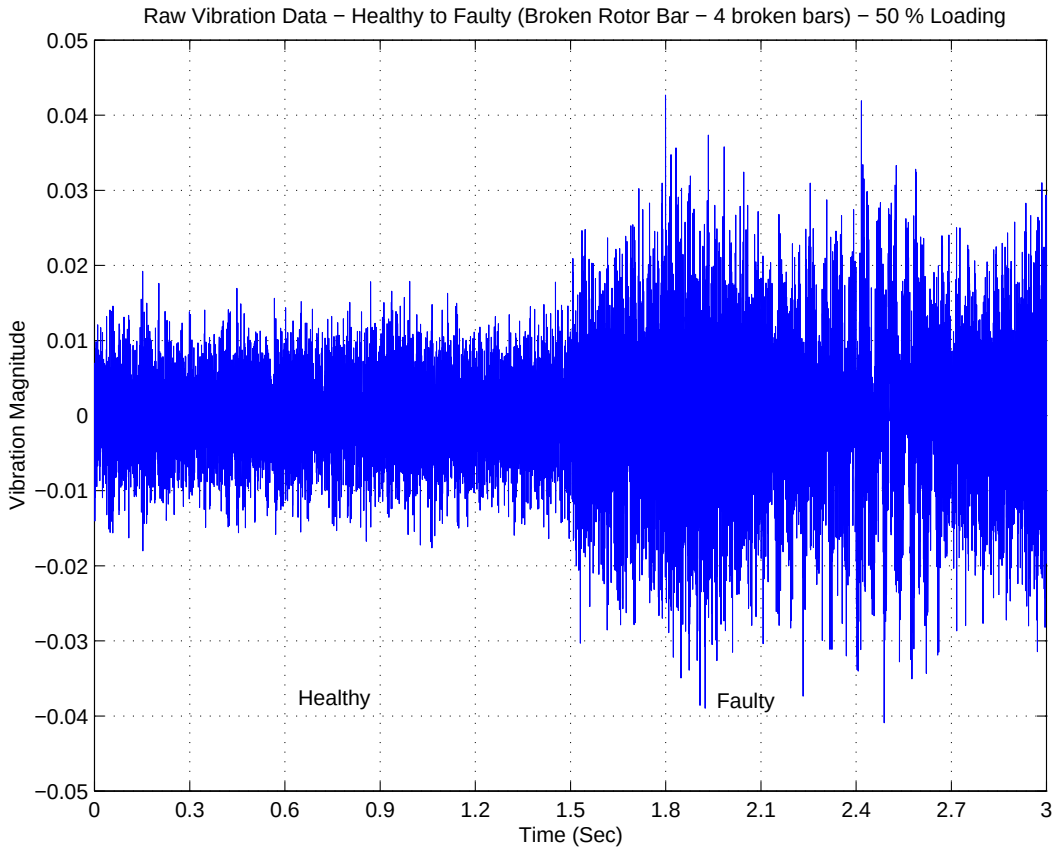

Fig. 89. Raw Vibration Signal - Four Broken Rotor Bars at 50% Loading

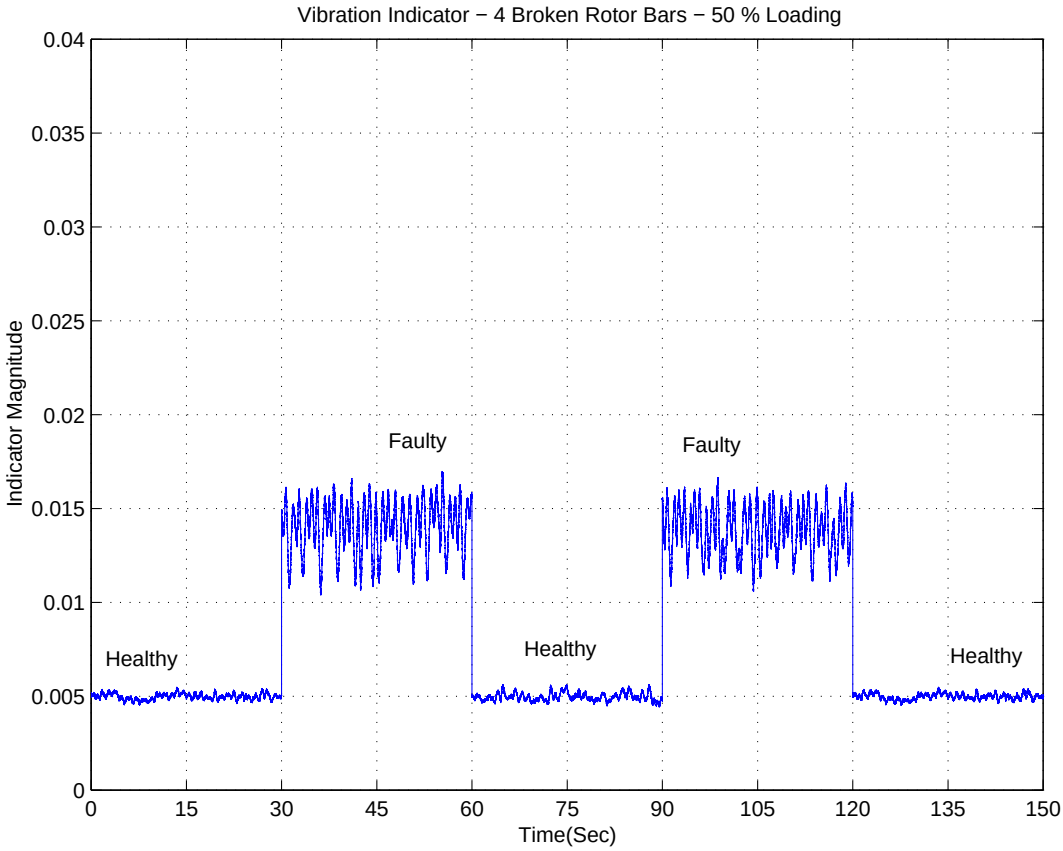

Fig. 90. Vibration-based Mechanical Indicator - Four Broken Rotor Bars at 50% Loading

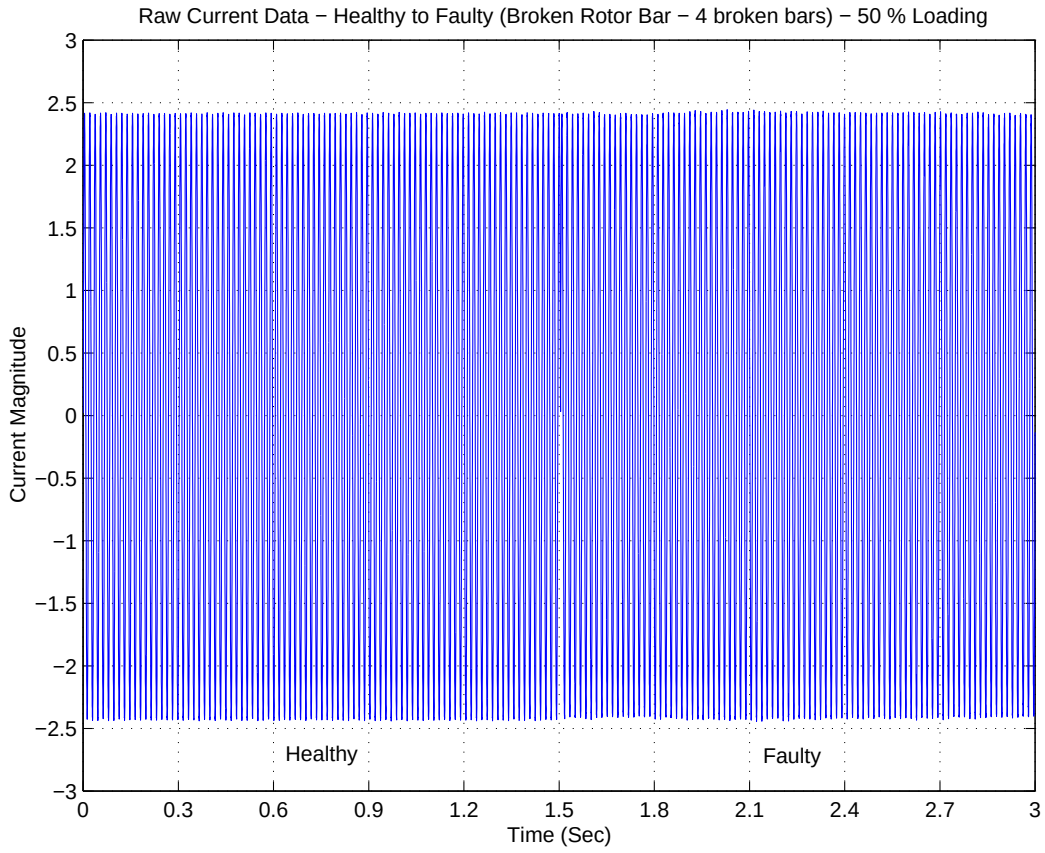

Fig. 91. Raw Current Signal - Four Broken Rotor Bars at 50% Loading

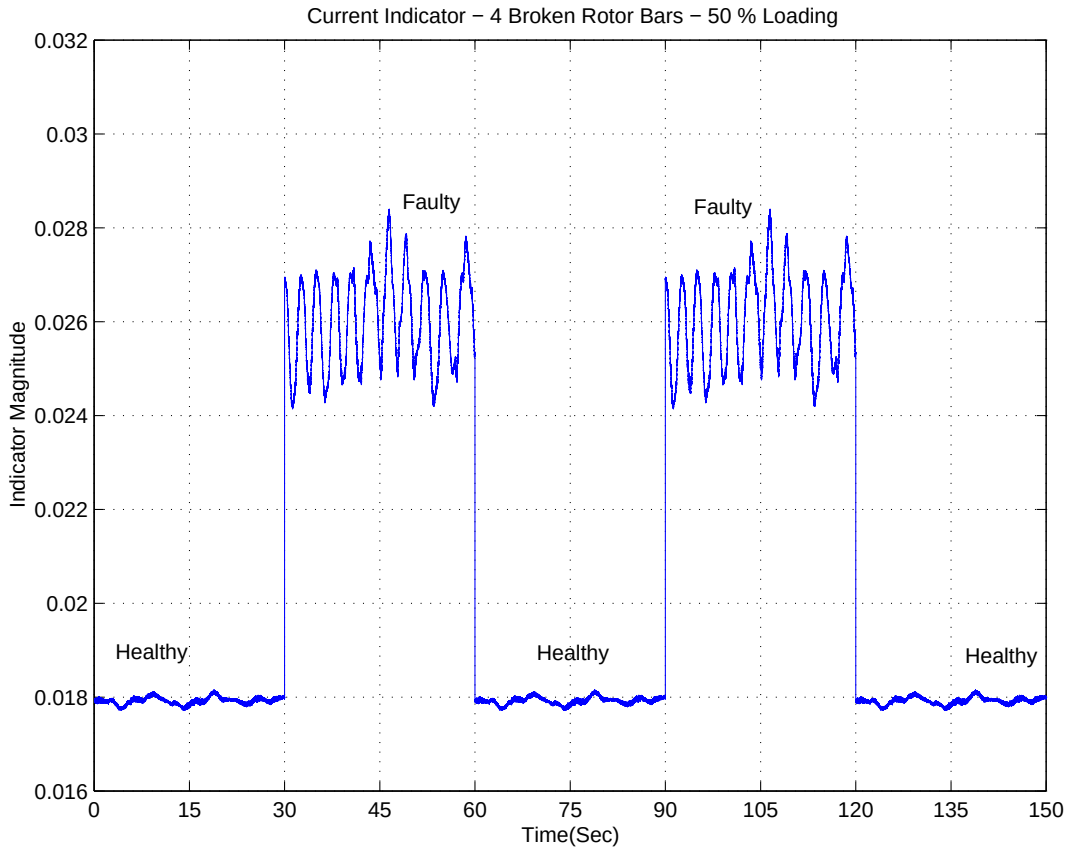

Fig. 92. Current-based Mechanical Indicator - Four Broken Rotor Bars at 50% Loading

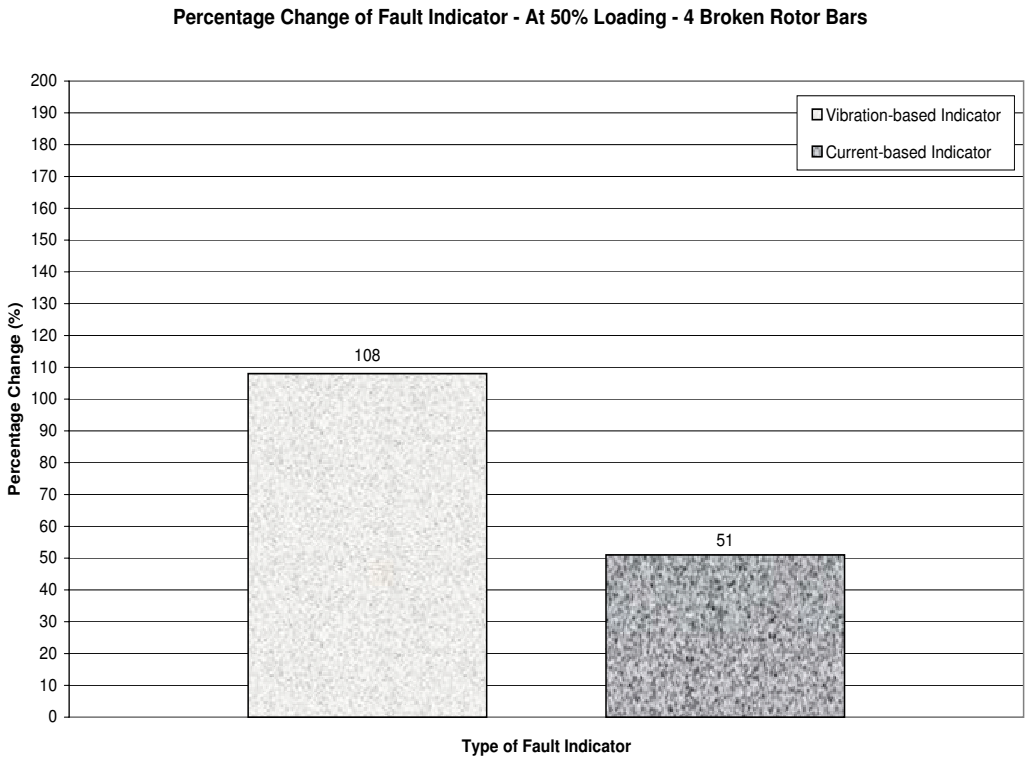

Fig. 93. Comparison of Current-based and Vibration-based Mechanical Fault Indicators - Four Broken Rotor Bars at 50% Loading

To summarize the Fault type (Broken Rotor Bars), we can say that at fully loaded conditions (100% loading level), the mean increases in the current-based indicator from healthy to faulty ranges from about 5% for the minimum severity of fault to about 20% for the maximum severity of fault.This in comparison to the vibration-based indicator (which ranges from 15% to 35%) is substantial. It is also observed that this pattern is more clearly observed at 50% loading than at 100% loading conditions.

C. Fault III: Air-Gap Eccentricity

1. Air-Gap Eccentricity - Case 1

For Eccentricity Case 1, there was an offset set to 25% Up Inboard. The data from experiments conducted with this setting, was compared to data from healthy operating conditions of the same motor. At 100% loading conditions for Eccentricity Case 1, Figures [94]-[98] show the raw vibration signal, vibration-based indicator, raw current signal, current-based indicator and the comparison chart between the two indicators, respectively. Both types of indicators are non-indicative of the fault being present in the system. This can be arrived at by looking at the low values of increase in the levels of the vibration-based indicator (about 4%) and the current-based indicator (about 6%).

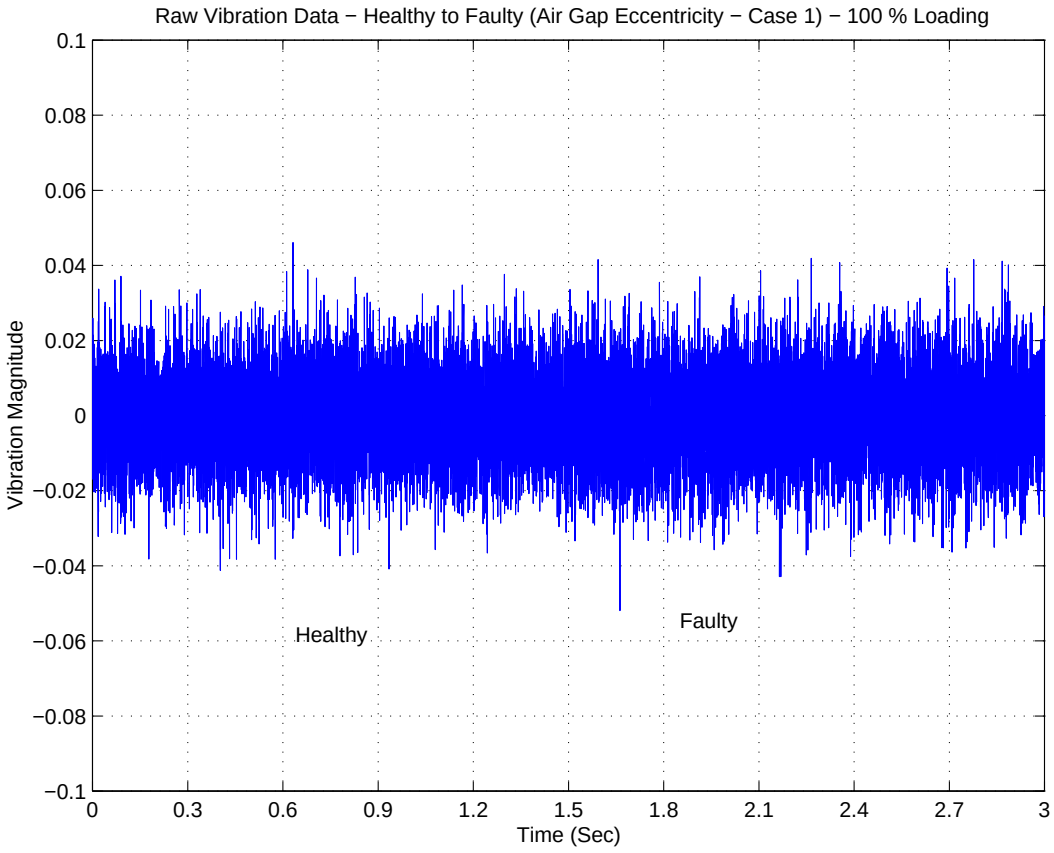

Fig. 94. Raw Vibration Signal - Eccentricity Case 1 at 100% Loading

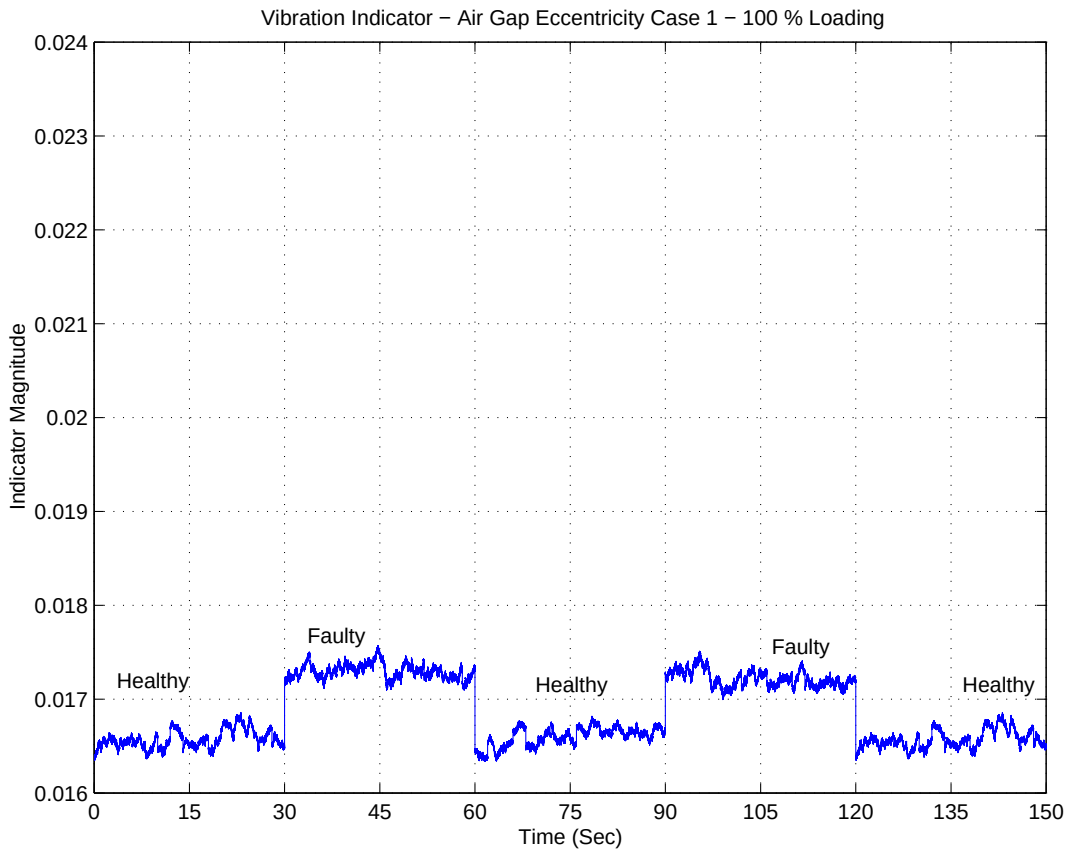

Fig. 95. Vibration-based Mechanical Indicator - Eccentricity Case 1 at 100% Loading

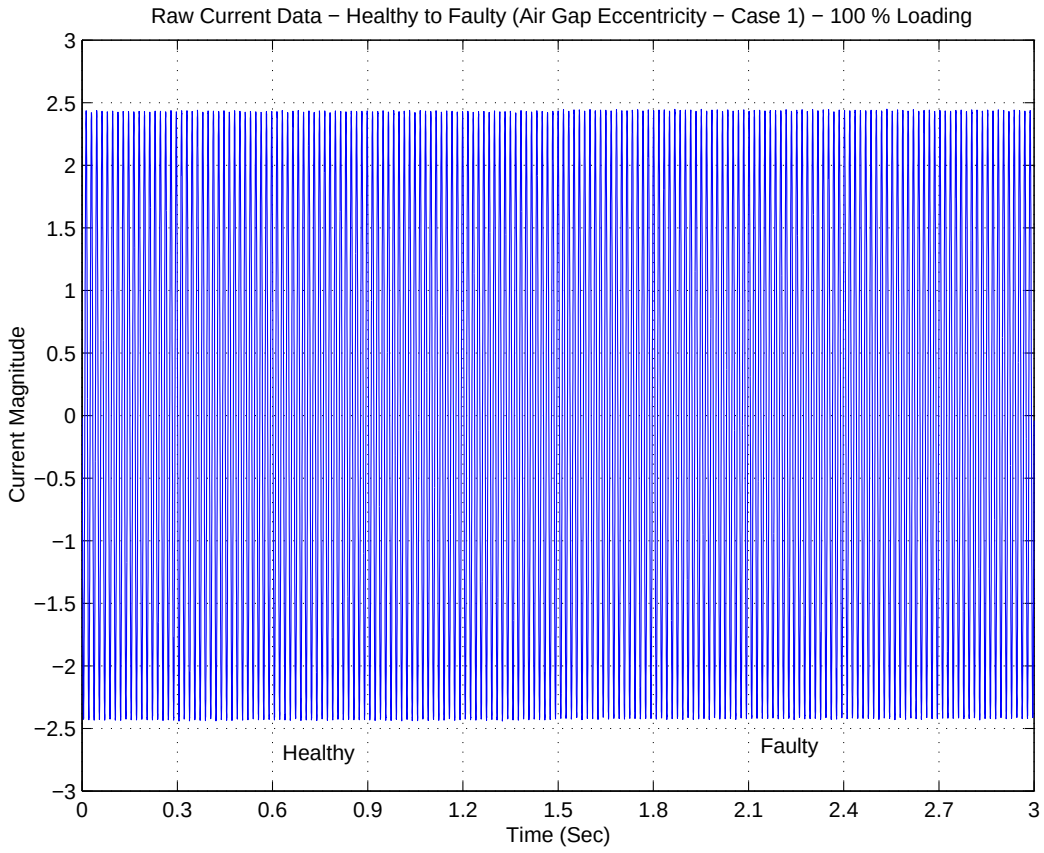

Fig. 96. Raw Current Signal - Eccentricity Case 1 at 100% Loading

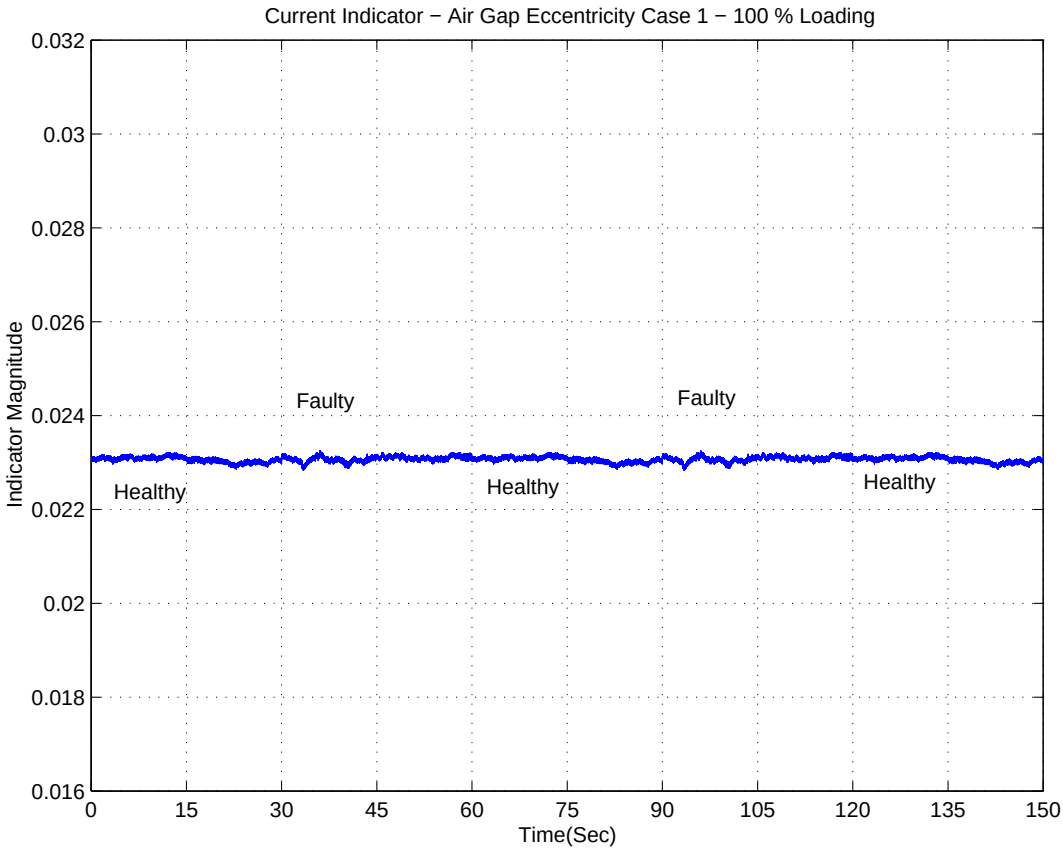

Fig. 97. Current-based Mechanical Indicator - Eccentricity Case 1 at 100% Loading

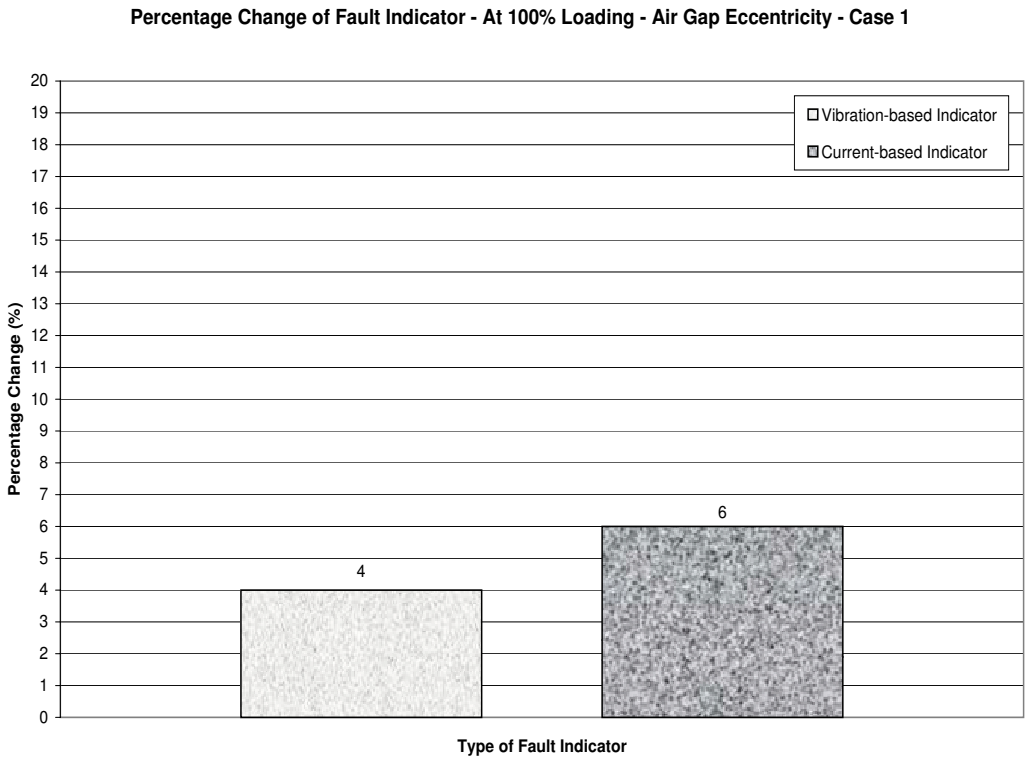

Fig. 98. Comparison of Current-based and Vibration-based Mechanical Fault Indicators - Eccentricity Case 1 at 100% Loading

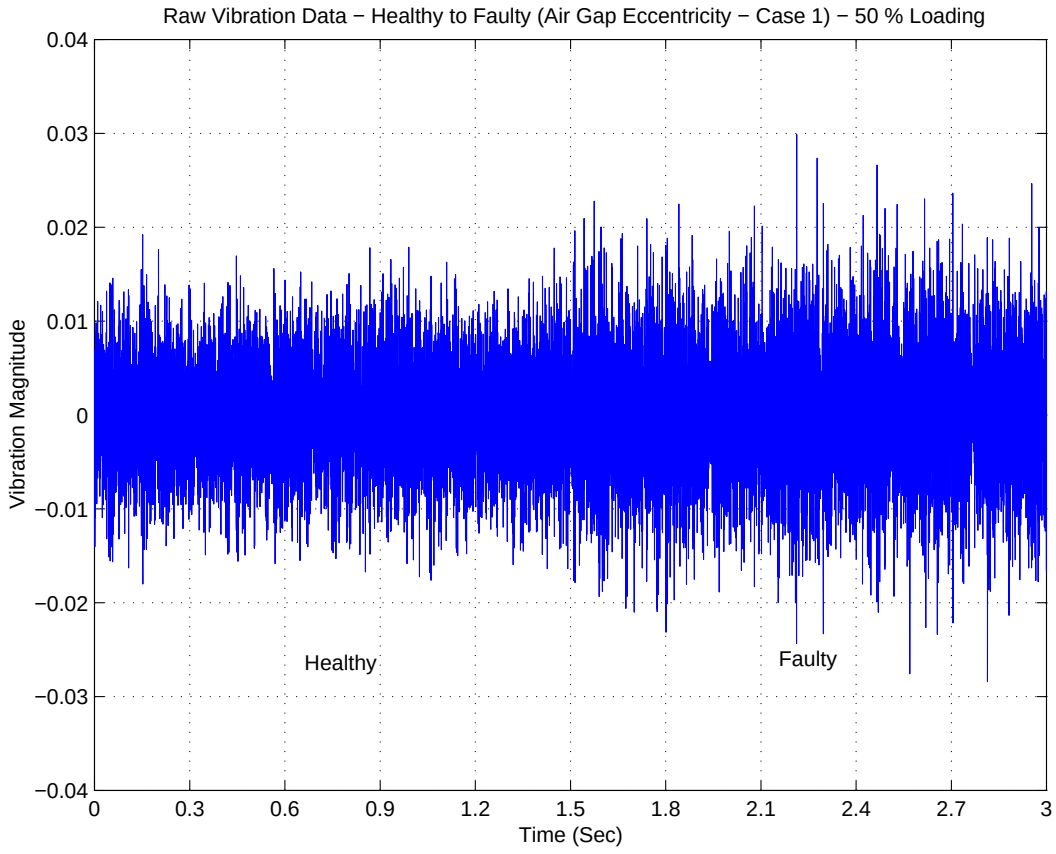

Fig. 99. Raw Vibration Signal - Eccentricity Case 1 at 50% Loading

At 50% loading for Eccentricity Case 1, Figures [99]-[103] show the raw vibration signal, vibration-based indicator, raw current signal, current-based indicator and the comparison chart between the two indicators, respectively. We can observe an increase in the magnitudes of fault indicators as compared to those obtained at 100% loading. While the increase in the vibration-based indicator is about 35.3%, the current-based indicator increases by about 38.2%. We can hence observe that for this case of eccentricity, at both levels of loading, the increases in both the indicator values are about the same.

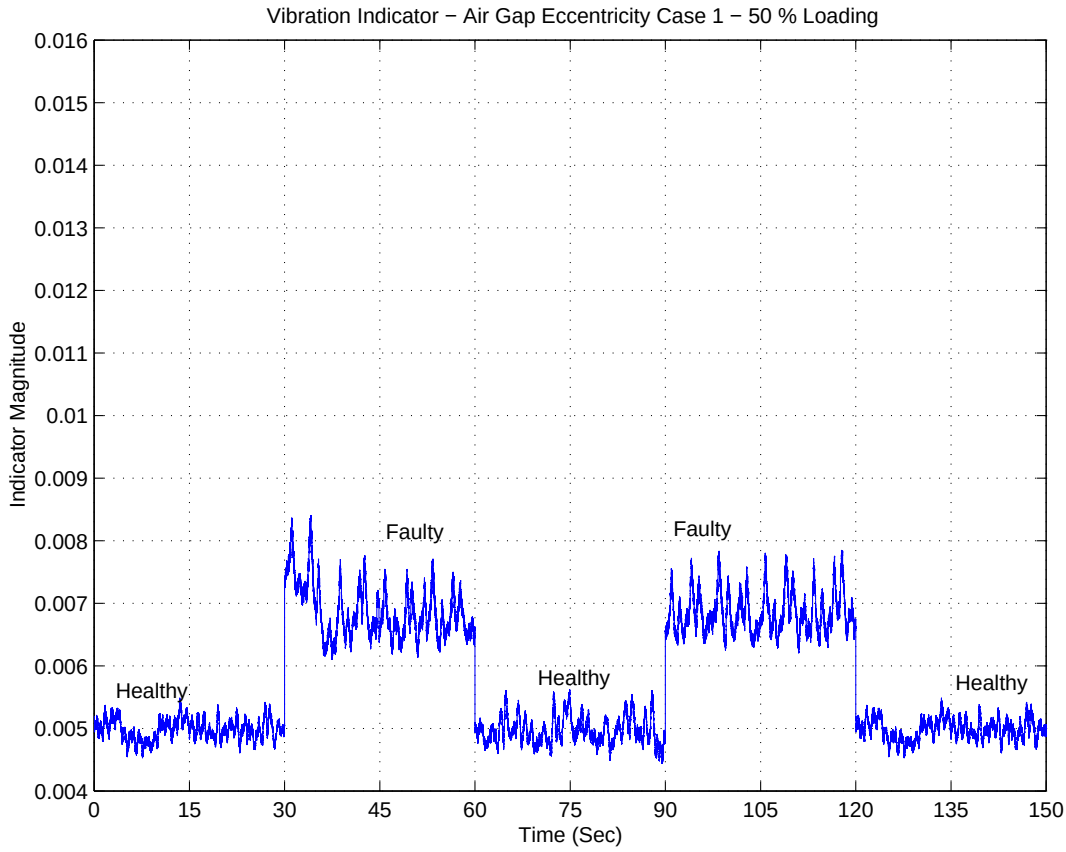

Fig. 100. Vibration-based Mechanical Indicator - Eccentricity Case 1 at 50% Loading

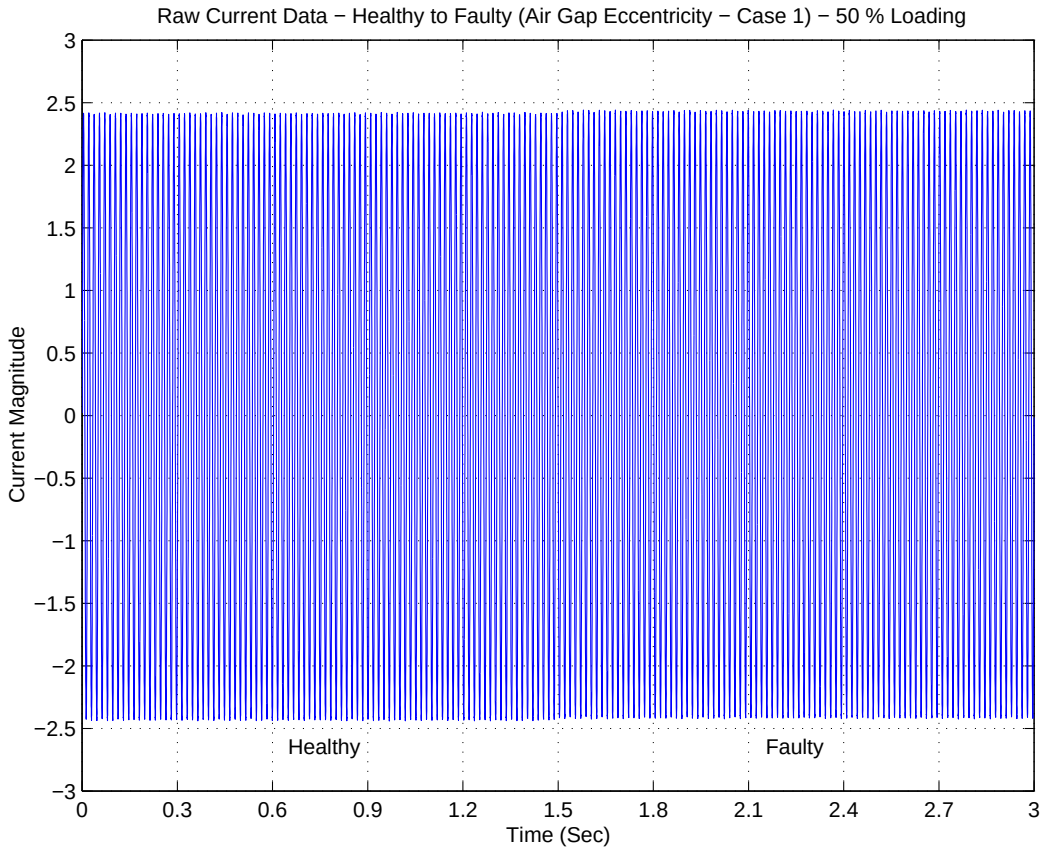

Fig. 101. Raw Current Signal - Eccentricity Case 1 at 50% Loading

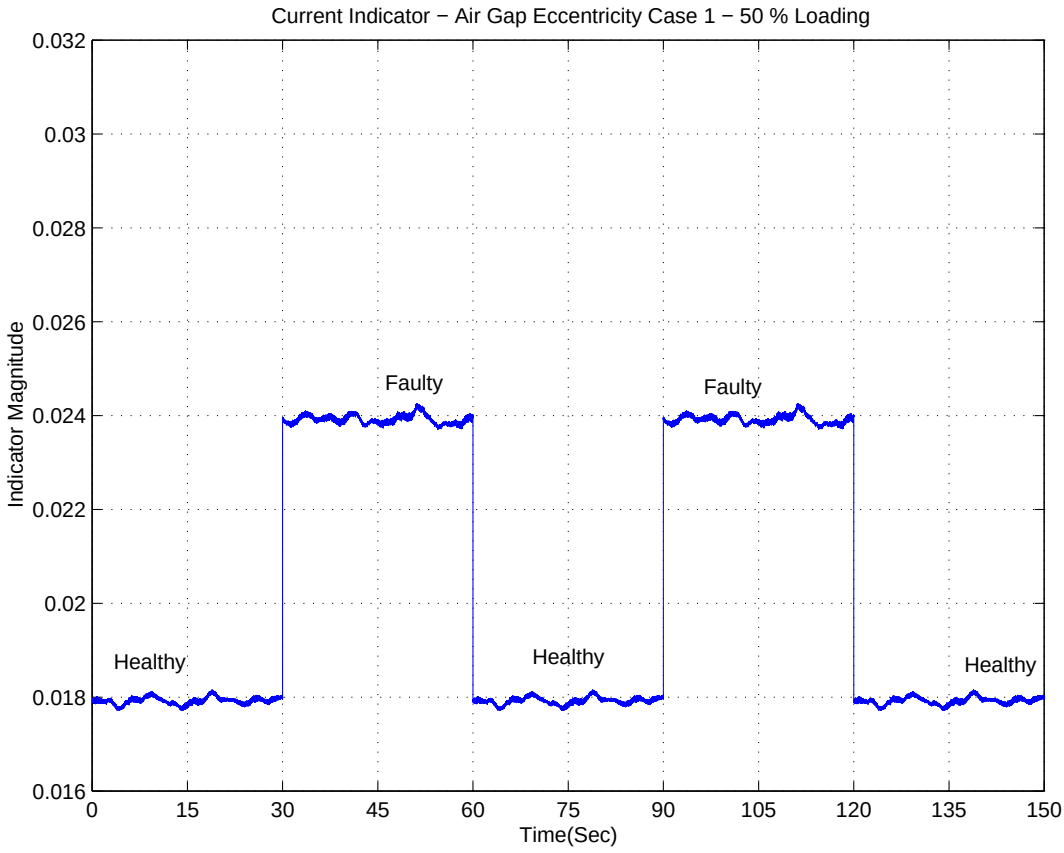

Fig. 102. Current-based Mechanical Indicator - Eccentricity Case 1 at 50% Loading

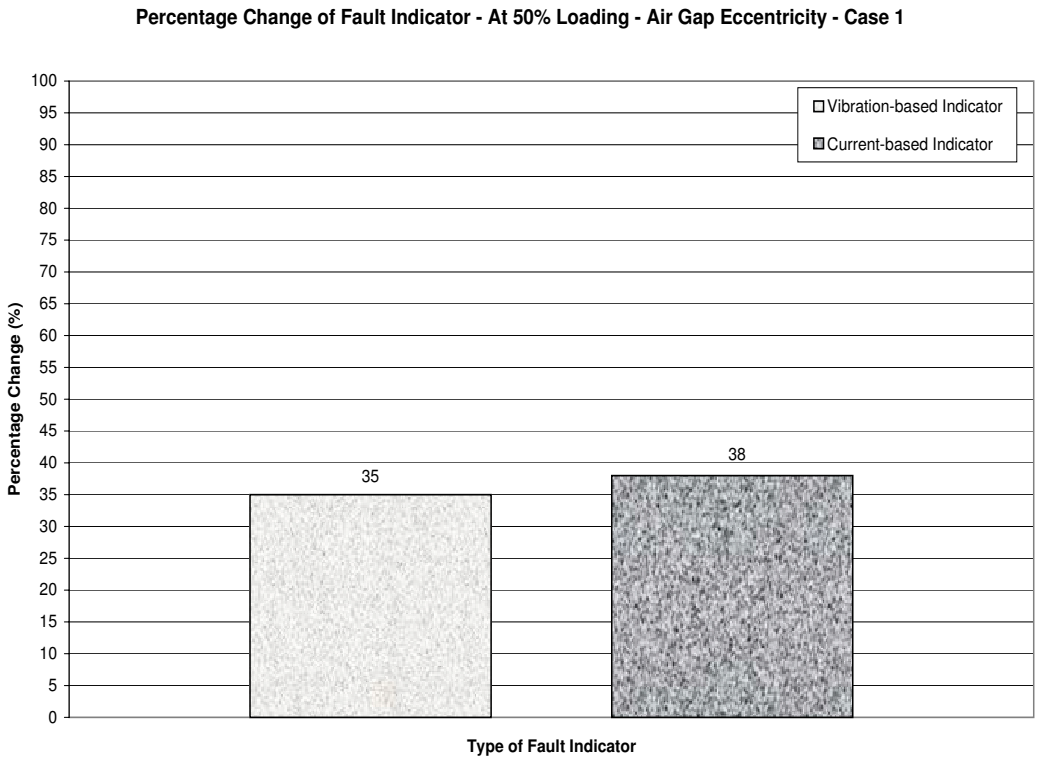

Fig. 103. Comparison of Current-based and Vibration-based Mechanical Fault Indicators - Eccentricity Case 1 at 50% Loading

2. Air-Gap Eccentricity - Case 2

For Eccentricity Case 2, there was an offset set to 20% Down 10% Right Outboard and 25% Up Inboard. The data from experiments conducted with this setting, was compared to data from healthy operating conditions of the same motor. At 100% loading conditions for Eccentricity Case 2, Figures [104]-[108] show the raw vibration signal, vibration-based indicator, raw current signal, current-based indicator and the comparison chart between the two indicators, respectively. Similar to Eccentricity Case 1 both types of indicators are non-indicative of the fault being present in the system (about 5.7% increase in the vibration-based indicator level about 5.4% increase in the current-based indicator level).

At 50% loading for Eccentricity Case 2, Figures [109]-[113] show the raw vibration signal, vibration-based indicator, raw current signal, current-based indicator and the comparison chart between the two indicators, respectively. We can observe an increase in the magnitudes of fault indicators as compared to those obtained at 100% loading. While the increase in the vibration-based indicator is about 62.9%, the current indicator-based increases by about 37.8%. We can observe that for this case, at 100% loading, the increases in both the indicator values are about the same. On lesser loading, the relative increase in the electrical indicator is about 50% as compared to the increase of the mechanical indicator.

For this fault type (Air-gap Eccentricity), we could see that at high levels of loading, the fault signatures are weak and it is hence very difficult to see a significant increase in the fault indicator levels. This is observed for both types of indicators. However, at lower levels of loading, we can see a significant increase in the vibration-based indicator and a reasonable increase in the current-based indicator.

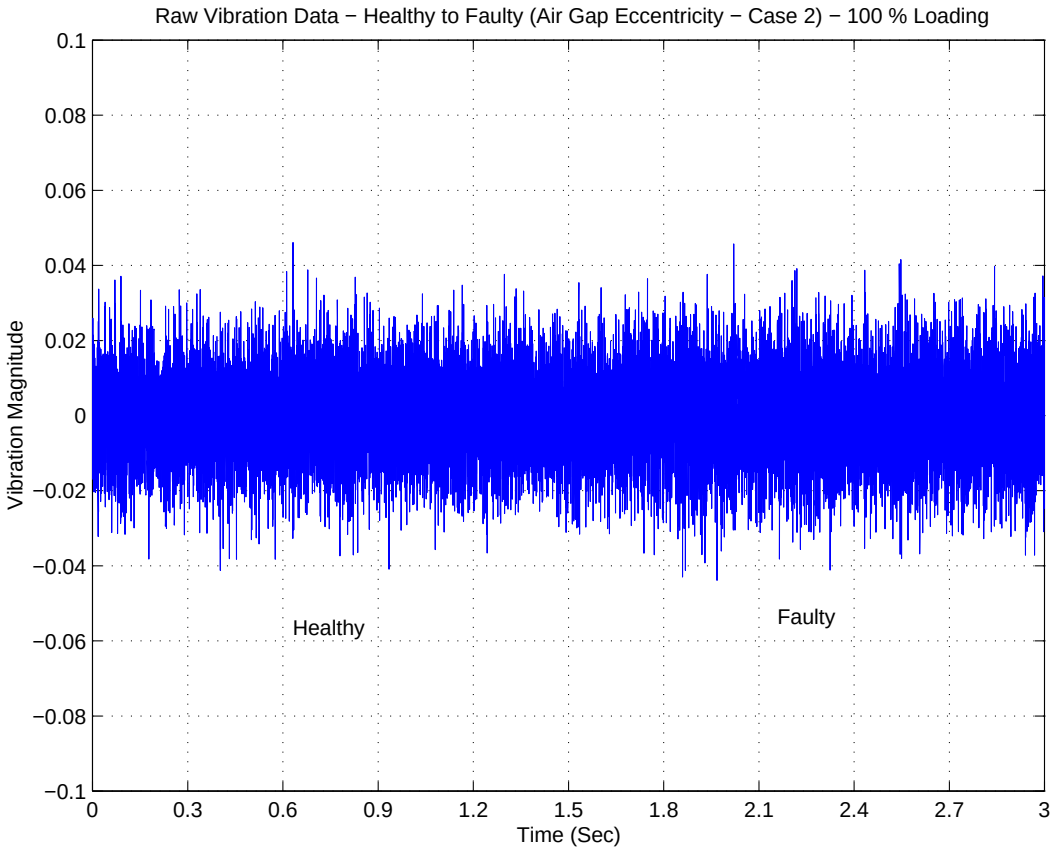

Fig. 104. Raw Vibration Signal - Eccentricity Case 2 at 100% Loading

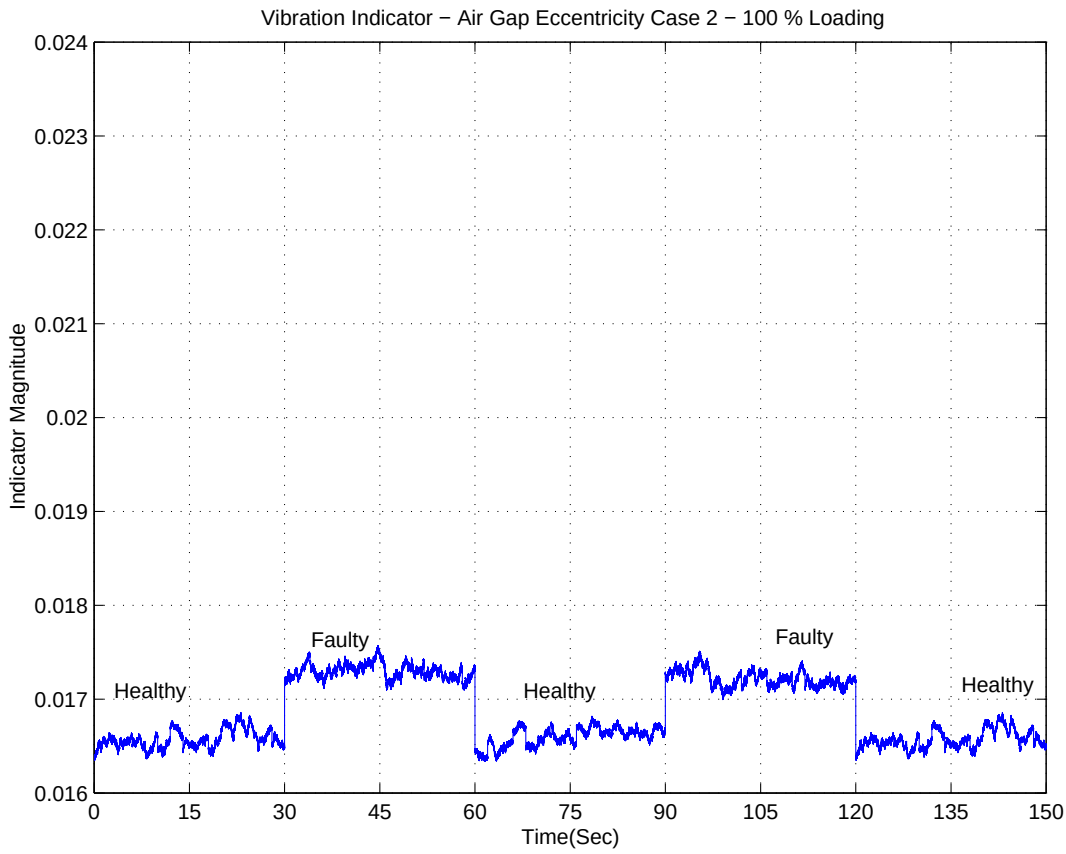

Fig. 105. Vibration-based Mechanical Indicator - Eccentricity Case 2 at 100% Loading

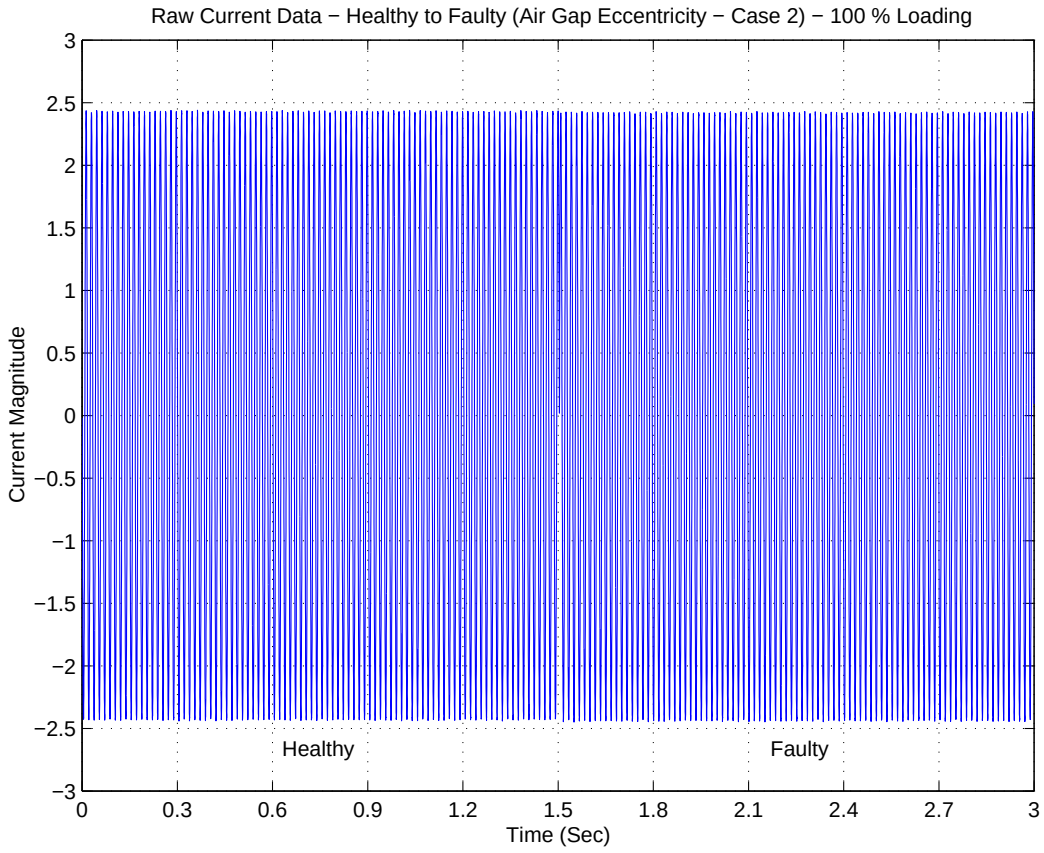

Fig. 106. Raw Current Signal - Eccentricity Case 2 at 100% Loading

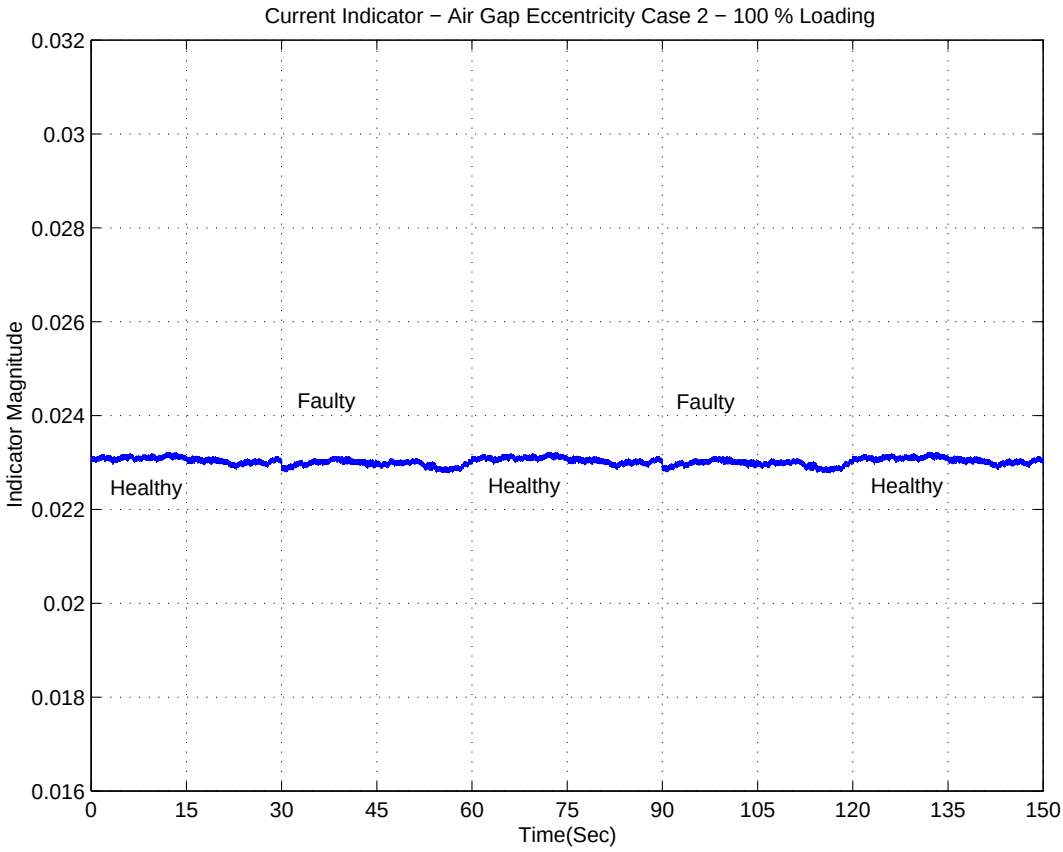

Fig. 107. Current-based Mechanical Indicator - Eccentricity Case 2 at 100% Loading

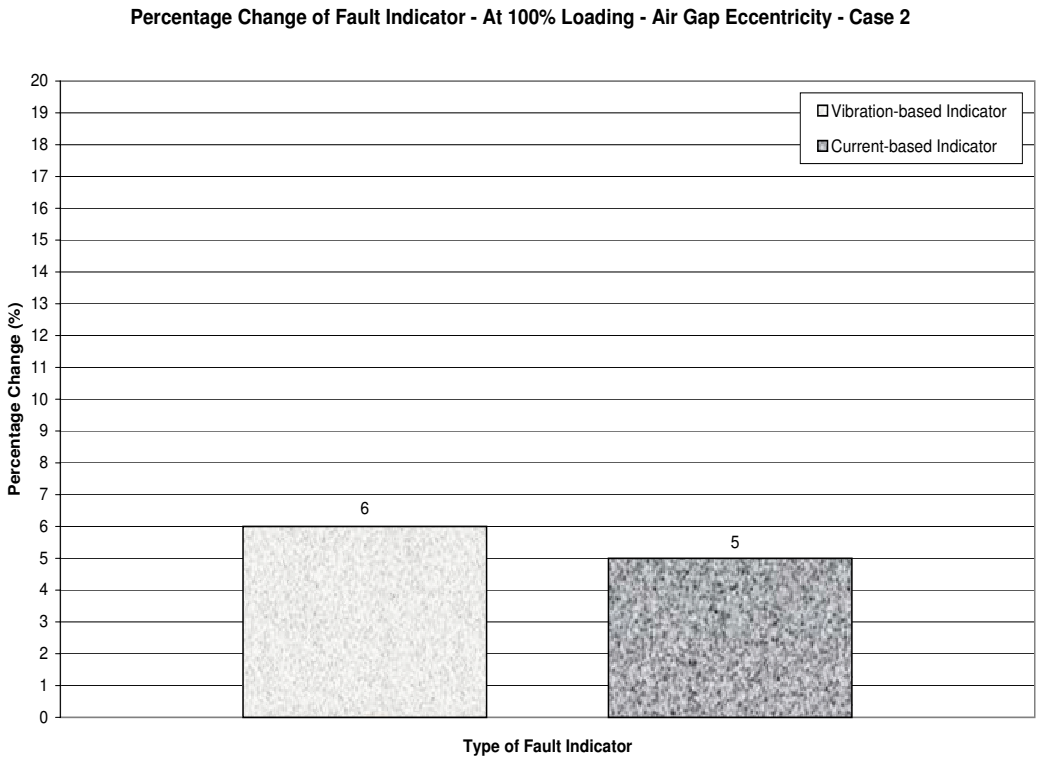

Fig. 108. Comparison of Current-based and Vibration-based Mechanical Fault Indicators - Eccentricity Case 2 at 100% Loading

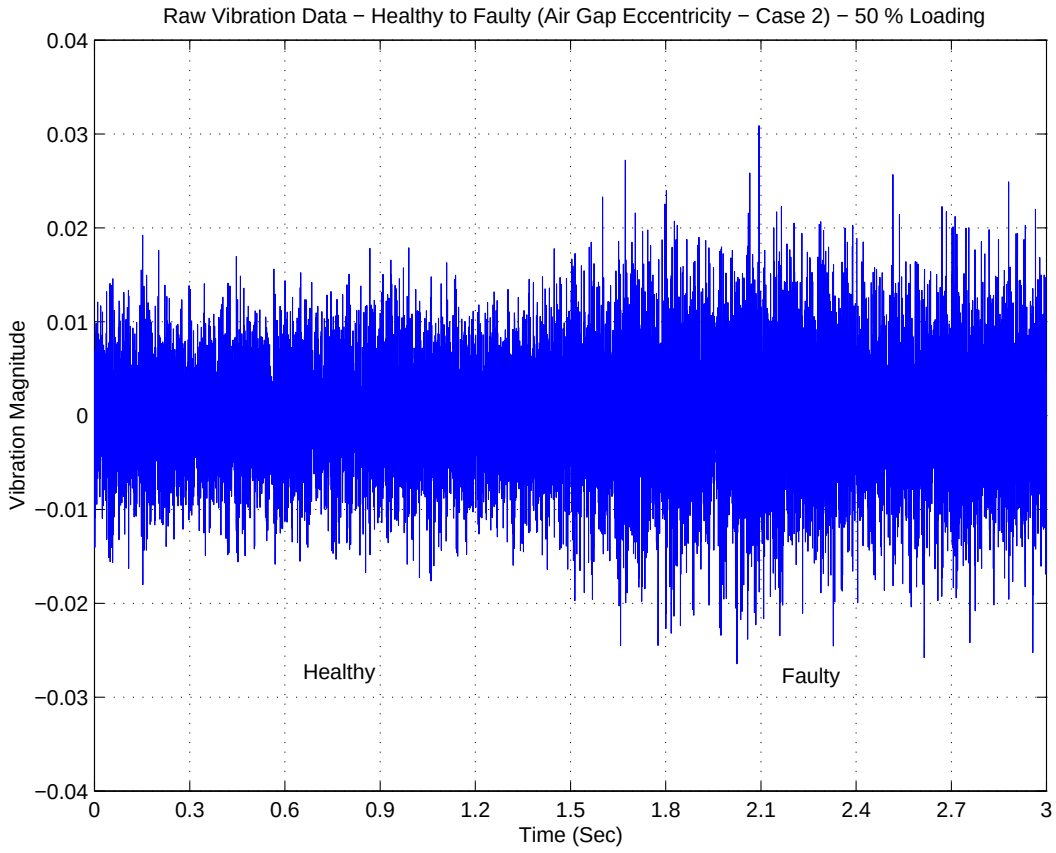

Fig. 109. Raw Vibration Signal - Eccentricity Case 2 at 50% Loading

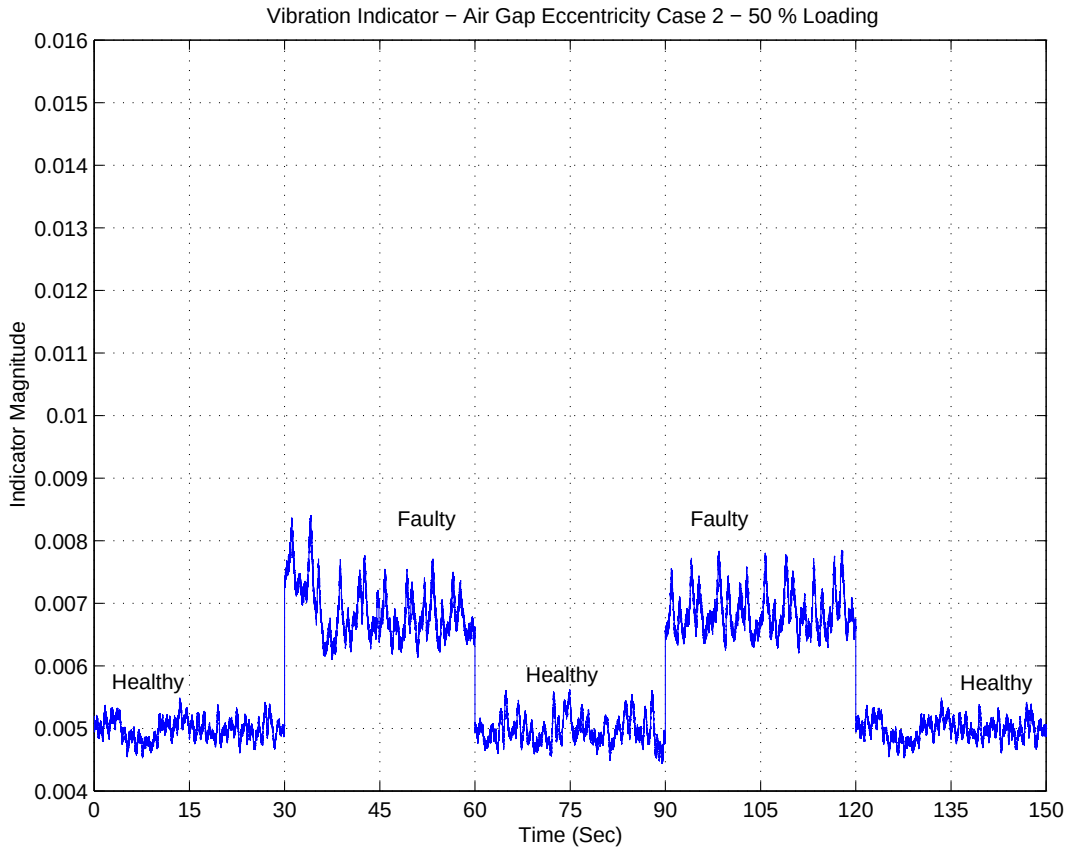

Fig. 110. Vibration-based Mechanical Indicator - Eccentricity Case 2 at 50% Loading

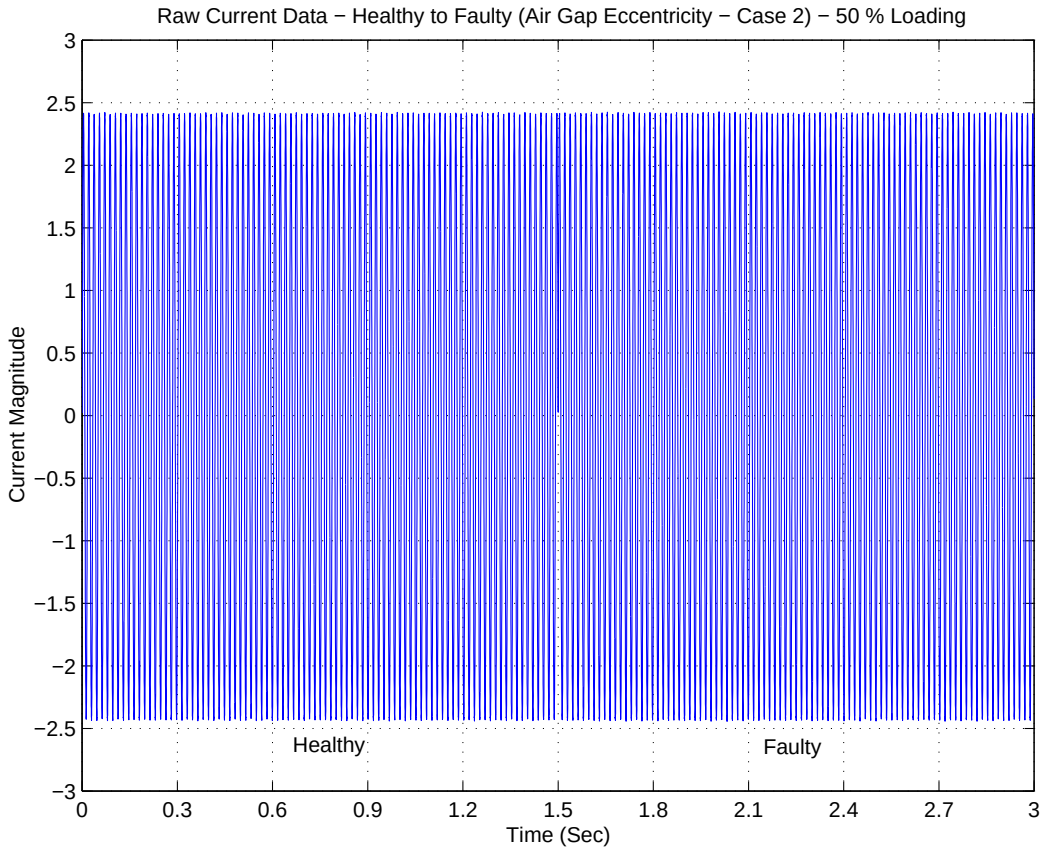

Fig. 111. Raw Current Signal - Eccentricity Case 2 at 50% Loading

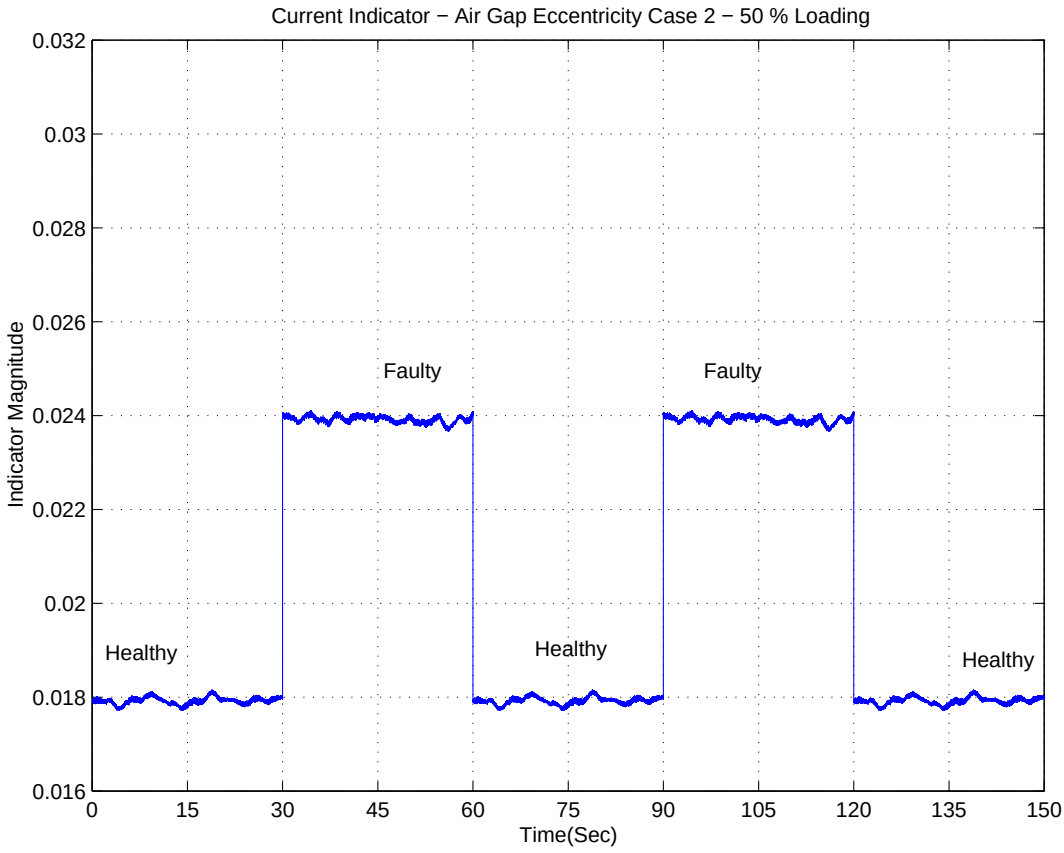

Fig. 112. Current-based Mechanical Indicator - Eccentricity Case 2 at 50% Loading

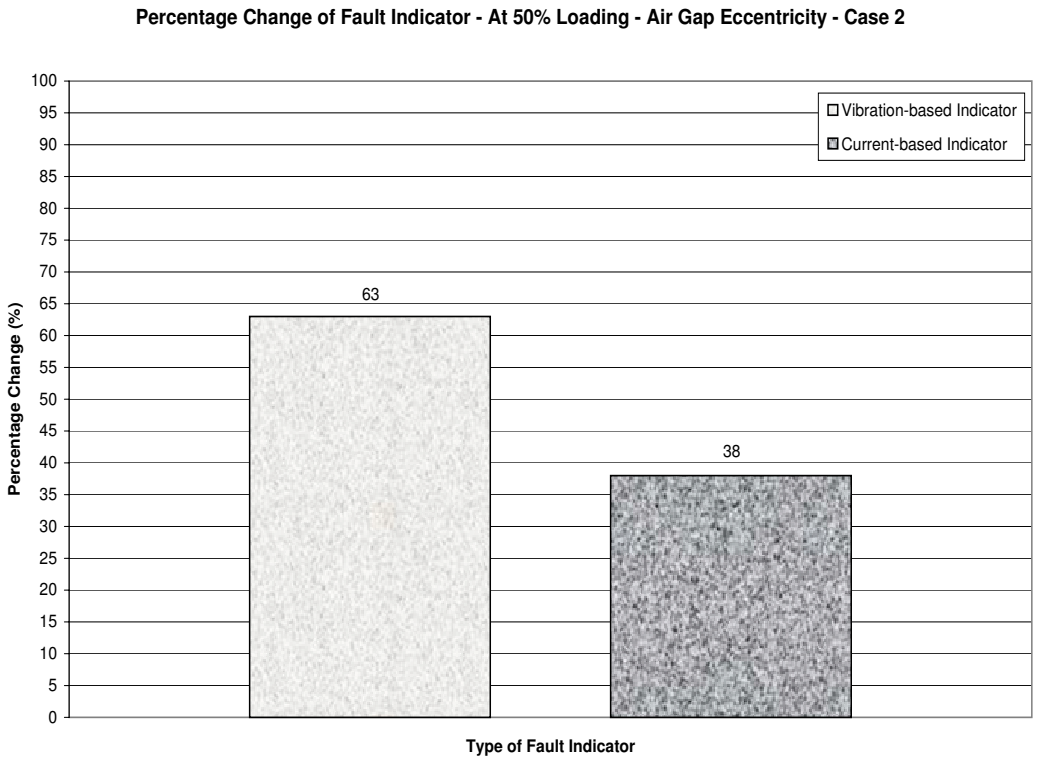

Fig. 113. Comparison of Current-based and Vibration-based Mechanical Fault Indicators - Eccentricity Case 2 at 50% Loading

D. Fault IV: Mechanical Imbalance

This experiments for this fault type was conducted on a 500 HP motor. The data obtained from a healthy condition of the motor is taken as the baseline (as in the analysis of the other fault types), and is compared with a mechanically unbalanced condition of the motor (unbalanced rotor). At 100% loading for the Imbalance Case, Figures [114]-[118] show the raw vibration signal, vibration-based indicator, raw current signal, current-based indicator and the comparison chart between the two indicators, respectively. It is observed that the vibration-based indicator level increases by about 11.5%, and there is almost no increase in the current-based indicator level (about 2%). Although there is a little increase in the vibration-based indicator level, it is not clearly indicative when one only looks at the raw vibration signals.

At 50% loading for the Imbalance Case, Figures [119]-[123] show the raw vibration signal, vibration-based indicator, raw current signal, current-based indicator and the comparison chart between the two indicators, respectively. Both the electrical and the mechanical fault signatures are more indicative of the fault present in the system. While there is about 85% increase in the vibration level from the mean healthy level of vibration, there is about 30% increase in the level of the current-based indicator. Hence, we can see that there is a 35% relative increase of the current-based indicator in comparison to the increase of the vibration-based indicator.

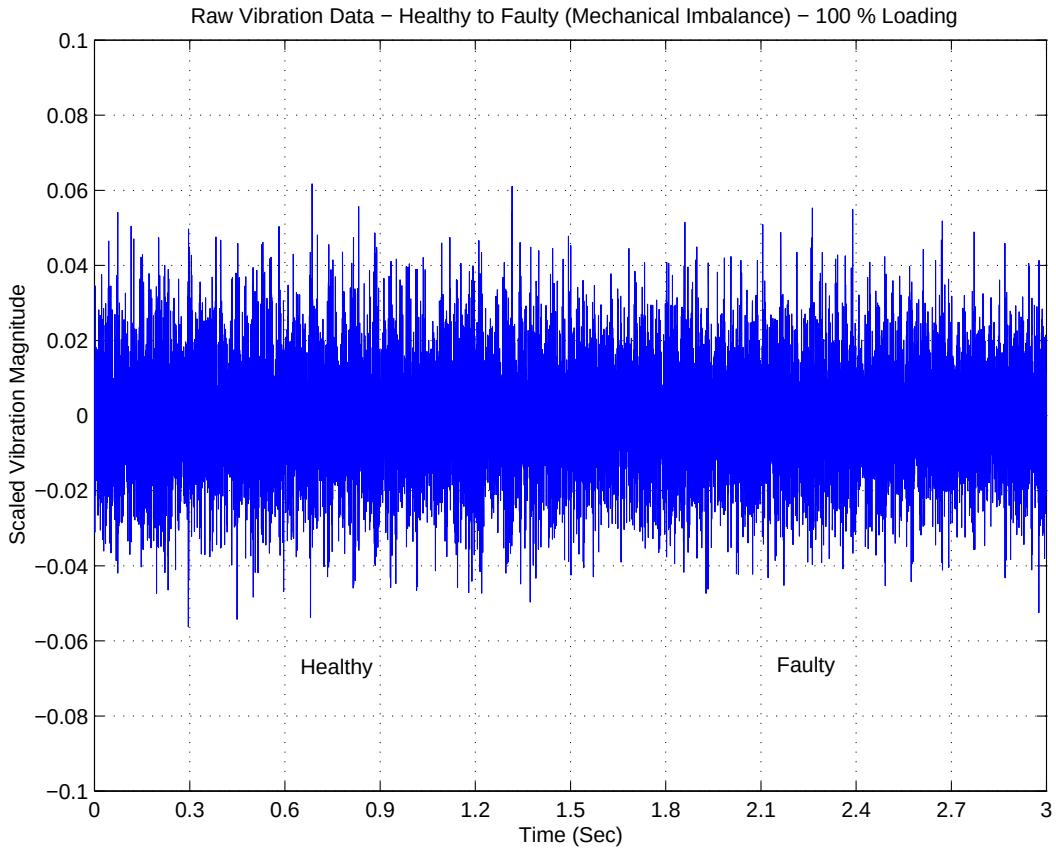

Fig. 114. Raw Vibration Signal - Mechanical Imbalance - at 100% Loading

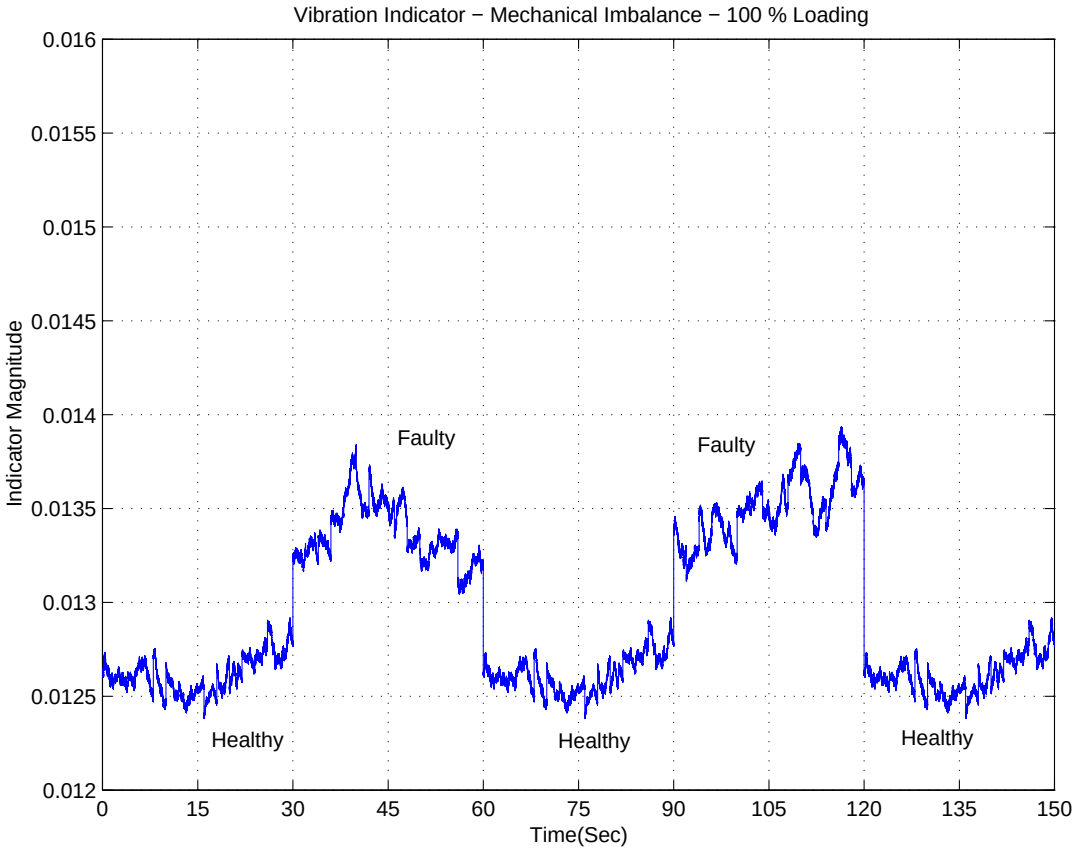

Fig. 115. Vibration-based Mechanical Indicator - Mechanical Imbalance at 100% Loading

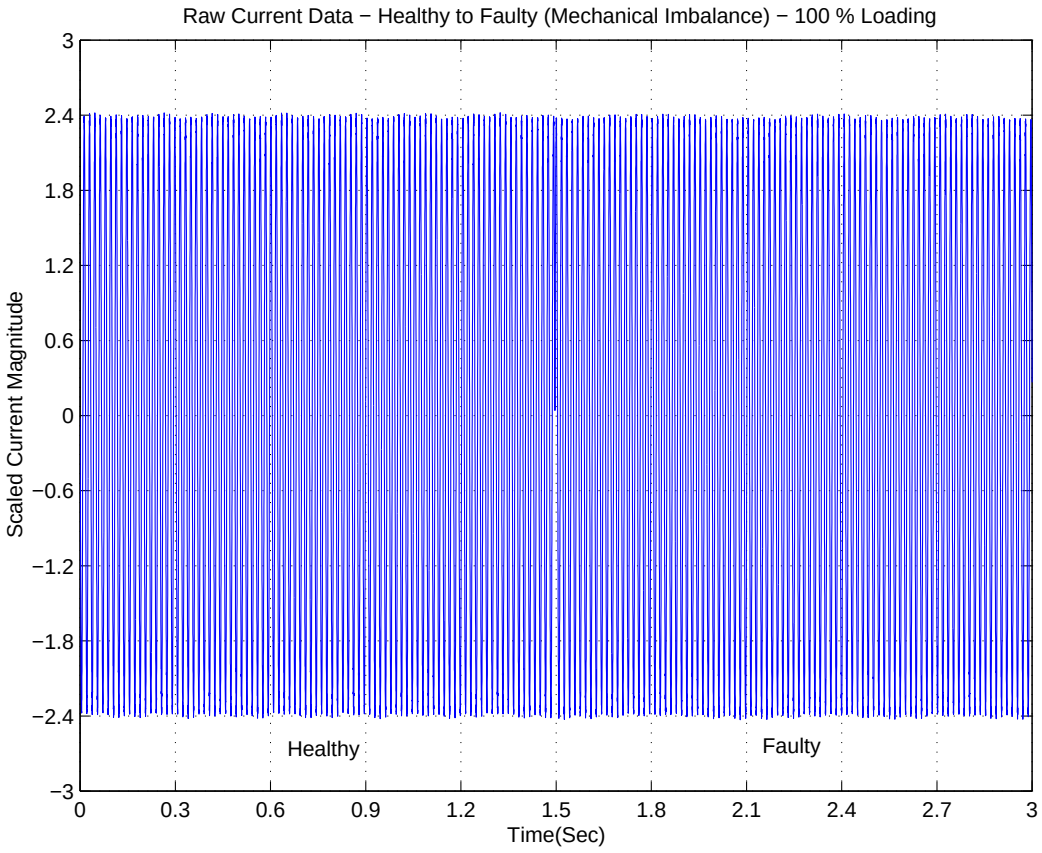

Fig. 116. Raw Current Signal - Mechanical Imbalance at 100% Loading

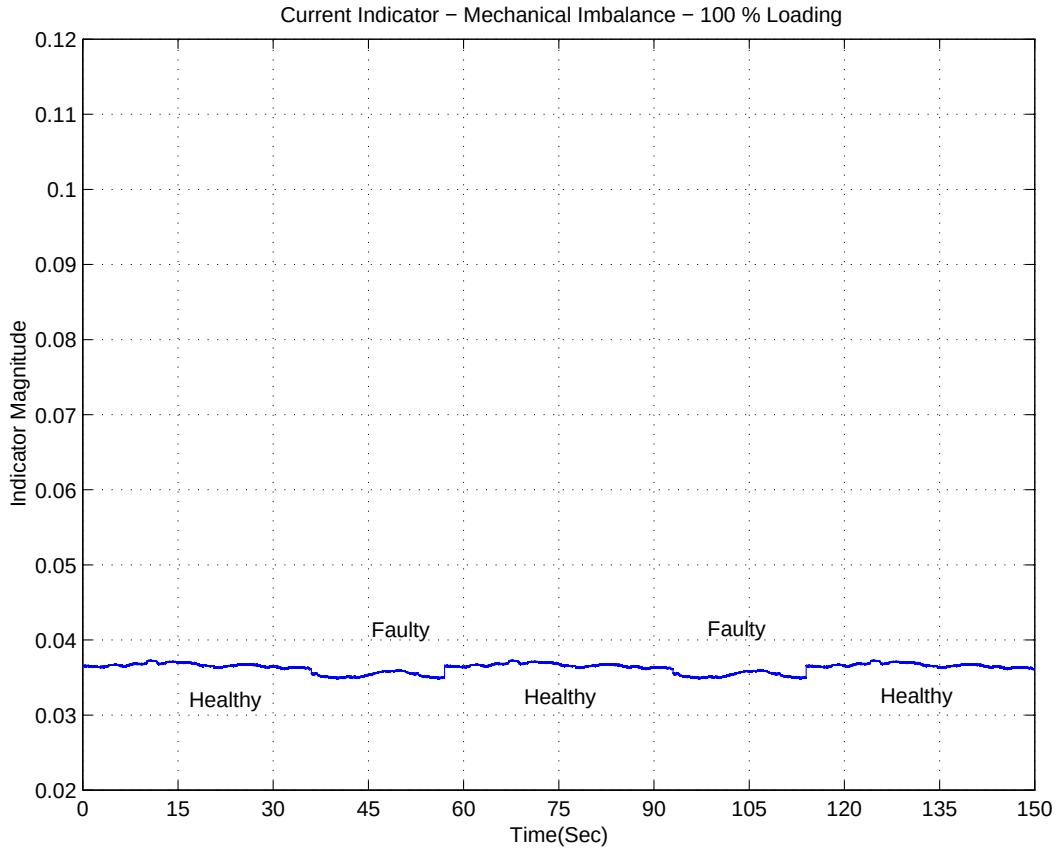

Fig. 117. Current-based Mechanical Indicator - Mechanical Imbalance at 100% Loading

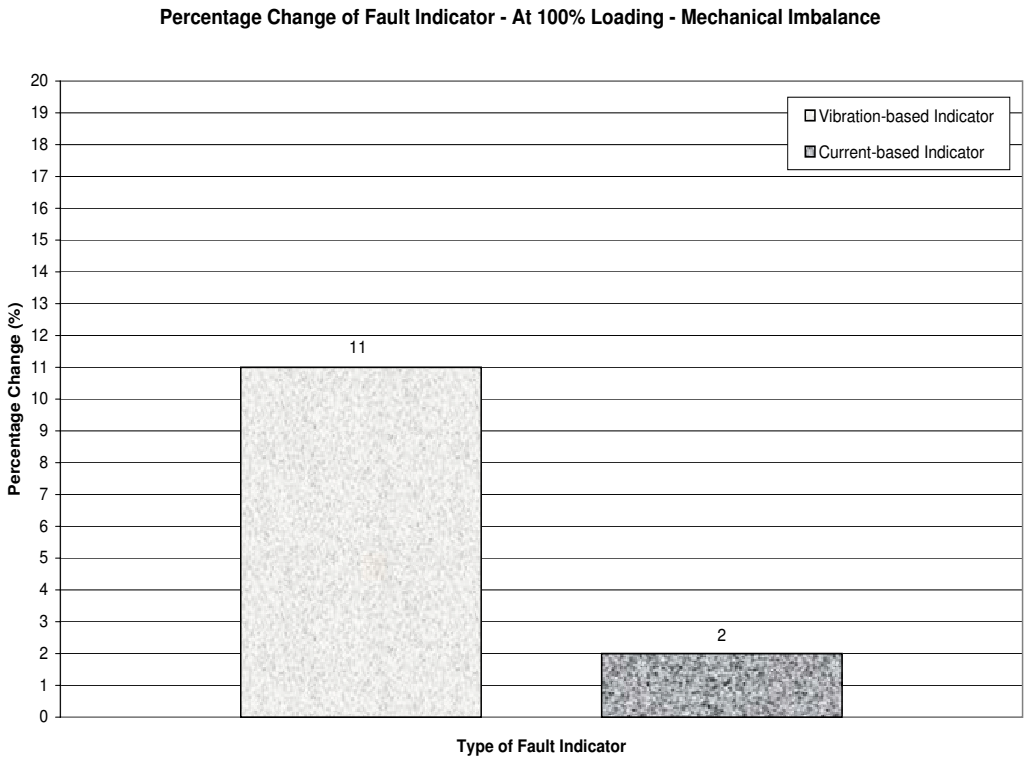

Fig. 118. Comparison of Current-based and Vibration-based Mechanical Fault Indicators - Mechanical Imbalance at 100% Loading

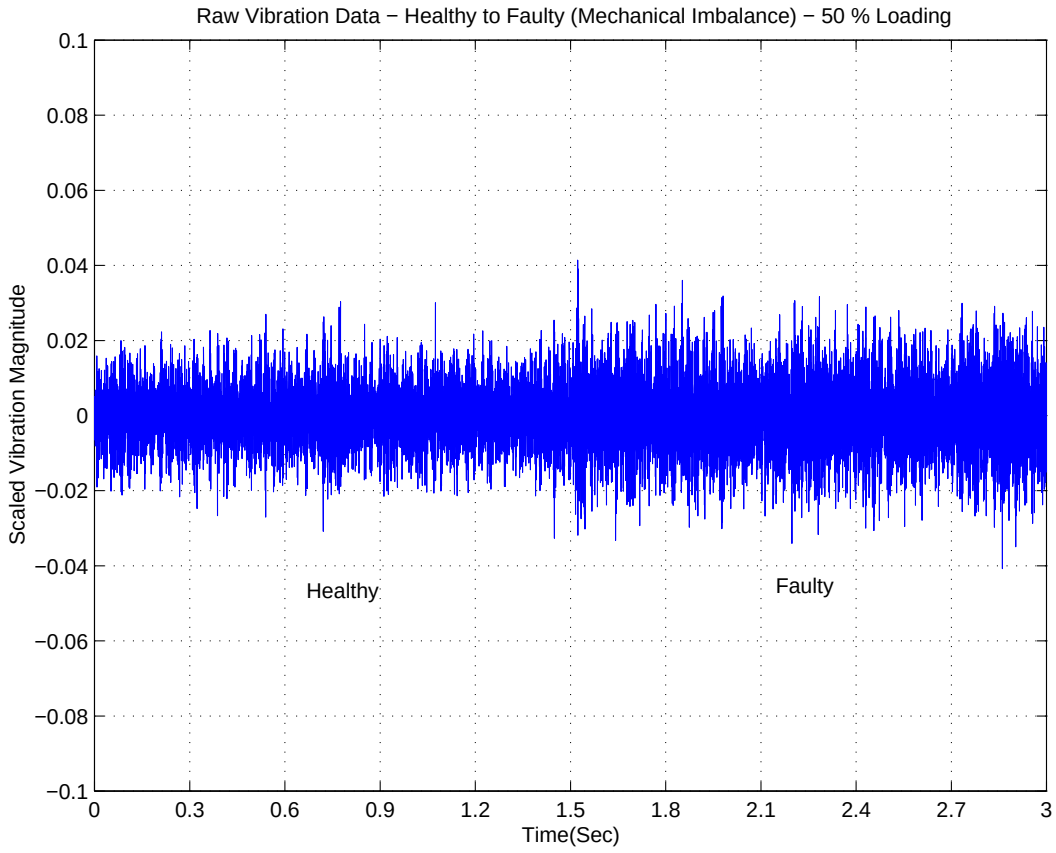

Fig. 119. Raw Vibration Signal - Mechanical Imbalance at 50% Loading

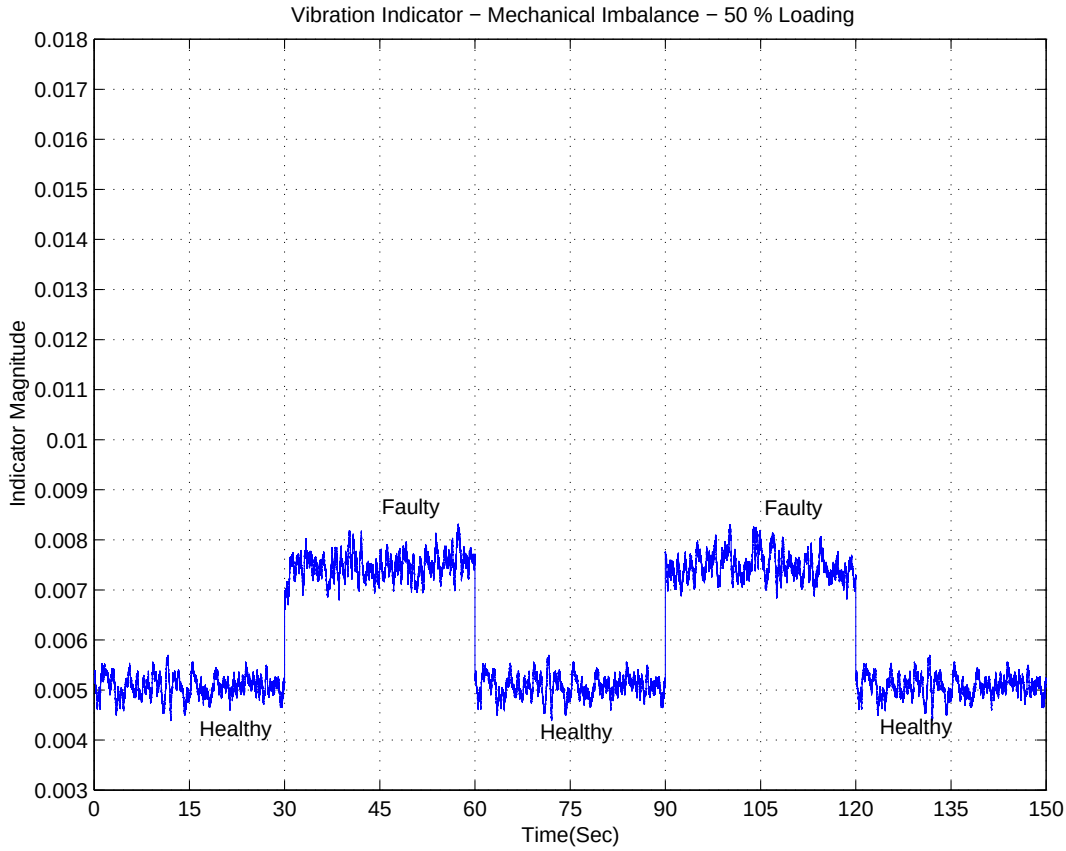

Fig. 120. Vibration-based Mechanical Indicator - Mechanical Imbalance at 50% Loading

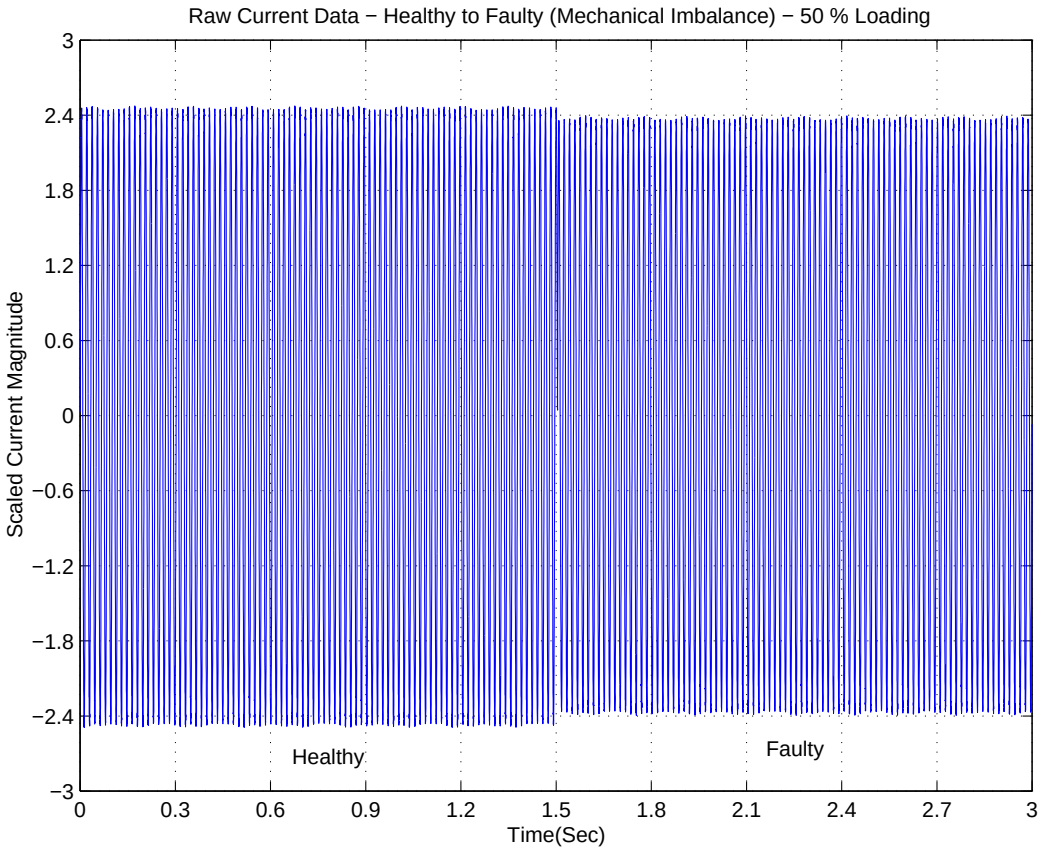

Fig. 121. Raw Current Signal - Mechanical Imbalance at 50% Loading

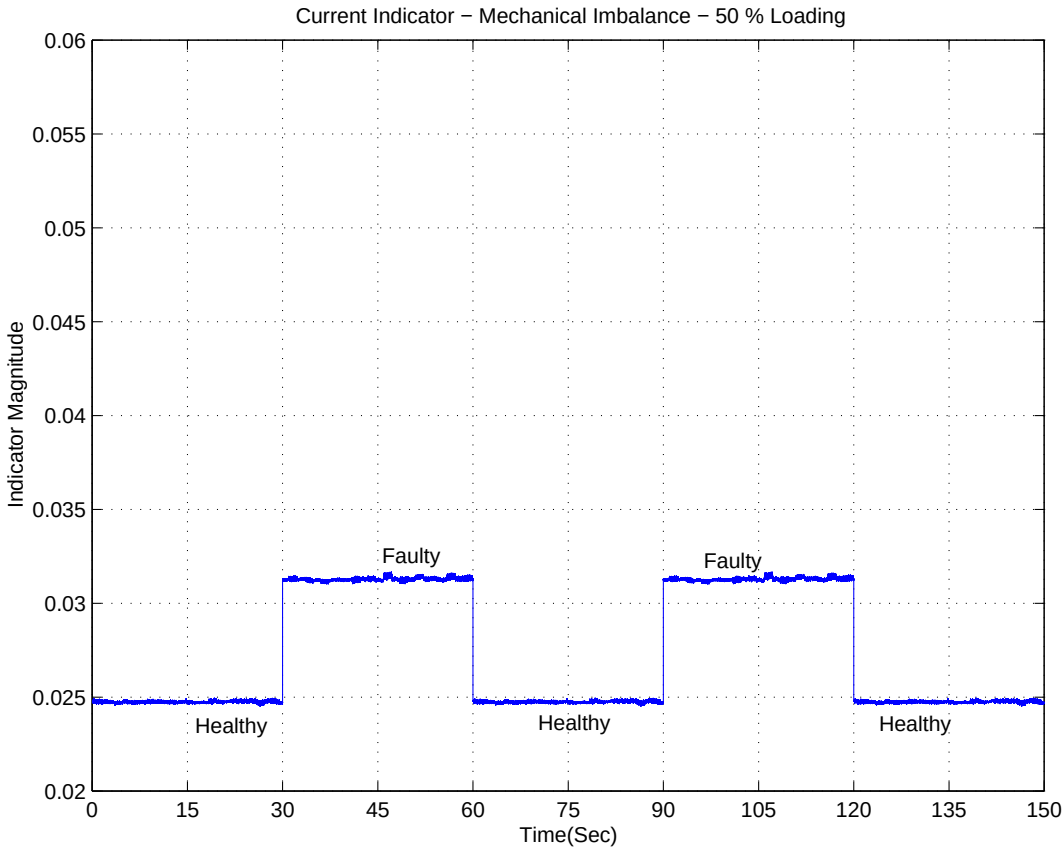

Fig. 122. Current-based Mechanical Indicator - Mechanical Imbalance at 50% Loading

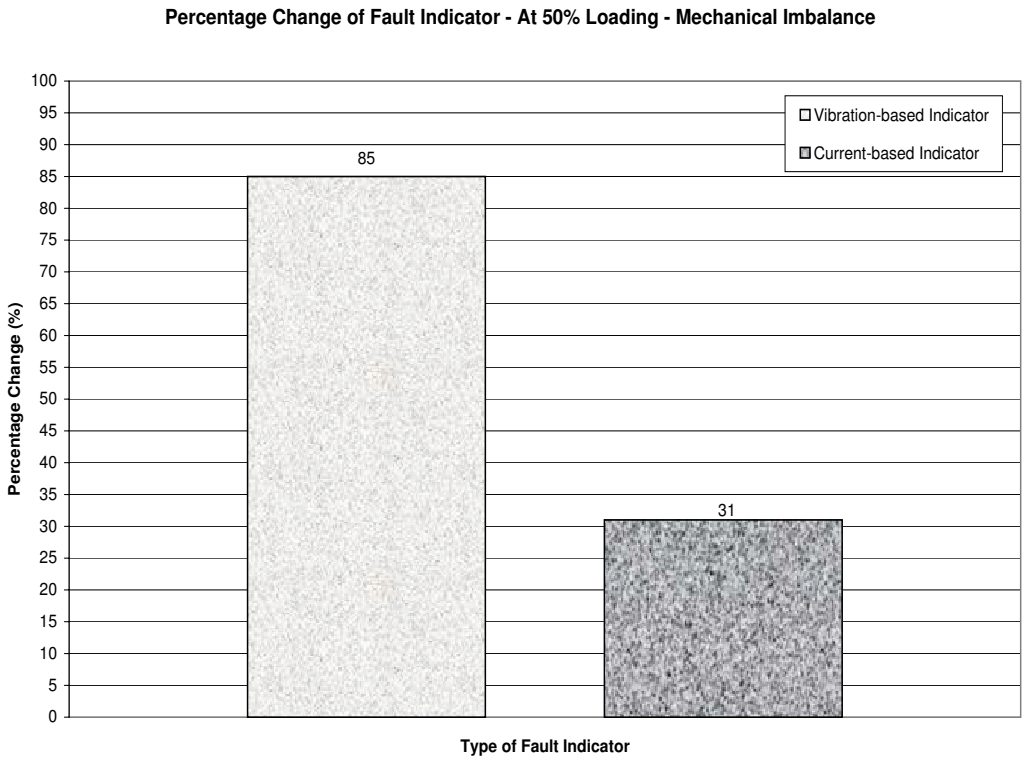

Fig. 123. Comparison of Current-based and Vibration-based Mechanical Fault Indicators - Mechanical Imbalance at 50% Loading

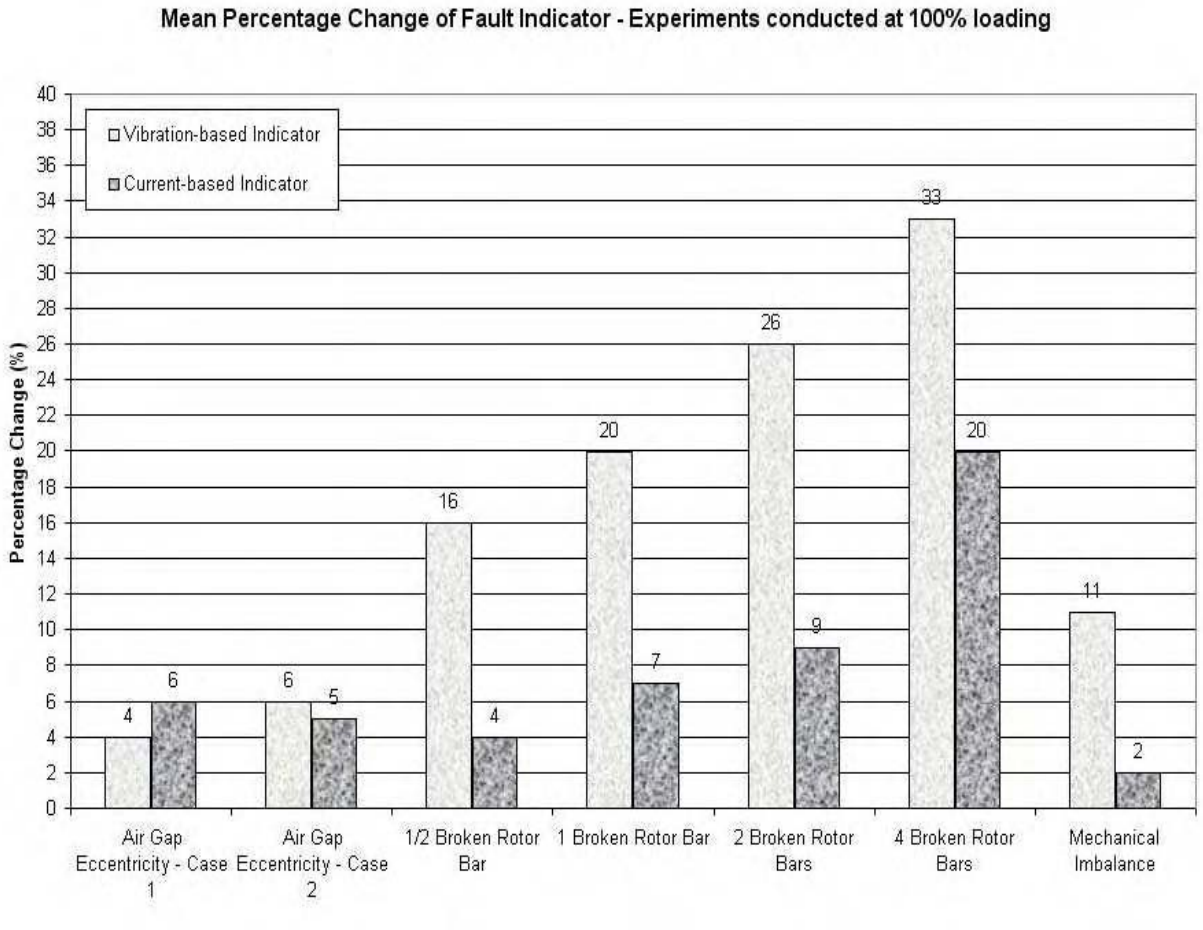

Fig. 124. Summary of the Comparison - At 100% Loading

E. Summary of the Comparison Based on the Load Levels

The experiments for the air-gap eccentricity cases, broken rotor bars and mechanical imbalance were performed at both 100% and 50% loading levels.

The summary chart for the 100% loading shown in Figure [124] depicts that the consistency in the pattern for the different fault cases. There is a clear indication of the magnitude fault in the case of experiments for broken rotor bar faults.

Although the pattern seems to be good at 100% loading conditions, the mag-

nitude of the mechanical indicator is not very significant. This is seen in both the vibration-based indicator as well as the current-based indicator. When we look at the 50% loading results shown in Figure [125], we can see that there is a significant indication of the fault for both the vibration-based and the current-based vibration fault indicators.

The experiments on the defective bearings were performed at 25% Loading (one case) and 0% (four cases of each severity level) loading conditions. The two summary charts are presented separately in Figure [126] and Figure [127] respectively. We can see that they reflect a similar pattern for discussion as the 100% and 50% loading case comparison.

In all the summary plots, we can see that the current-based mechanical indicator does not have a comparable magnitude as the vibration-based indicator. However, we can infer that the magnitude of the current-based mechanical indicator is significant for fault detection, especially at the lower loading level of operation.

F. Summary of the Comparison Based on Motor Ratings

Experiments were conducted on three motors of different ratings. The bearing fault experiments were done using a 3 HP induction motor, the mechanical imbalance experiments were done using a 500 HP induction motor. The experiments on air-gap eccentricities and broken rotor bars were done using a 800 HP induction motor.

The bearing fault experiments comprise of experiments with a single faulty bearing in the rotor, and both the rotor bearings faulty. Both were performed using a 3 HP motor. Four cases of each were considered without any loading, and one case was considered with 25% loading. When we look at the summarized comparison for the various cases in Figure [128], we can clearly see the expected pattern according to the

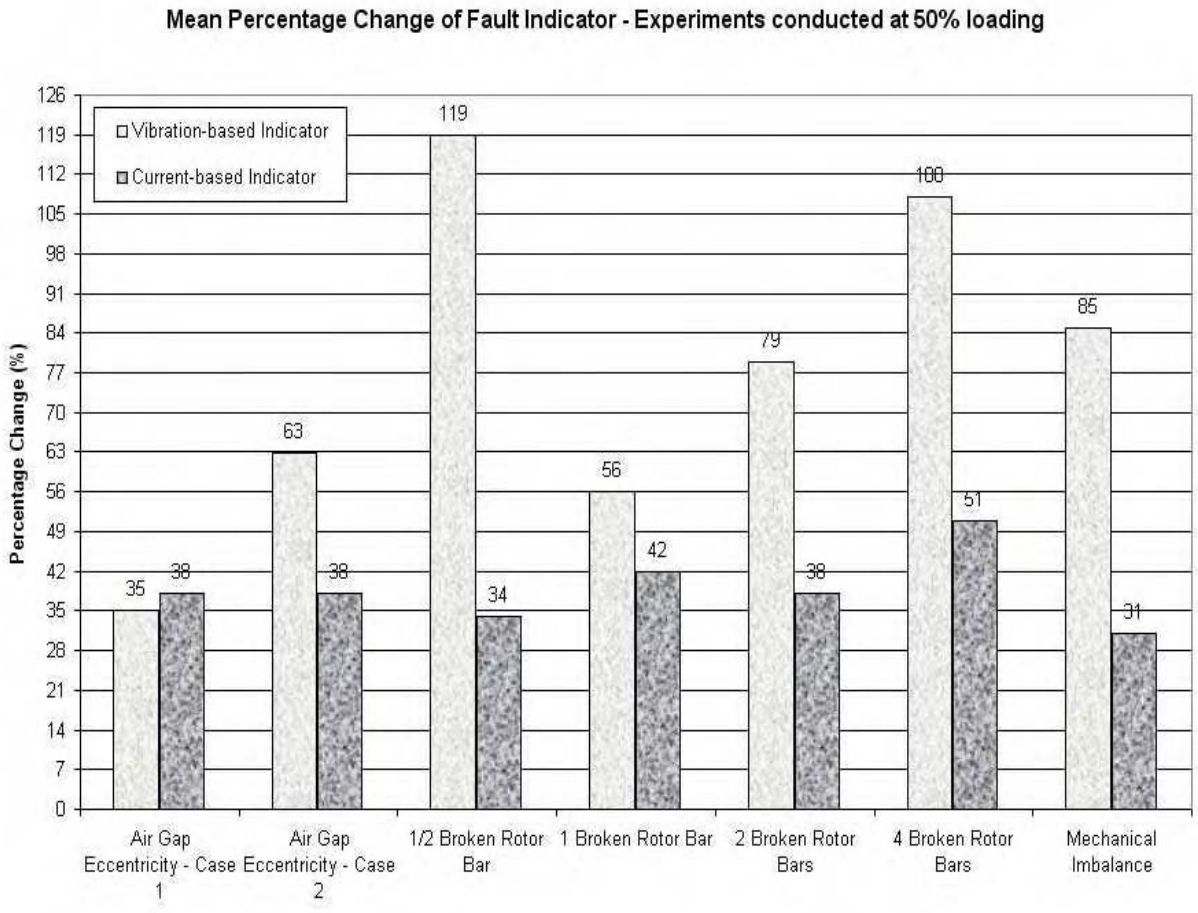

Fig. 125. Summary of the Comparison - At 50% Loading

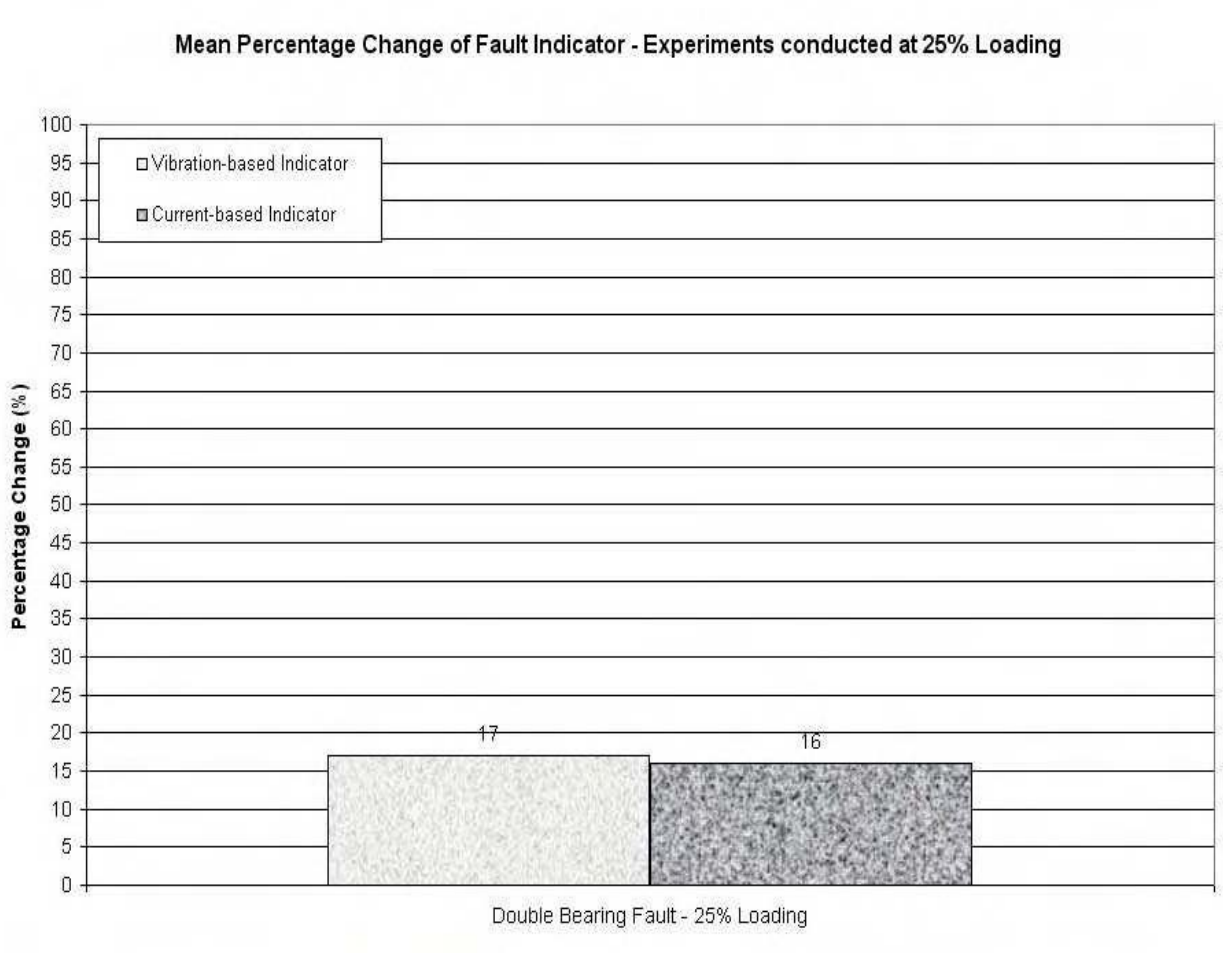

Fig. 126. Summary of the Comparison - At 25% Loading

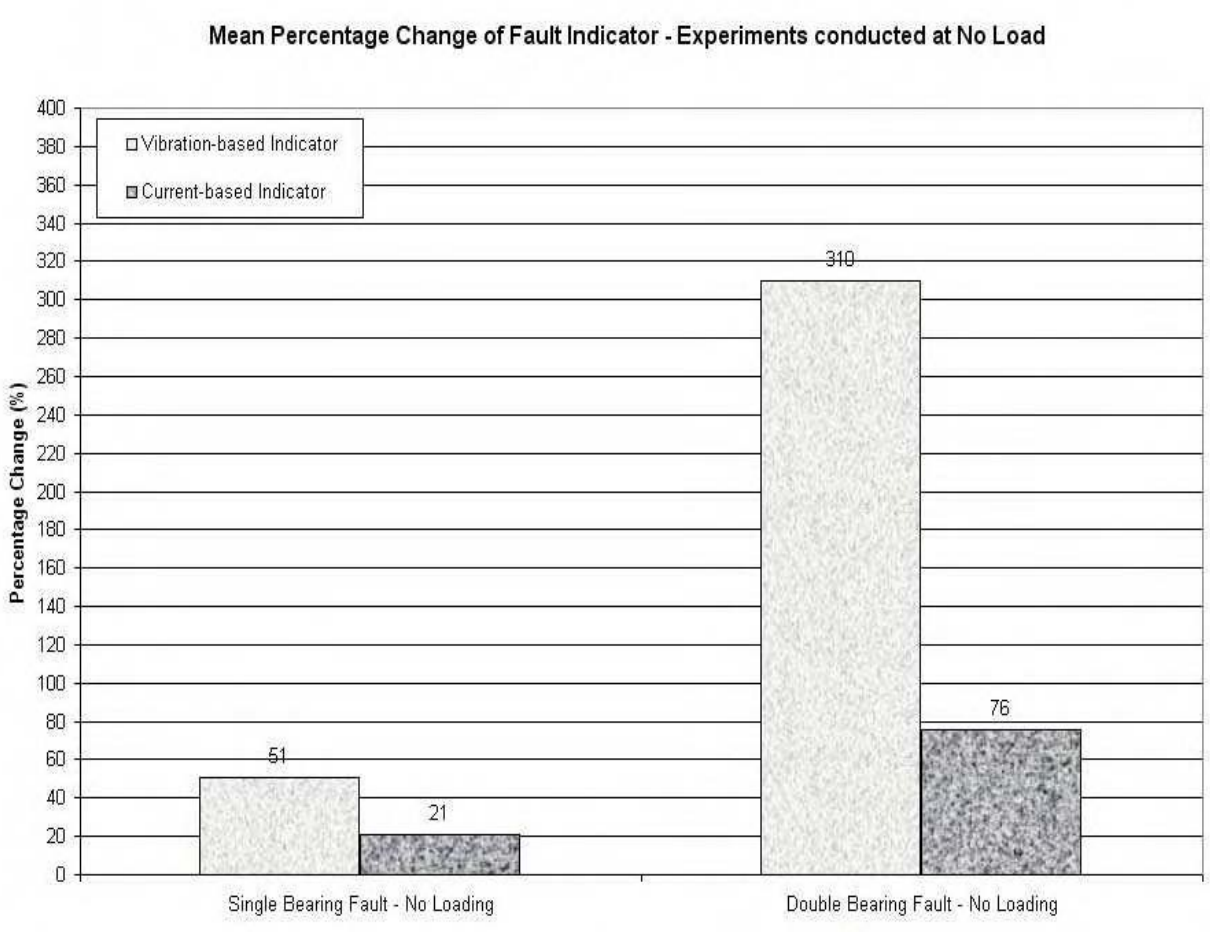

Fig. 127. Summary of the Comparison - At 0% Loading

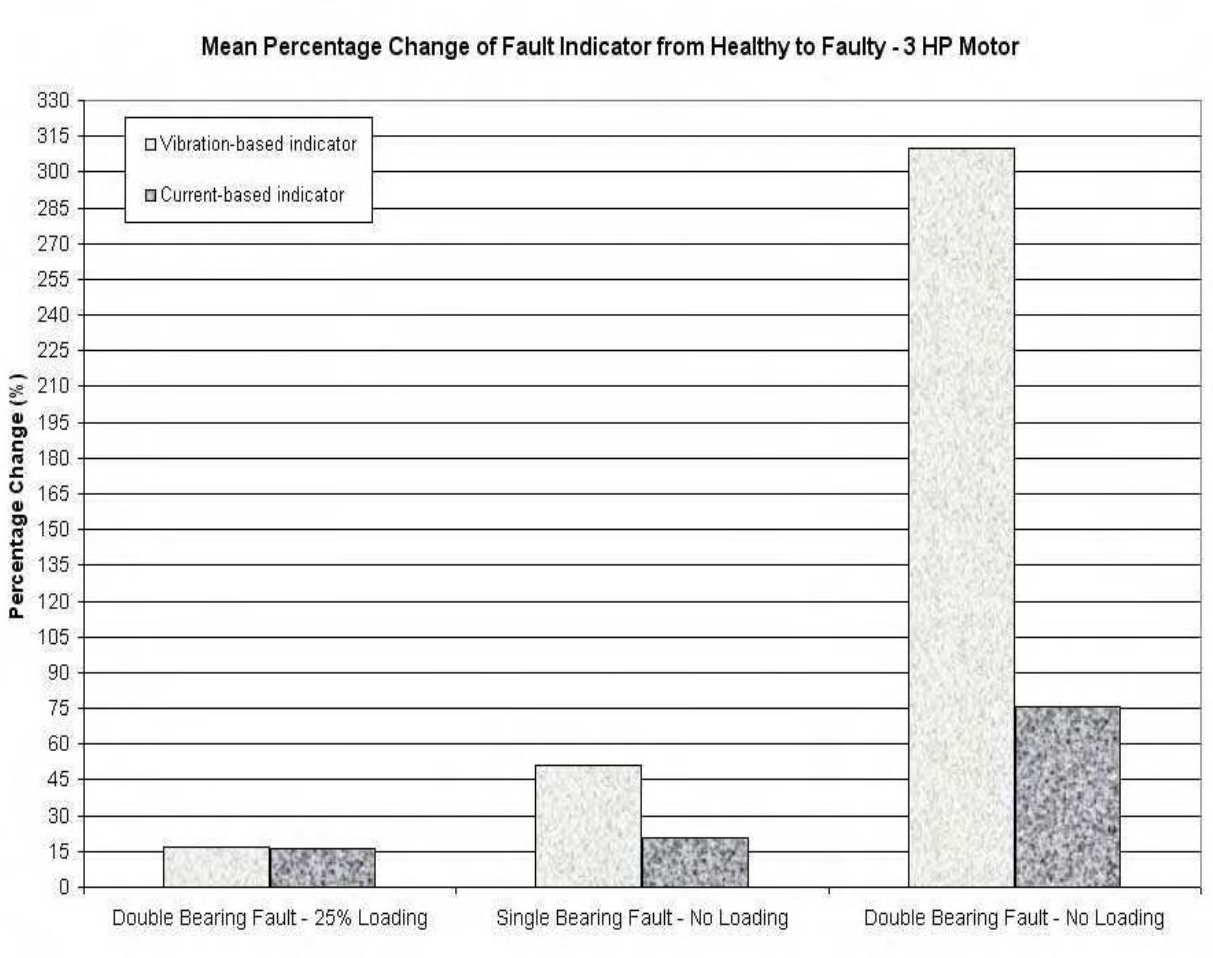

Fig. 128. Summary of the Comparison - 3 HP Motor

severity of the fault. We can also observe that in both the cases (single and double faulty bearing cases) the magnitude of the current-based mechanical fault indicator is not as significant as the vibration-based mechanical fault indicator. It can also be observed that the magnitudes of the indicators is much higher for the double faulty cases as compared to the single faulty cases.

Experiments were done on a 500 HP motor for the mechanical imbalance case. They were done at both 100% loading and at 50% loading. The summary chart in

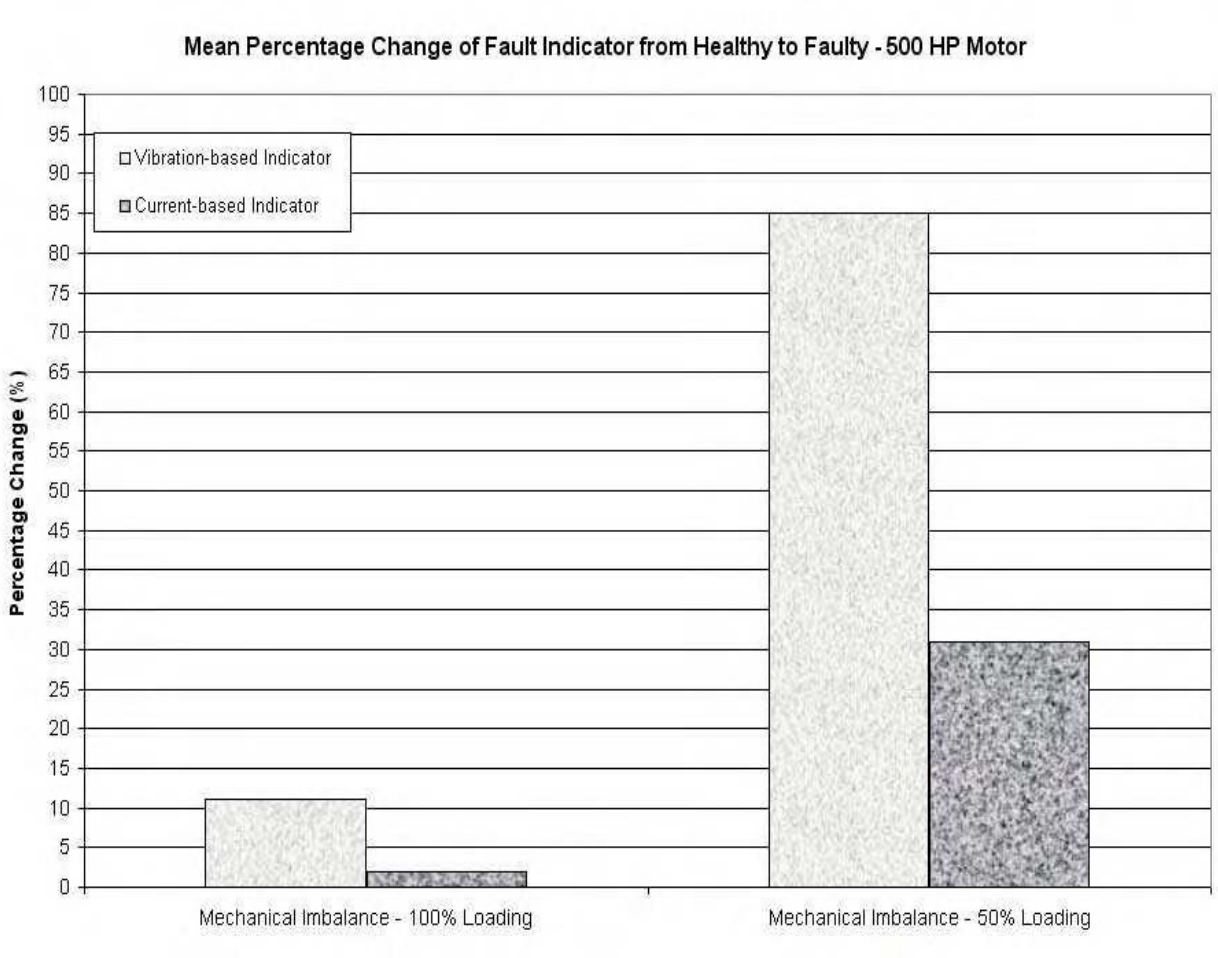

Fig. 129. Summary of the Comparison - 500 HP Motor

Figure [129] for this motor shows that for both the loading levels the vibration-based mechanical fault indicator is higher in magnitude than the current-based mechanical fault indicator. We can also observe that the magnitudes themselves are at much higher values at a lower loading level.

Air-gap eccentricity cases and the broken rotor bar experiments were done on a 800 HP motor. The summary chart for experiments performed (both at 100% and 50% loading levels) shown in Figure [130] clearly depicts the pattern. The current-based

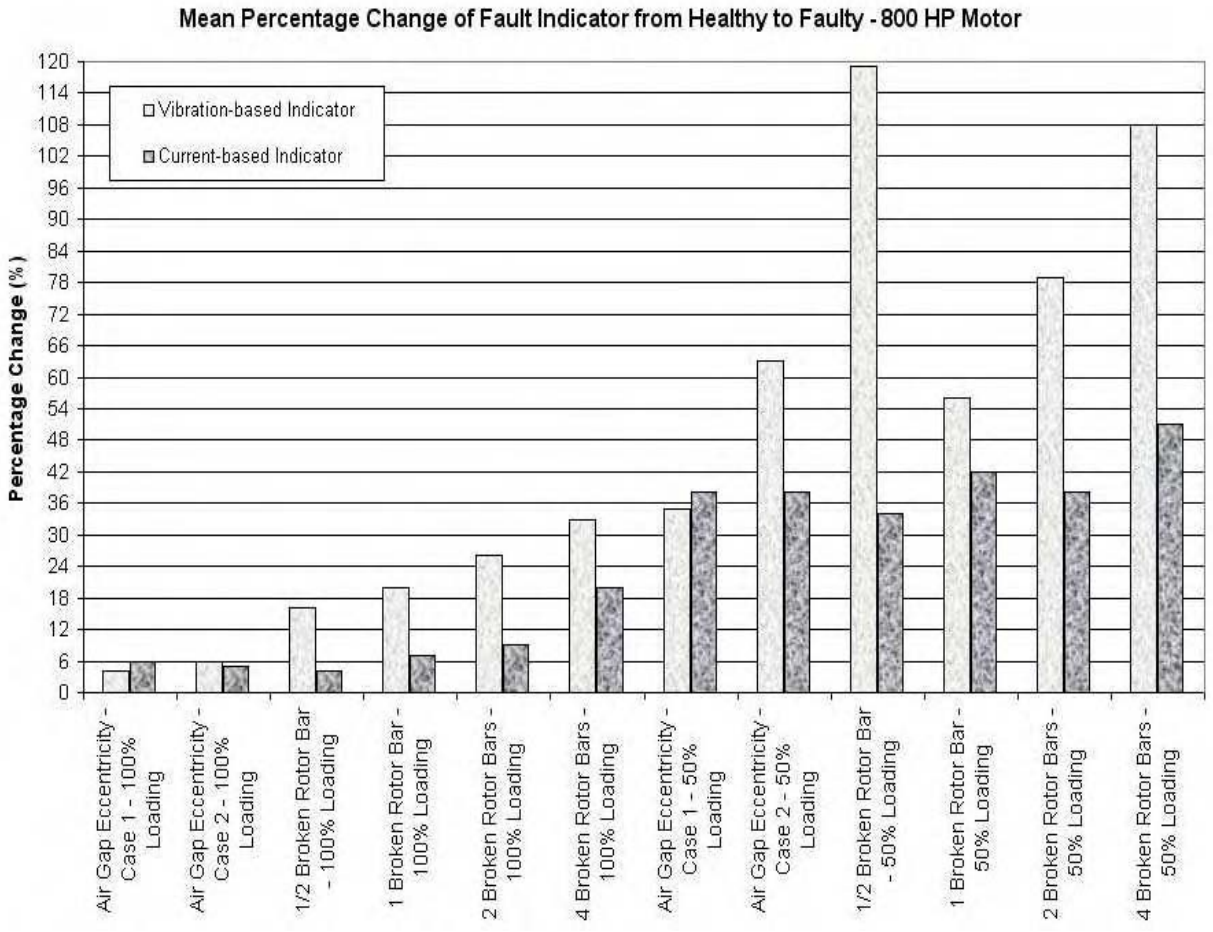

Fig. 130. Summary of the Comparison - 800 HP Motor

mechanical indicator is not as large in magnitude as the vibration-based indicator for the different cases. However, at lower levels of operation, we can observe that the magnitudes are significant and can aid in the fault detection, when applied to a real-time fault.

G. Chapter Summary

In this Chapter, the results obtained for the various experiments were discussed. For every Fault type being considered, the raw vibration and current signals were presented. The Fault indicators computed from the mechanical signatures and the electrical signatures were also presented along with a comparative chart of the two types of Fault Indicators. The patterns observed in these graphs were discussed, taking into consideration the effects of factors like loading and motor rating. It was then followed by discussions of the comparison based on the loading levels and the motor ratings.

CHAPTER IV

SUMMARY AND CONCLUSIONS

A. Summary of Research

The purpose of this research is to analyze and observe the behavior of electrical signatures in comparison to mechanical signatures when applied to mechanical faults in induction motors.

In Chapter II, the experimental setups were explained. It included discussions with specific details on the data acquisition hardware and experimental procedures. Four distinct types of mechanical faults were considered for the research. Experiments were conducted for multiple cases of Single and Double Bearing Faults (faulty at a single side of the rotor and at both sides of the rotor correspondingly) and their data was were considered for the analysis. Data from experiments conducted at the Public Service Electric and Gas Motor Repair Facility, Sewaran, New Jersey for Rotor Faults (Broken Rotor Bars), multiple cases of Air-Gap Eccentricities and Mechanical Imbalance were analyzed. For all fault types, experiments were conducted at steady state operating conditions. But different levels of loading were separately considered for the analysis. This was done to study the effects of loading on the results. The bearing faults were conducted with a smaller motor (3 hp Motor) while the other experiments were conducted with larger motors (Imbalance with a 500 hp Motor, Broken Rotor Bars and Air-Gap Eccentricities with a 800 hp Motor). This was done primarily to demonstrate the adaptability of the procedure to motors of different sizes and ratings. In this chapter, different fault detection schemes were also discussed, and the signal processing approach was further discussed. The signal processing algorithms based on the electrical and mechanical signatures were then discussed. The vibration signals

were analyzed by passing them through a moving window averaging algorithm and the vibration-based mechanical fault indicators were computed. The current signals were analyzed by first passing them through a wavelet packet decomposition algorithm to remove the fundamental frequency of the signal. They were then passed through a moving window averaging algorithm and the current-based mechanical fault indicators were computed. The above mentioned procedure was performed for all the data sets obtained for the different Healthy and Faulty Cases.

In Chapter III, the various cases were presented and discussed. For each case of the fault types, raw signals (vibrations and the currents) were presented along with the computed indicators. The mean percentage increase of these fault indicators from the mean healthy indicators were then compared. An indication of close to or more than about 10 to 15% is usually considered sufficient for effective fault detection. With this in mind, in every case, the electrical signature based mechanical fault indicator (or the current-based mechanical fault indicator) was compared to the corresponding mechanical signature based mechanical fault indicator (or the vibration-based mechanical fault indicator). It was followed by a discussion or an explanation of the observed behavior. The comparison of the fault indicators was then summarized based on the loading level. Bar plots of the indicators for the various loading levels were presented and discussed. A summary based on the motor ratings was then presented. This was done to achieve the desired scalability of the scheme across different sizes of motors.

B. Conclusions from the Research

Based on the discussions of the different results obtained, the conclusions drawn from this research can be summarized as follows:

- The mechanical signatures analyzed are indicative of mechanical faults in the system and this is reflected in the vibration indicators obtained. In addition to this expected outcome, we could also see a similar pattern in the behaviour of the electrical signatures. The results from the electrical signatures provide a consistent indication of the same faults in the electric current indicators for the different fault cases.

- The summary based on the loading levels clearly indicates the relative ease of fault detection when the operating conditions are at lower load levels. This can be seen from the results obtained for broken rotor bars, mechanical imbalance, air-gap eccentricities and defective bearings using both mechanical and electrical signatures.

- From observing the similarities of pattern in the summary charts presented based on the motor ratings, we can say that the relative behavior of the fault signatures is very similar for both small machines as well as large machines, thus demonstrating the scalability of the proposed scheme to motors of different ratings and manufacturers.

- For the various mechanical fault types that were considered, the relative behavior of the electrical signatures with respect to the mechanical signatures has been found to follow a constant pattern irrespective of the fault type. As expected the mechanical signatures are stronger in almost all cases, compared to electrical signatures. However the strength of the electrical fault signatures is in most instances sufficient to allow fault detection. The exception is the case of mechanical imbalance where only a low threshold fault detection system would enable its effective detection. This demonstrates the adaptability of the procedure to different types of mechanical faults.

C. Future Work

On the basis of the research discussions in this thesis, some recommendations for future work are as follows.

- The present research applies to 3ϕ induction motors. However, it can also be extended to other electrical machinery fault detection.
- The effects of dynamic loading can be studied and related experiments can be carried out. This can especially be helpful when dealing with the fault diagnosis of systems like pumps, compressors, fans, etc. using the induction motor.
- Similar studies can be carried out when the system operates in a closed loop and the motor is fed through an inverter. The control loop modifies the behavior of the system, and hence a more enhanced procedure might be required to be developed based on the proposed scheme.
- Effects on the fault signatures when the system has a set of motors being operated from the set voltage bus can be studied. The objective of fault detection can have a scope as simple as a single motor being faulty, to a complex one where multiple motors are in faulty operating conditions.
- More enhanced signal processing techniques that would allow more pronounced induction motor fault detection based on electrical signatures.

REFERENCES

[1] P. J. Tavner and J. Penman, *Condition Monitoring of Electrical Machines*, Letchworth, UK: Research Studies Press, 1987.

[2] P. F. Albrecht, J. C. Appiarius, R. M. McCoy, E. L. Owen, and D. K. Sharma, "Assessment of the Reliability of Motors in Utility Applications - Updated," *IEEE Transactions on Energy Conversion*, vol. EC-1, no. 1, pp. 39–46, March 1986.

[3] N. M. Elkasabgy, A. R. Eastham, and G. E. Dawson, "Detection of Broken Bars in the Cage Rotor on an Induction Motor," *IEEE Transactions on Industry Applications*, vol. 28, pp. 165–171, January 1992.

[4] B. Liang, B. Payne, and A. Ball, "Detection and Diagnosis of Faults in Induction Motors Using Vibration and Phase Current Analysis," in *Proceedings of the 1st International Conference on the Integration of Dynamics, Monitoring and Control (DYMAC '99)*, Manchester, UK, September 1999, pp. 337–341.

[5] B. Payne, B. Liang, and A. Ball, "Modern Condition Monitoring Techniques for Electric Machines," in *Proceedings of the 1st International Conference on the Integration of Dynamics, Monitoring and Control (DYMAC '99)*, Manchester, UK, September 1999, pp. 325–330.

[6] R. R. Schoen, T. G. Habetler, F. Kamran, and R. G. Bartheld, "Motor Bearing Damage Detection Using Stator Current Monitoring," *IEEE Transactions on Industry Applications*, vol. 31, pp. 1274–1279, November/December 1995.

[7] B. Yazici and G. B. Kliman, "An Adaptive Statistical Time-Frequency Method for Detection of Broken Bars and Bearing Faults in Motors Using Stator

Current," *IEEE Transactions on Industry Applications*, vol. 35, pp. 442–452, March/April 1999.

[8] A. M. Trzynadlowski and E. Ritchie, "Comparative Investigation of Diagnostic Media for Induction Motors: A Case of Rotor Cage Faults," *IEEE Transactions on Industrial Electronics*, vol. 14, no. 4, pp. 1417–1423, December 2000.

[9] J. R. Cameron, W. T. Thomson, A. B. Dow, "Vibration and Current Monitoring for Detecting Airgap Eccentricity in Large Induction Motors," *IEEE Transactions*, vol. 133, pt. B, no. 3, pp. 155–163, May 1986.

[10] W. T. Thomson, D. Rankin, D. G. Dorrell, "On-line Current Monitoring to Diagnose Airgap Eccentricity in Large Three-Phase Induction Motors-Industry Case Histories Verify the Predictions," *IEEE Transactions on Energy Conversions*, vol. 14, no. 4, pp. 1372–1378, December 1999.

[11] K. Kim, "Sensorless Fault Diagnosis of Induction Motors," Ph.D. dissertation, Texas A&M University, College Station, May 2001.

[12] K. Kim, and A. G. Parlos, "Induction Motor Fault Diagnosis Based on Neuropredictors and Wavelet Signal Processing," IEEE/ASME Transactions on Mechatronics, vol 7, no. 2, pp. 201–219, June 2002.

[13] M. Benbouzid, M. Vieira, C. Theys, "Induction Motor's Fault Detection and Localization Using Stator Current Advanced Signal Processing Techniques," *IEEE Transactions on Power Electronics*, vol. 14, no. 1, pp. 14–22, January 1999.

[14] P. D. McFadden, J. D. Smith, "A Signal Processing Technique for Detecting Local Defects in a Gear from the Signal Average of the Vibration," in *IMechE Proceedings*, vol. 199, pt. C, no. 4, pp. 287–292, February 1985.

[15] M. Benbouzid, "A Review of Induction Motors Signature Analysis as a Medium for Faults Detection," *IEEE Transactions on Industrial Electronics*, vol. 47, no. 5, pp. 984–993, October 2000.

[16] M. Benbouzid, "Bibliography on Induction Motors Faults Detection and Diagnosis," *IEEE Transactions on Energy Conversion*, vol. 14, no. 4, pp. 1065–1074, December 1999.

[17] G. Strang, and T. Nguyen, *Wavelets and Filter Banks*, Wellesley, MA: Cambridge Press, 1997.

[18] B. Liu and J. Si, "Machinery Diagnostics Based on Wavelet Packets," *Journal of Vibration Control*, vol. 3, no. 1, pp. 5–17, January 1997.

[19] G. G. Yen and Kuo-Chung Lin, "Wavelet Packet Feature Extraction for Vibration Monitoring," *IEEE Transactions on Industrial Electronics*, vol. 47, no. 3, pp. 650–667, June 2000.

VITA

Arvind M. Venugopal was born in Bangalore, India and completed his B.E. from the University of Madras. He entered Texas A&M University to pursue his Master's degree starting Fall 2000 and received his M.S. in mechanical engineering in December 2003. Arvind conducted research under the guidance of Dr. Alexander G. Parlos. He can be reached through: Networked Intelligent Machines Laboratory, 167 Wisenbaker Engineering Research Center, Texas A&M University, College Station, TX-77843

The typist for this thesis was Arvind M. Venugopal.